5-2024

Structure and Dynamics of Complex Fluids Formed by Ionomers: Experimental-Computational Insight

Chathurika Kosgallana
ckosgal@clemson.edu

STRUCTURE AND DYNAMICS OF COMPLEX FLUIDS FORMED BY IONOMERS: EXPERIMENTAL-COMPUTATIONAL INSIGHT

A Dissertation
Presented to the
Graduate School of
Clemson University

In Partial Fulfillment of the
Requirements for the Degree
Doctor of Philosophy
Chemistry

by
Chathurika Kosgallana
May 2024

Accepted by:
Dr. Dvora Perahia, Committee Chair
Dr. Gary S. Grest
Dr. Rhett C. Smith
Dr. Brian N. Dominy
Dr. Leah B. Casabianca

ABSTRACT

The current study focuses on understanding the effect of clustering on the structure, dynamics, and response of ionomers in melts and solutions using neutron scattering methods combined with atomistic large-scale molecular dynamics (MD) simulations. Ionizable polymers are used in a wide range of applications, such as in clean energy and biotechnology, where ion transport is integral to the application. Ionizable groups drive cluster formation and often become the dominating force in determining the structure and dynamics of these polymers.

The work consists of five studies. The first study probes the structure of sulfonated polystyrene in toluene solutions tweaked by the addition of ethanol using small-angle neutron scattering (SANS) and MD simulations. We find that a network is formed driven by ionic cluster formation. The addition of ethanol impacts the size of the clusters and their size distribution, which affects the overall structure of these systems. Following the understanding of the structure of these ionomers in solution, neutron spin echo (NSE) and MD simulations were used to study the dynamics of these systems. From this study, the relationship between polymer dynamics and ionic clusters was established. Two distinctive time scales were needed to describe the motion in these systems, where the slower motion correlated with the effects of the clusters and the faster motion correlated with the non-confined motion of the highly solvated chain segments.

Following the understanding of dynamics of polymers in solutions, the systems were studied under external perturbations, including temperature and solvent dielectrics, using NSE and MD simulations. With increasing the dielectric constant of the solvent, the cluster size decreases, and the dynamics of the system increase. With increasing temperature, the long-lived clusters remain stable, and the polymer remains dynamic. The next chapter focuses on structure and dynamics of THF swollen melts studied by large scale atomistic MD simulations. THF is as close as possible to a mutual solvent for both the ionic groups and the chains. We measured structure parameters, including the static structure factor, ionic cluster size and distribution, and dynamic parameters, such as mean square displacement and dynamic structure factor. The study finds that THF resides throughout the system and releases constrains of both the chain and ionic groups. While the addition of THF results in larger ionic clusters, all segments become more dynamic.

The last chapter probes the response of THF swollen melts to shear by large scale MD simulations of the same systems whose structure was probed in the previous chapter. Similar to dielectric constant and temperature, shear affects the stability of the ionic clusters. The neutral polymer was compared to the ionic polymer as THF amounts are increased. For all compositions, the shear viscosity decreases with increasing shear rate. However, the decrease depends strongly on the degree of solvation. With increasing solvent, shear affects packing of polymer bundles but only breaks the clusters at higher shear rate.

DEDICATION

This work is dedicated to my loving son Trivone Perera for being the motivation to succeed and push forward. My husband, Rachitha Perera, for always being there. My loving parents, Wasantha Nandalal and Hemalie Nandalal, for encouraging and motivating me throughout this journey, and my sister Warunie Kosgallana, for her support.

ACKNOWLEDGMENTS

TABLE OF CONTENTS

LIST OF TABLES

LIST OF FIGURES

CHAPTER ONE

INTRODUCTION

Controlling the structure and dynamics of ionomers is critical to their technological uses. Ionizable polymers are used in a broad range of applications; examples include ion exchange membranes,[1] clean energy,[2] dialysis[3] and drug delivery.[4] Among the most common ionomer is Nafion[TM,5, 6] a perfluorinated ionomer that is used in numerous ion exchange membranes. One application is hydrogen fuel cells where Nafion has served as the electrolytic membrane. The ionic groups form transport challengers and the rest of the polymer, often referred to as "the matrix" form the membrane. The ionic groups associate and minimize the contact between incompatible segments or clusters that enable transport. However, they also act as physical crosslinks that offer additional mechanical stability. As transport takes place, the ionic clusters are often affected and the stability of these type of membranes is reduced leading to failures of devices.

This study explores the relation between formation of ionic clusters in polystyrene sulfonate and the structure and dynamics of the different constituents of a model polystyrene sulfonate co-polymer. Polystyrene was chosen as the model system because it has been one of the most prevalent materials in different applications. Therefore, there is a rich knowledge base that allow us to focus on the interrelation of cluster characteristics and overall structure and dynamics of the system.[7-11]

To probe SPS in solutions and melts the study uses small angle neutron scattering (SANS)[12-15] and classical atomistic molecular dynamics (MD) simulation. The ionic clusters will be altered by addition of solvents of different polarity. The following the structure and dynamics of all constituents will be followed.

This section will first discuss the background of ionic polymers, including physics that controls clustering. In the following sections, SANS principals will be briefly introduced followed by large scale classical MD methods.

1.1 Ionic Polymers

Ionic polymers are polymers containing ionizable groups. These are often divided into two groups, ionomers and polyelectrolytes. While the properties of ionomers are determined by both the ionic groups and polymer backbone. In polyelectrolytes the properties are dominated by the ionic groups. The uniqueness of these polymers is that even a small number of ionic groups strongly affect the structure and dynamics of macromolecules.[16] This study will focus on ionomers where the ionic groups provide their functionality, and their backbone provides the mechanical stability. Even though the unique properties of ionomers have been realized decades ago, the balance between electrostatic interactions and van der Waals forces that together determine both the structure and dynamics of the system, remains an open question. The co-existence of van der Waals forces, that are relatively weak and ionic forces that are relatively strong often results in materials whose structures are far from equilibrium, resulting in challenges to the design of materials with designed properties. Understanding the interrelation of the ionic interactions and the van der Waals forces will allow the control over properties of polymers, crucial in designing polymers for targeted applications.

Due to electrostatic interactions the ionic groups assemble into clusters of 30-50 nm in diameter where the rest of the backbone is confined by these aggregates, forming materials whose structure features extend across length scales, presents a challenge to both experimental and computational studies.

1.2 Polymer-Solvent Interactions

Most studies that have been done so far have been in SPS melts. Here we probe SPS in solution. Compared to melts, solutions have interactions that are more complex. In order to obtain membranes with high mechanical performance they need to be swelled by significant amounts of solution. A polymer dissolves when a solvation lowers free energy. The equation for free energy change of mixing is given by,

$$\Delta G_{mix} = \Delta H_{mix} - T\Delta S_{mix} \qquad (1.1)$$

Here, ΔH_{mix} is the enthalpy change of mixing, T is temperature and ΔS_{mix} is entropy change of mixing.
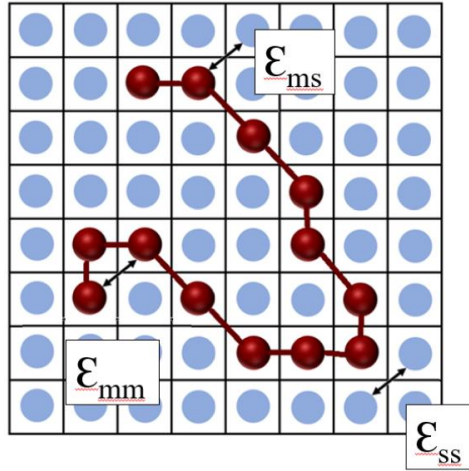
Figure 1.1: Flory-Huggins lattice model. Blue: solvent molecules on lattice. Red: monomers on lattice.

The Flory-Huggins[17] parameter gives the energy change upon polymer-solvent mixing. This model defines the system as particles on a lattice. Each lattice point is occupied by solvent or monomer.[18] The equation is given below,

$$\chi = \left(\frac{z}{k_B T}\right)\left[\varepsilon_{ms} - \frac{1}{2}(\varepsilon_{mm} + \varepsilon_{ss})\right] \qquad (1.2)$$

3

In this equation, z is the number of nearest neighbors per monomer and, k_B is Boltzman constant. The interaction energies between monomer-solvent, monomer-monomer, solvent-solvent are given by $\varepsilon_{ms}, \varepsilon_{mm}$ and ε_{ss}. When monomer-solvent interactions are less favored than monomer-monomer, solvent-solvent contacts χ is positive. When monomer-solvent interactions are more favored than monomer-monomer, solvent-solvent contacts χ is negative. When χ is negative, solvation occurs.

Good Solvent	Theta Solvent	Poor Solvent
$\chi < 0$	$\chi = 0.5$	$\chi > 0$
$R_g \propto N^{3/5}$	$R_g \propto N^{1/2}$	$R_g \propto N^{1/3}$
$\varepsilon_{ms} > \varepsilon_{mm}, \varepsilon_{ss}$	$\varepsilon_{ms} \sim \varepsilon_{mm}, \varepsilon_{ss}$	$\varepsilon_{ms} < \varepsilon_{mm}, \varepsilon_{ss}$
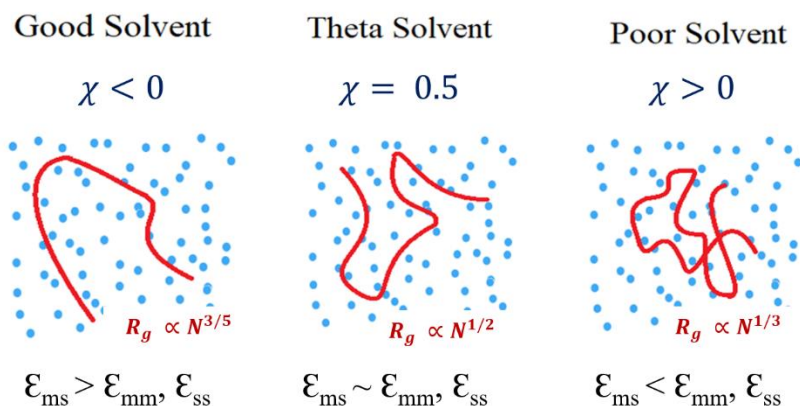
Figure 1.2: Single polymer chain in good, theta and poor solvents. blue: solvent molecules, red: polymer chain

The strength of the monomer-solvent interaction determines if the solvent quality for the polymer is good, theta or poor. In a good solvent, monomer-solvent interactions are stronger that the monomer-monomer interactions. A poor solvent, monomer solvent interactions are weaker than monomer-monomer interactions. A theta solvent is a solvent where monomer-solvent and monomer-monomer interactions are the same. The structure of the polymer is governed by the quality of the solvent. Depending on the polymer, the good and poor solvent differs. Toluene is a good solvent for polystyrene, but as ionic groups are added toluene becomes a poor solvent for sulfonated polystyrene.[19]

1.3 Cluster formation
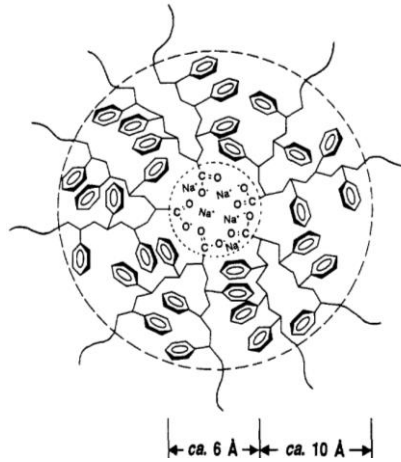
Figure 1.3: Schematic deconstruction of a cluster. (*Reprinted with permission from ref [21]. Copyright {1970} American Chemical Society)*

Eisenberg and co-workers were the first to quantify the balance between electrostatic forces and elastic energy of a polymer backbone[20-22]. They showed that the formation of ionic clusters depends on elastic forces of hydrophobic chains and electrostatic interactions between ionizable groups. Ion pairs formed by ionic sites on the polymer chains and counter ions could be from either multiplets of a few ionic groups or clusters.[23] Collection of several multiplets form a cluster. Clusters, which contain both ionic material and significant amount of organic polymer,[21] dominates the structure and the dynamics of ionomers. Elastic forces play a significant part in cluster formation.

Elastic force *f* is given by,

$$f = \frac{3k_B T h}{\bar{h}^2} \qquad (1.3)$$

Where $\bar{h}^2$ is the mean square end to end distance for the free chain and *h* is the actual separation of the ends.

The nearest neighbor distance between multiplets is given by,

5

$$R_0 = \sqrt[3]{n_0 M_c / \rho N_{AV}}$$

where n_0 is number is ion pairs in multiplet, M_c is molecular weight of chain between ionic groups, N_{Av} is Avogadro number and ρ is density.

Upon cluster formation, work is done to stretch and contract the polymer chain due to elastic forces acting upon the polymer chain.

Work for stretching a polymer chain,

$$\int_{R_0}^{R} f \, dh = W_1 = \left(\frac{3k_B T}{2\bar{h}^2}\right)(R^2 - R_0^2) \qquad (1.4)$$

where R_0 is the nearest neighbor distance between multiplets. R is the distance of stretched polymer.

Work for contraction a polymer chain,

$$\int_{R_0}^{0} f \, dh = W_2 = -\left(\frac{3k_B T}{2\bar{h}^2}\right)(R_0^2) \qquad (1.5)$$

Half the chains will expand, and other half will collapse. Using the two equations 1.4 and 1.5 we could obtain the net work done upon cluster formation per chain due to elastic forces, which is given by,

$$W_{ch} = \left(\frac{3k_B T}{4\bar{h}^2}\right)(R^2 - 2R_0^2) \qquad (1.6)$$

Considering Electrostatic forces, according to Eisenberg cluster model[22], the work required to separate a contact ion pair into separate ions is,

$$W = -e^2 / (r 4\pi \epsilon_0 K) \qquad (1.7)$$

where K is the dielectric constant, $1/4\pi\epsilon_0 = 1$ dyn cm^2/statcoulomb^2, e is the electronic charge and r is the distance between the centers of positive and negative charges in the contact ion pair. Therefore, work done per ion pair upon cluster formation by electrostatic energy is given by,

$$W' = {k'e^2}\big/{r4\pi\epsilon_0 K} \qquad (1.8)$$

Where k' is energy released upon formation of an ion pair from energy released upon formation of an ion pair from isolated ions for a system.

At temperatures below Tc the clusters are thermodynamically stable, while at temperature Tc the cluster is thermodynamically unstable and at that temperature the elastic force and electrostatic forces balance each other. Since elastic force was calculated per chin and the electrostatic force per ion pair, W_{ch} can be set equal to W' at Tc. By equations 1.6 and 1.8 we can obtain the cluster size n.

$$n = \frac{\rho N_{AV}}{Me}\left[\frac{4l^2}{3kT_c}\frac{\overline{h^2}}{\overline{h_0^2}}\frac{M_c}{M_0}\frac{k'}{K}\frac{1}{4\pi\epsilon_0}\frac{e^2}{r} + 2\left(\frac{n_0 M_c}{\rho N_{AV}}\right)^{2/3}\right]^{3/2}$$

Where l is length of a C-C bond and M_c/M_o is average number of C-C links in a chain between ionic groups.
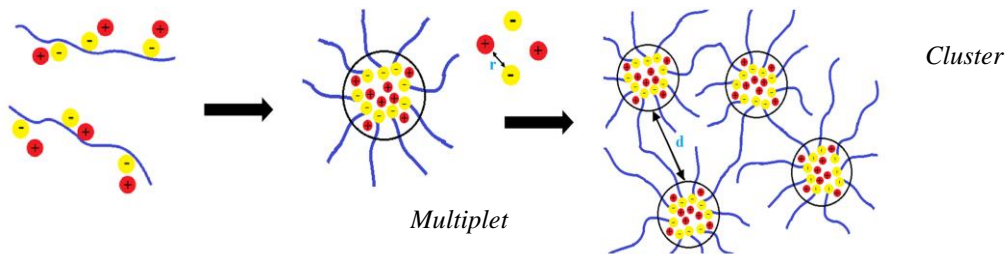
Figure 1.4: Schematic diagram of formation of ionic clusters

1.4 Sulfonated polystyrene: what is known

This study uses sulfonated polystyrene which is an excellent model system because it is possible to experimentally control the molecular weight, charge distribution and topography of the polymer. In addition, SPS has been well studied and therefore there is preexisting knowledge which enables to focus on the current questions. Another desirable property of SPS is that it displays solubility in a variety of different solvents ranging from low polarity to high polarity.[24]

SPS is incorporated in many uses from traditional clean energy applications to recent innovative biotechnology. One such example of medicinal recent uses is SPS-Na$^+$ as short-term treatment for hyperkalaemia.[25, 26] This is a condition in which the potassium level in the blood is high. These high levels are found in patients with chronic kidney disease, heart failure, and diabetes. SPS is ingested and operates as an ion exchanger and captures potassium.[27] On the other side of the spectrum of uses are innovative piezoelectric crystals where SPS in combination with PEDOT (poly(3,4-ethylenedioxythiophne)) forms PEDOT:SPS a flexible electric-responsive media. Further this complex is used as a hole transport layer or as a coating on microelectrode arrays in order to reduce impedance for both in vitro and in vivo electrophysiology.[28, 29]

For improvements of current applications and deriving new ones, the structure and internal dynamics of SPS must be fully controlled. Further corelating the structure and dynamics of the ionic clusters with that of the entire polymer becomes critical. Despite the many uses and numerous studies of basic properties, this correlation remains an open question. The challenges in full characterization of such system lies in the need to capture multiple time and length scales simultaneously.

Significant number of studies that have been done in SPS melts. Among these studies those of are Weiss and co-workers[30-36] who established correlations between sulfonation levels of the

polymer with structure and dynamics of the system. This group used small angle X-ray scattering (SAXS) to probe the correlations between sulfonation levels of the polymer and its structure. They showed that aggregation of ionic groups had a large effect on the structure and dynamics of the SPS. In addition, they were able to resolve the response to external perturbation. One study done compared SAXS data for sulfonation level $f = 0$ and $f = 1.00$ as shown in Figure 1.5. The fully sulfonated $f = 1.0$ system shows a clear ionomer peak around 1.6 nm^{-1} which is not present in the non-sulfonated system.
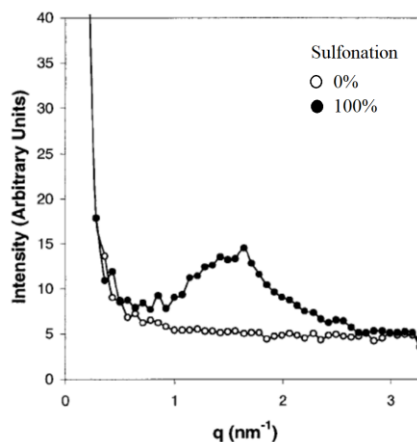
Figure 1.5: SAXS intensity as a function of scattering vector for f = 0 (open) and f = 1.0 (closed) for PS and Zn-SPS melts at room temperature. Molecular weight M_w = 64,600 g/mol. (*Reprinted with permission from ref [37] Copyright {2001} John Wiley and Sons and Copyright Clearance Center'*)

Other studies focus on solutions,[34, 35] where similar features are observed. Solution studies by several group shows that aggregates driven by ionic clusters are formed.

Dynamics of SPS solutions and melts are being dominated by the ionic clusters. Rheology is one convenient technique to study the effect of the ionic clusters on dynamics.[31, 32, 37-39] Rheological measurements of SPS have shown that even small quantity of sulfonation groups act as if they arrest the motion where even low molecular weight polymers behave act like high molecular

weight polymers in presence of very few sulfonation fraction. One of the objectives of the current

study is to understand molecular basis of the arrest of motion of SPS observed by rheology.
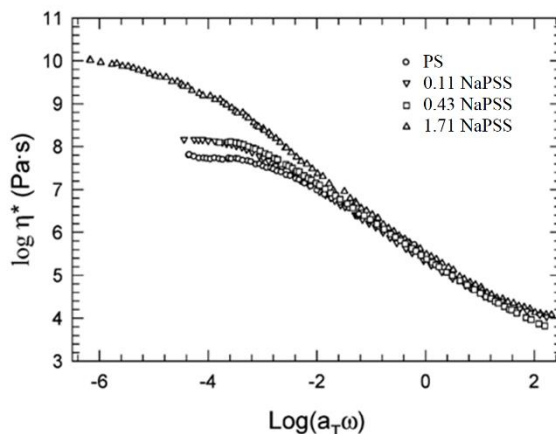
Figure 1.6: Complex Viscosity-frequency master-curves for PS and SPS ionomers with Na^+ counterions at T=140 °C. Molecular weight M_n = 400 000 g/mol. (*Reprinted with permission from ref [37] Copyright {2001} John Wiley and Sons and Copyright Clearance Center'*)

In the Figure 1.6, very low sulfonation fractions were considered to observe which fraction would

form ionic clusters. From this study Weiss and coworkers observed that at f = 0.0011, 0.0043 the

polymer behaved more closely to PS while the sulfonation fraction was increased to f = 0.017

showed a large increase in viscosity compared to the other two sulfonation fractions.[36] This study

shows that even a sulfonation fraction as low as 0.017 has an impact on the dynamics of SPS.

Through these studies it is apparent that ionic clusters control both structure and dynamics of SPS.

SAXS and STEM provide a macroscopic picture. To attain an atomistic view, classical large-scale atomistic MD simulation were carried out, which provide new insight on the atomistic length scale. One example are the studies done by Agrawal et al who studied the effect of sulfonation and cation valency on the formation of ionic clusters. S(q) vs q plot gives an idea about the structure of the polymer system. The peak in the low q region is the characteristic signature of the ionic cluster signature which can be used to extract the average distance between ionic clusters. Here the peak is observed 0.2 Å^{-1} for both SPS samples. This peak corresponds distance between ionic clusters of ~30 Å. Polystyrene does not show any features at low q range as expected since there are no ionic groups present.
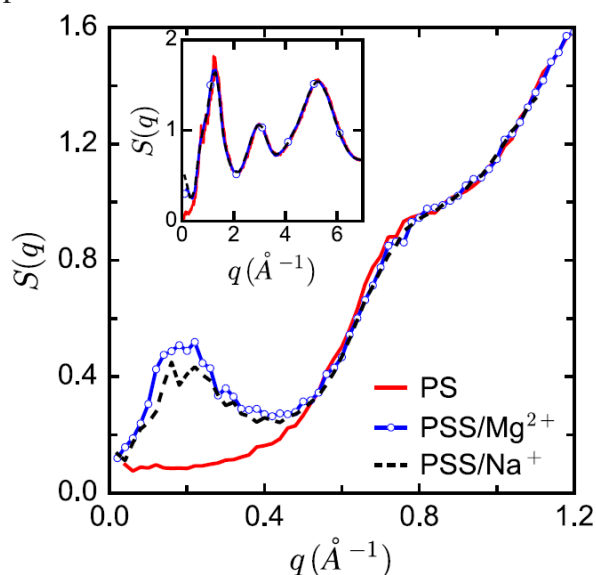
Figure 1.7: S(q) vs q for polystyrene and 5% sulfonated polystyrene with Na$^+$ and Mg^{2+} counterions[30] (R*eprinted (Figure) with permission from ref [30] Copyright (2016) by the American Physical Society)*

The dynamics of the polymer could be studied using mean square displacement (MSD) of the chains. In the following study, polystyrene, and sulfonated polystyrene with two sulfonation fractions (*f* = 0.05, 0.1) were studied.[40] With increasing sulfonation fraction, the mobility of the chains is considerably reduced. Internal dynamics of the polymer is compared using the phenyl rings with and without the sulfonated groups. The sulfonation phenyl ring motion is seen to be slower than the non-sulfonated rings.
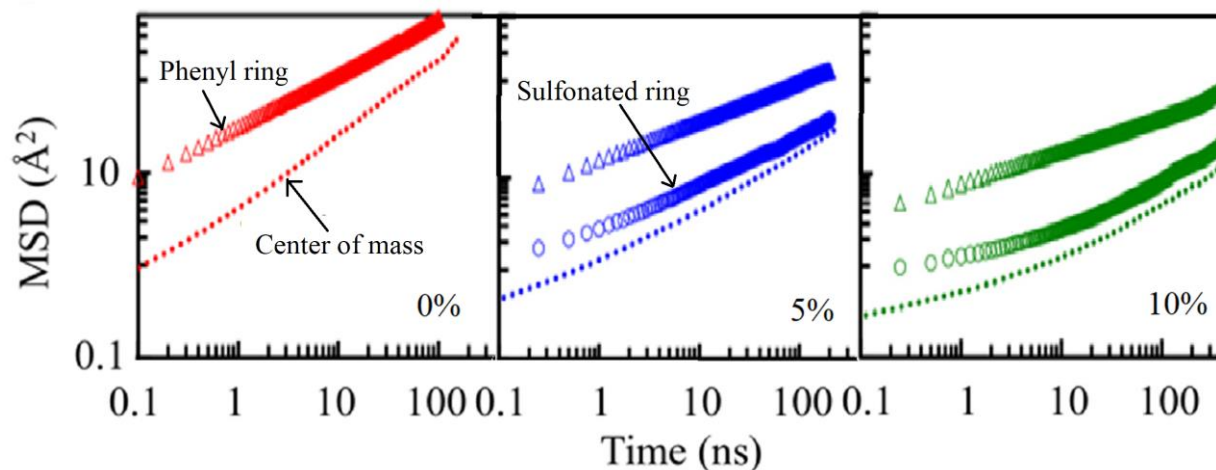
Figure 1.8: Mean square displacement versus time at 600 K of a sulfonated polystyrene melt with (a) 0%, (b) 5%, and (c) 10% sulfonation for chain length N = 40. (*Reprinted (Figure) with permission from ref[41] Copyright (2015) by the American Physical Society)*

Both experiment and computational studies point to direct correlations between the ionic clusters and structure dynamics in SPS melts. The current work aims to resolve the correlation of structure and dynamics in SPS solutions as a function of cluster properties.

1.5 References

(1) Castagna, A. M.; Wang, W.; Winey, K. I.; Runt, J. Influence of the degree of sulfonation on the structure and dynamics of sulfonated polystyrene copolymers. *Macromolecules* **2010**, *43* (24), 10498-10504.
(2) Balsara, N. P.; Newman, J. Comparing the energy content of batteries, fuels, and materials. *Journal of chemical education* **2013**, *90* (4), 446-452.
(3) Molmeret, Y.; Chabert, F.; Kissi, N. E.; Iojoiu, C.; Mercier, R.; Sanchez, J.-Y. Towards extrusion of ionomers to process fuel cell membranes. *Polymers* **2011**, *3* (3), 1126-1150.
(4) Yoshida, T.; Lai, T. C.; Kwon, G. S.; Sako, K. pH-and ion-sensitive polymers for drug delivery. *Expert opinion on drug delivery* **2013**, *10* (11), 1497-1513.
(5) Mauritz, K. A.; Moore, R. B. State of understanding of Nafion. *Chemical reviews* **2004**, *104* (10), 4535-4586.
(6) Gebel, G. Structural evolution of water swollen perfluorosulfonated ionomers from dry membrane to solution. *polymer* **2000**, *41* (15), 5829-5838.
(7) Lopez, C. G. Scaling and entanglement properties of neutral and sulfonated polystyrene. *Macromolecules* **2019**, *52* (23), 9409-9415.
(8) Chen, Q.; Huang, C.; Weiss, R.; Colby, R. H. Viscoelasticity of reversible gelation for ionomers. *Macromolecules* **2015**, *48* (4), 1221-1230.
(9) Lerman, M. J.; Lembong, J.; Muramoto, S.; Gillen, G.; Fisher, J. P. The evolution of polystyrene as a cell culture material. *Tissue Engineering Part B: Reviews* **2018**, *24* (5), 359-372.

(10) Wang, K.; Zhang, Z.; Liu, C.; Fu, Q.; Xu, W.; Huang, C.; Weiss, R.; Gong, X. Efficient polymer solar cells by lithium sulfonated polystyrene as a charge transport interfacial layer. *ACS applied materials & interfaces* **2017**, *9* (6), 5348-5357.

(11) Arslanova, A.; Sanginov, E.; Dobrovol'skii, Y. A. New composite proton-conducting membranes based on nafion and cross-linked sulfonated polystyrene. *Russian Journal of Electrochemistry* **2018**, *54*, 318-323.

(12) Pranzas, P. K.; Heinemann, A. Small-Angle Neutron Scattering. *Neutrons and Synchrotron Radiation in Engineering Materials Science: From Fundamentals to Applications* **2017**, 207-216.

(13) Wang, Y.; Wang, W.; Hong, K.; Do, C.; Chen, W.-R. Quantitative examination of a fundamental assumption in small-angle neutron scattering studies of deformed polymer melts. *Polymer* **2020**, *204*, 122698.

(14) Fumagalli, M.; Lyonnard, S.; Prajapati, G.; Berrod, Q.; Porcar, L.; Guillermo, A.; Gebel, G. Fast water diffusion and long-term polymer reorganization during Nafion membrane hydration evidenced by time-resolved small-angle neutron scattering. *The Journal of Physical Chemistry B* **2015**, *119* (23), 7068-7076.

(15) Cabry, C. P.; D'Andrea, L.; Shimizu, K.; Grillo, I.; Li, P.; Rogers, S.; Bruce, D. W.; Lopes, J. N. C.; Slattery, J. M. Exploring the bulk-phase structure of ionic liquid mixtures using small-angle neutron scattering. *Faraday Discussions* **2018**, *206*, 265-289.

(16) Castagna, A. M.; Wang, W.; Winey, K. I.; Runt, J. Structure and dynamics of zinc-neutralized sulfonated polystyrene ionomers. *Macromolecules* **2011**, *44* (8), 2791-2798.

(17) Ogg, C. Determination of Molecular Weight. *Journal of the Association of Official Analytical Chemists* **1966**, *49* (4), 744-749.

(18) Rubinsten, M. *Polymer physics*; United States of America, 2003.

(19) Rasouli, S.; Moghbeli, M. R.; Nikkhah, S. J. A comprehensive molecular dynamics study of a single polystyrene chain in a good solvent. *Current Applied Physics* **2018**, *18* (1), 68-78.

(20) Eisenberg, A.; Hird, B.; Moore, R. A new multiplet-cluster model for the morphology of random ionomers. *Macromolecules* **1990**, *23* (18), 4098-4107.

(21) Eisenberg, A. Clustering of ions in organic polymers. A theoretical approach. *Macromolecules* **1970**, *3* (2), 147-154.

(22) Bazuin, C.; Eisenberg, A. Ion containing polymers: Ionomers. ACS Publications: 1981.

(23) Rigdahl, M.; Eisenberg, A. Viscoelastic properties of sulfonated styrene ionomers. *Journal of Polymer Science: Polymer Physics Edition* **1981**, *19* (10), 1641-1654.

(24) Lundberg, R.; Phillips, R. Solution behavior of metal-sulfonate ionomers. ACS Publications, 1986.

(25) Kamel, K. S.; Schreiber, M. Asking the question again: are cation exchange resins effective for the treatment of hyperkalemia? *Nephrology Dialysis Transplantation* **2012**, *27* (12), 4294-4297.

(26) Watson, M.; Abbott, K. C.; Yuan, C. M. Damned if you do, damned if you don't: potassium binding resins in hyperkalemia. *Clinical journal of the American Society of Nephrology* **2010**, *5* (10), 1723-1726.

(27) Lepage, L.; Dufour, A.-C.; Doiron, J.; Handfield, K.; Desforges, K.; Bell, R.; Vallee, M.; Savoie, M.; Perreault, S.; Laurin, L.-P. Randomized clinical trial of sodium polystyrene sulfonate for the treatment of mild hyperkalemia in CKD. *Clinical journal of the American Society of Nephrology: CJASN* **2015**, *10* (12), 2136.

(28) Dijk, G.; Rutz, A. L.; Malliaras, G. G. Stability of PEDOT: PSS-coated gold electrodes in cell culture conditions. *Advanced Materials Technologies* **2020**, *5* (3), 1900662.

(29) Lu, B.; Yuk, H.; Lin, S.; Jian, N.; Qu, K.; Xu, J.; Zhao, X. Pure pedot: Pss hydrogels. *Nature communications* **2019**, *10* (1), 1043.

(30) Agrawal, A.; Perahia, D.; Grest, G. S. Cluster morphology-polymer dynamics correlations in sulfonated polystyrene melts: computational study. *Physical review letters* **2016**, *116* (15), 158001.

(31) Ling, G. H.; Wang, Y.; Weiss, R. Linear viscoelastic and uniaxial extensional rheology of alkali metal neutralized sulfonated oligostyrene ionomer melts. *Macromolecules* **2012**, *45* (1), 481-490.

(32) Qiao, X. Nonlinear Rheology of Lightly Sulfonated Polystyrene Ionomers. *Macromolecules* **2013**, *v. 46* (no. 6), pp. 2417-2424-2013 v.2446 no.2416. DOI: 10.1021/ma3026496 From National Agricultural Library PubAg.

(33) Lu, X.; Steckle, W.; Weiss, R. Ionic aggregation in a block copolymer ionomer. *Macromolecules* **1993**, *26* (22), 5876-5884.

(34) Chakrabarty, K.; Weiss, R.; Sehgal, A.; Seery, T. Characterization of ionomer solutions. 2. Dynamic light scattering studies on sulfonated polystyrene ionomers in a nonpolar solvent. *Macromolecules* **1998**, *31* (21), 7390-7397.

(35) Chakrabarty, K.; Seery, T.; Weiss, R. Characterization of ionomer solutions. 1. Phase behavior and gelation of sulfonated polystyrene ionomers in decalin. *Macromolecules* **1998**, *31* (21), 7385-7389.

(36) Weiss, R.; Yu, W.-C. Viscoelastic behavior of very lightly sulfonated polystyrene ionomers. *Macromolecules* **2007**, *40* (10), 3640-3643.

(37) Chan, R. W. Estimation of viscoelastic shear properties of vocal-fold tissues based on time–temperature superposition. *The Journal of the Acoustical Society of America* **2001**, *110* (3), 1548-1561.

(38) Huang, C.; Chen, Q.; Weiss, R. Nonlinear rheology of random sulfonated polystyrene ionomers: The role of the sol–gel transition. *Macromolecules* **2016**, *49* (23), 9203-9214.

(39) Zhang, Z.; Huang, C.; Weiss, R.; Chen, Q. Association energy in strongly associative polymers. *Journal of Rheology* **2017**, *61* (6), 1199-1207.

(40) Agrawal, A.; Perahia, D.; Grest, G. S. Clustering effects in ionic polymers: Molecular dynamics simulations. *Physical Review E* **2015**, *92* (2), 022601.

CHAPTER TWO

METHODOLOGY

In this study three techniques are used to probe structure and dynamics of ionic polymer in solution, these include small angle neutron scattering, neutron spin echo and classical atomistic molecular dynamic simulations These three methodologies are discussed below.

2.1 Small angle neutron scattering (SANS)

Small angle scattering is an elastic scattering technique that studies structure characterization of materials (solids, liquid and even gases). There are several small angle scattering methods. Here I use small angle neutron scattering. The technique depends on size and contrast desired.[1]
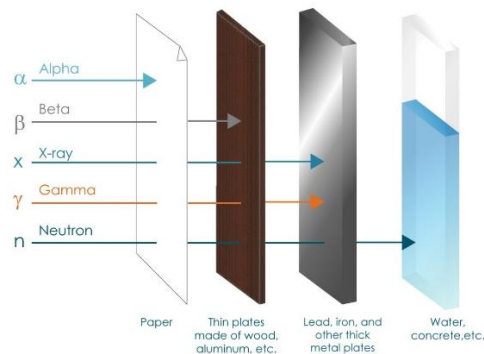
Figure 2.1: Schematic illustration of penetration of different electromagnetic radiation[2] (*Reprinted (Figure) with permission from ref [2] Copyright (2023) by the SNCSC'*)

Neutrons interact with the nuclei while X-ray interact with electrons. Scattering results due to interaction between waves and the objects that have same dimension of wavelength. Due to these factors, neutron scattering is able to differentiate between isotopes like hydrogen and deuterium while X-ray cannot. Another advantage of using neutron scattering is there is no sample damage, but it is more expensive compared to x-ray scattering.

As the incident beam hits the sample the scattering changes direction. Since elastic scattering occurs, there is no energy exchanged. Therefore, the magnitude of the incident wave vector k_i is equal to the scattered wave vector k_f. However, since the direction is changed a momentum difference is created and it is called momentum transfer vector q.
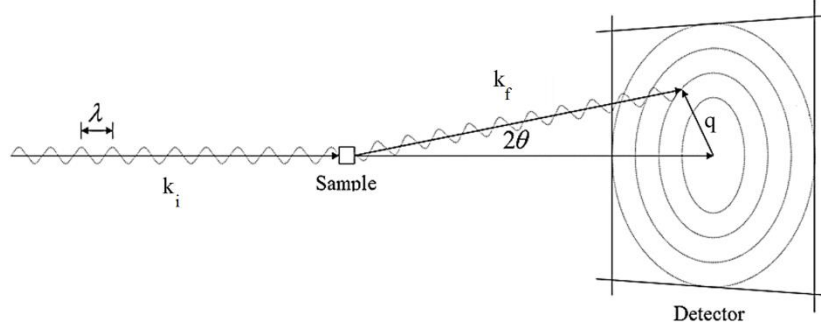
Figure 2.2: Diagram of elastic scattering which illustrates the relationship between incident and scattered wave vector (k_i, k_f), scattering angle (θ), wavelength (λ) and momentum transfer vector (q).

In elastic scattering energy or momentum is not exchanged. Thus, change of energy is zero and wave vectors are unchanged upon scattering.

$$|\mathbf{k_i}| = |\mathbf{k_f}| = \frac{2\pi}{\lambda} \qquad (3.1)$$

Momentum transfer vector q is the difference between incident and final wave vector. q depends on scattering angle θ and corresponding wavelength λ is,

$$\mathbf{q} = \mathbf{k}_i - \mathbf{k}_f \qquad (3.2)$$

$$q = \frac{4\pi sin\theta}{\lambda} \qquad (3.3)$$

For constructive interference to occur scattered neutrons should follow the Braggs equation.

$$2d\ sin\theta = n\lambda \qquad (3.4)$$

Here d is the spacing between two scattering points and n is an integer.

In order to understand the relationship between q and d, equation 3.3 and 3.4 can be used. As shown below we can see that q and d are inversely proportional to each other. Therefore, large dimensions are captured at low q while small dimensions are captured at high q.

$$q = \frac{2\pi n}{d} \qquad (3.5)$$

Scattering length density is a characteristic of the nucleus, which gives an idea about the interaction between the nucleus and neutrons. Normalized sum of scattering length (b) of all the elements in the scattering object is shown in the equation 3.6. Where b_i is the scattering length of each element, ρ is the density of the scattering object, and M_w is the molecular weight of the object.

$$b = \frac{\rho N_A}{M_W} \sum_0^i b_i \qquad (3.6)$$

In SANS absolute intensity I(q) is measures as a function of q,

$$I(q) = \left[\frac{N}{V}\right] V_p^2 \, \Delta\rho P(q) S(q) \quad (3.7)$$

Here, N/V is the number density, V_p is particle volume, $\Delta\rho$ is contrast factor, $P(q)$ is form factor of the object and $S(q)$ is the structure factor.

The contrast factor is the scattering length density difference between two objects. The scattering length density is given by,

$$\Delta\rho^2 = (\rho_A - \rho_B)^2 \qquad (3.8)$$

Here scattering length density is the strength of the scattering (b)

The structure factor $S(q)$ depends on correlation of the objects or atoms.

$$S(q) = 1 + \int d\boldsymbol{r}.\{g(r) - 1\}\rho.\,e^{-iq.r} \qquad (3.9)$$

The structure factor $S(q)$ is related to the Fourier transform of the pair correlation function $g(r)$ which is given by,

$$g(r) = \frac{V}{4\pi r^2 N\rho}\left\langle \sum_i \sum_{j\neq i} \delta\left(r - r_{ij}\right)\right\rangle \qquad (3.10)$$

In dilute solutions there is no correlation between objects thus $g(r) = 1$ and hence $S(q) = 1$.

The form factor $P(q)$ determines the shape of the object. Since SANS is performed in q space, scattering pattern alone does not give direct information of the scattered object. To extract real space information the scattering data should be fitted in to a model. Few examples of form factors are shown in the table 3.1.
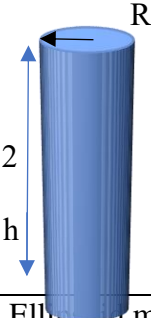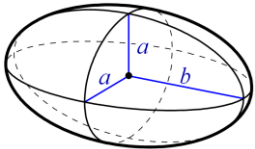
Form factor geometry	Form factor
Spherical[3]	$$P(q) = \frac{[\sin(qR) - qR\cos(qR)}{qR^3}$$ R=Radius of sphere
Cylindrical[4]	$$P(q) = \frac{scale}{V_{cyl}} \int_o^{\pi/2} f^2(q,\alpha)\sin\alpha d\alpha$$ $$f(q,\alpha) = 2(\rho_{cyl} - \rho_{solv})V_{cyl}j_0(qh\cos\alpha)\frac{J_1(qr\sin\alpha)}{(qr\sin\alpha)}$$ h=Length of the cylinder r = Radius of the cylinder α = Orientation of the cylinder J_1 = first order Bessel function
Ellipsoid model[5]	$$P(q) = \frac{scale}{V} \frac{(3(\Delta\rho)V\sin[qr(R_a,R_b,\alpha)] - qr\cos[qr(R_a,R_b,\alpha)])^2}{[qr(R_a,R_b,\alpha)]^3}$$ R_a = Minimum radius R_b = Maximum radius α = angle
Beaucage[6]	$$I(q) = \sum_{i=0}^{N} G_i \exp\left(-\frac{q^2 R_{g,i}^2}{3}\right) + B_i[\text{erf}\left(\frac{qR_{g,i}}{\sqrt{6}}\right)]^{3P_i}/q^{P_i}$$ G_i = Guinier scaling factor $R_{g,i}$ = Guinier radius Q = Scattering vector B_i = G/R^2_g P = Constant

Table 2.1: Different form factors used in SANS analysis[3-6]

As the complexity of the shape of the aggregate increases, higher number of variables are required to obtain the form factor.

2.2 Neutron Spin Echo (NSE)

Neutron spin echo is a complimentary technique to SANS that measures the dynamics of the system using neutron scattering. This method measures the velocity change of neutrons to infer the energy transfer. NSE techniques gives access to the largest length scales and longest time scales and has the highest resolution.

NSE measures the intermediate scattering function S(q,t) which gives relative motion of the polymer. The fundamental idea of this method is to follow the energy change of the neutrons in the scattering process.[7]

Due to the magnetic field applied perpendicular to the beam the spin of each neutron will turn 90 degrees and initiates a Larmor precession. The Larmor precession angle is given by.

$$\emptyset = \gamma H l / v \quad (3.11)$$

Where Larmor constant $\gamma = 2.916$ kHz/Oe, H is the average strength of magnetic field of length l.

Scattering off the sample results in an energy change of the neutron,

$$\hbar\omega = \frac{mv'^2}{2} - \frac{mv^2}{2} \quad (3.12)$$

Here m is the neutron mass and v' is the final neutron velocity. Since the relative velocity change is assumed to be small the momentum transfer Q is

$$\hbar Q = mv' - mv \quad (3.13)$$

Lamor frequency after the sample is changed to ϕ' in the second field region,

$$-\phi + \phi' = \frac{\gamma H l}{v} - \frac{\gamma H' l'}{v'} \quad (3.14)$$

If $Hl = H'l'$

$$-\phi + \phi' = \gamma H l \left(\frac{1}{v} - \frac{1}{v'}\right) \approx \frac{\gamma H'l'}{mv^3} \hbar\omega \quad (3.15)$$

NSE measures the polarization,

$$P_x = \langle \cos\left(-\phi + \phi'\right)\rangle = \langle \cos \frac{\gamma H'l'}{mv^3} \hbar\omega \rangle \quad (3.16)$$

The average describes the probability distribution of ω. This can be expressed by S(Q, ω) and with the notation $t = \frac{\gamma \hbar H'l'}{mv^3}$,

$$P = \frac{\int S(Q,\omega) \cos(\omega t)d\omega}{\int S(Q,\omega)d\omega} \quad (3.17)$$

The nominator of the above equation is the cosine Fourier transform of S(Q, ω), which is the real part of the time dependent correlation function. The denominator is the static structure factor S(Q). The direct result observed by NSE is

19

$$P = s(Q, t) = \frac{ReI(Q,t)}{S(Q)} \qquad (3.18)$$

2.3 Molecular dynamics simulations

To understand the structure and dynamics of the system at the atomic scale a method other than SANS is required. One such approach is atomistic MD simulations in which one follows the motion of all the atoms in the system.

In classical molecular dynamic simulations Newtons law of motion,

$$F_i = m_i a_i \qquad (3.19)$$

are solved for a set of interacting particles. Here F_i is the force acting on particles i which has a mass m_i the mass and acceleration a_i. Force can be expressed as gradient of potential energy.

$$F_i = \frac{\partial U_i}{\partial r} \qquad (3.20)$$

where U_i is the potential energy. To integrate Newton's equations, time is discretized in time steps of size Δt. The position and velocity of each particle of the system are updated each time step using Velocity-Verlet algorithm,

$$r(t + \delta t) = 2r(t) - r(t - \delta t) + \delta t^2 a(t) \qquad (3.21)$$

$$v(t + \delta t) = v(t) + \frac{1}{2}\delta t[a(t) + a(t + \delta t)] \qquad (3.22)$$
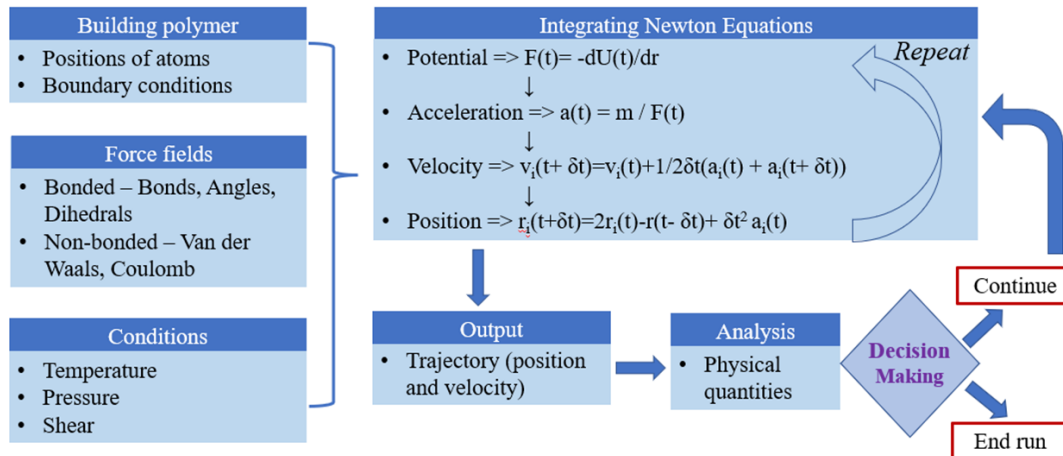
Figure 2.3: Flow chart of classical MD simulations.

In order to understand MD simulations better a flow chart is illustrated in Figure 2.3. The first step to build a system is to assign the position, bond, angles and velocities. Next the forces on

each atom are calculated and then the equations of motion are solved at a given time Δt by an integrator to generate the new position and velocities of each atom. The last steps repeat in a loop until the system reaches the desired state.

2.4 Force fields

The proposed study requires a proper choice of potentials to describe the interactions between the atoms. For this study, the Optimized Potentials for Liquid Simulations – all atom (OPLS/AA)[8, 9] force fields are used. The mathematical expressions and constants are essential to reproduce the geometry and properties of the structures.

$$U_{OPLS} = U_{bonded} + U_{nonbonded} \qquad (3.23)$$

The bonded interactions are given by bond, angle and dihedral potentials and are mathematically defined by the following equations.

$$U_{bonded} = U_{bond} + U_{angle} + U_{torsion} \qquad (3.24)$$

$$U_{bond}(r_{ij}) = k_r(r_{ij} - r_0)^2 \qquad (3.25)$$

where r_{ij} is the distance between atoms i and j, r_0 is their equilibrium separations and k_r is strength of the interaction. Similarly, the three-body angle term are also described as harmonic potentials of the form,

$$U_{angle}(\theta_{ijk}) = k_\theta(\theta_{ijk} - \theta_0)^2 \qquad (3.26)$$

where θ_{ijk} is the angle between the vectors r_{ji} and r_{jk}, and θ_0 the equilibrium value and k_θ is the force constant. The torsional component of the OPLS potential is

$$U_{torsion}(\phi_{ijkl}) = \sum_{n=i}^{n=l} \frac{k_n}{2} [1 - (1-1)^n \cos(n\phi)] \qquad (3.27)$$

where, ϕ is the dihedral angle and k_n are the interaction energies.

The non-bonded interactions equations are given by the sum of a short-range Lennard-Jones potential and a long-range Coulomb potential,

$$U_{non-bonded} = U_{Lj} + U_{Coul} = 4\varepsilon_{ij}\left[\left[\frac{\sigma_{ij}}{r_{ij}}\right]^{12} - \left[\frac{\sigma_{ij}}{r_{ij}}\right]^{6}\right] + \frac{q_i q_j}{4\pi\varepsilon_0 r_{ij}} \quad (3.28)$$

Here, r_{ij} is the distance between atoms i and j, ε_{ij} is the Lennard-jones energy, σ_{ij} is the distance where inter particle potential is zero, q_i,q_j are partial charges for atoms i and j, ε_0 is the permeability of free space.[10]
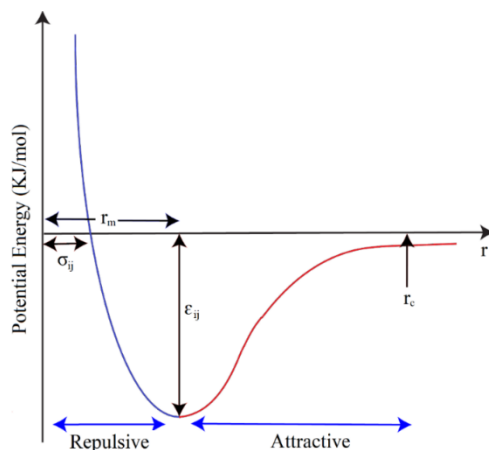
Figure 2.4: Illustration of Lennard-jones potential. σ_{ij} is the distance where inter particle potential is zero for atom, ε_{ij} is the well depth, r_m is distance where potential reaches its minimum and r_c is the cut off radius.

Lennard-Jones potential gives the interaction potential between two atoms as a function of the distance between them. At close distance, the repulsive component of the force dominates. As the distance between the particles increases, the repulsive force decreases. The attractive and repulsive forces are balanced at r_m where the potential energy is minimum. For $r > r_m$ the attraction decreases and goes to zero as r goes to infinity.

The most expensive part of a MD simulation is the calculation of the nonbonded terms in the potential energy function, electrostatic and van der Waals forces. The electrostatic interactions decay slowly and simply cutting off the Coulomb interaction is not adequate. Particle-particle particle mesh (PPPM)[11] with a real space cut-off of 1.2 nm was used to calculate the electrostatic interactions.

From the simulation, it is possible to calculate several quantities to obtain quantitative

details of the systems. These measurements include radius of gyration R_g, mean square displacement of the chains and the static and dynamic structure factors $S(q)$ and $S(q,t)$. As shown in Figure 2.3 as part of the decision-making process we use the analyzed data in order to continue the run or to end.

- Pair correlation function

$$g(r) = \frac{V}{4\pi r^2 N\rho} \left| \left\langle \sum_i \sum_{j\neq i} \delta(r - r_{ij}) \right\rangle \right| \qquad (3.10)$$

- Static scattering function

$$S(q) = \sum_{i,j=1}^{N} b_i b_j \exp\left(iq.(r_i - r_j) \right) \qquad (3.29)$$

- Properties such as Density, Pressure

- Polymer specific properties (Cluster analysis, crystallinity analysis)

- Radius of gyration

$$R_g^2 = \sum_{i=1}^{N} m_i (r_i - r_{COM})^2 / \sum_{i=1}^{N} m_i \qquad (3.30)$$

- Mean square displacement → chains move at least their own size

$$\begin{aligned} MSD(t) &= \langle \Delta r_i(t)^2 \rangle \\ &= \langle (r_i(t) - r_i(0))^2 \rangle \end{aligned} \qquad (3.31)$$

- Dynamic scattering function → longer time than the slowest motion in the system

$$\begin{aligned} S(q,t) = \sum_{i,j=1}^{N} b_i\, b_j \langle exp[iq.(r_i(t) \\ - r_j(0)] \rangle \end{aligned} \qquad (3.32)$$

These quantities could be used to determine whether to continue or terminate the simulation.

There are many methods that could be used experimentally and computationally to probe the structure and dynamics of ionic polymers. The current study uses neutron scattering and classical molecular dynamics simulations.

2.5 References

(1) Hammouda, B. Probing nanoscale structures-the sans toolbox. *National Institute of Standards and Technology* **2008**, 1-717.

(2) Kovach, V.; Iatsyshyn, A.; Pylypchuk, I.; Gurkovskyi, V.; Romanenko, Y. Analysis of Existing Types and Protection Methods Against Neutron Radiation from Different Sources. In *Systems, Decision and Control in Energy IV: Volume II. Nuclear and Environmental Safety*, Springer, 2023; pp 77-89.

(3) Guinier, A.; Fournet, G.; Walker, C. B.; Vineyard, G. H. Small-angle scattering of X-rays. American Institute of Physics: 1956.

(4) Roe, R.-J. Methods of X-ray and neutron scattering in polymer science. *(No Title)* **2000**.

(5) Higgins, J.; Benoit, H. Polymers and Neutron Scattering Clarendon. Oxford: 1994.

(6) Beaucage, G. Small-angle scattering from polymeric mass fractals of arbitrary mass-fractal dimension. *Journal of applied crystallography* **1996**, *29* (2), 134-146.

(7) Mezei, F.; Pappas, C.; Gutberlet, T. *Neutron spin echo spectroscopy: Basics, trends and applications*; Springer Science & Business Media, 2002.

(8) Jorgensen, W. L.; Maxwell, D. S.; Tirado-Rives, J. Development and testing of the OPLS all-atom force field on conformational energetics and properties of organic liquids. *Journal of the American Chemical Society* **1996**, *118* (45), 11225-11236.

(9) Jorgensen, W. L.; Madura, J. D.; Swenson, C. J. Optimized intermolecular potential functions for liquid hydrocarbons. *Journal of the American Chemical Society* **1984**, *106* (22), 6638-6646.

(10) Allen, M. P.; Tildesley, D. J. *Computer simulation of liquids*; Oxford university press, 2017.

(11) Isele-Holder, R. E.; Mitchell, W.; Ismail, A. E. Development and application of a particle-particle particle-mesh Ewald method for dispersion interactions. *The Journal of chemical physics* **2012**, *137* (17).

CHAPTER THREE

CLUSTERING EFFECTS ON THE STRUCTURE OF IONOMER SOLUTIONS:
A COMBINED SANS AND SIMULATIONS STUDY

3.1 Abstract

Ionic assemblies, or clusters, determine the structure and dynamics of ionizable polymers and enable their many applications. Fundamental to attaining well-defined materials is controlling the balance between van der Waals interactions that govern the backbone behavior and the forces that drive the formation of ionic clusters. Here, using small angle neutron scattering and fully atomistic molecular dynamics simulations, the structure of a model ionomer, sulfonated polystyrene in toluene solutions, was investigated as the cluster cohesion was tweaked by the addition of ethanol. The static structure factor was measured by both techniques and correlated with the size of the ionic clusters as the polymer concentration was varied. The conjunction of SANS results and molecular insight from MD simulations enabled the determination of the structure in these inhomogeneous networks on multiple length scales. We find that across the entire concentration range studied, a network driven by the formation of ionic clusters was formed, where the size of the clusters drives the inhomogeneity of these systems. Tweaking the ionic clusters through the addition of ethanol impacts the packing of the sulfonated groups, their shape, and their size distribution, which, in turn, affects the structure of these networks.

3.2 Introduction

Ionizable polymers are used in a wide range of applications, particularly lightweight clean energy devices,[1, 2] and responsive materials for biotechnology.[3, 4] These polymers consist of ionizable groups that assemble into clusters,[5-7] forming distinctive hydrophilic and hydrophobic domains in

25

melts and solutions, where the ionic assemblies control transport pathways in membranes.[8-11] In the presence of solvents and electric fields that are in the core of the many applications of these polymers, the domains adapt, affecting the structure and consequently the functionality and stability of the materials.[8, 12, 13] Controlling the structure and mobility of ionizable polymers is fundamental to their current and potential applications. However, the correlation between the characteristics of the ionic clusters and the structure of ionomers remains a critical open question. One roadblock to resolving the interrelation between clustering and the structures formed on multiple length scales is the formation of highly inhomogeneous networks in solutions, whose structure is only partially accessible by traditional scattering techniques that captures well defined structures in solution. The current study couples small angle neutron scattering (SANS) with real space exascale large scale molecular dynamics (MD) simulations results, that together is able to provide direct atomistic level to mesoscopic insight into these networks.

Specifically, we probe the correlation between the properties of the ionic clusters and the structure of a model ionomer in solutions. Since much of the structuring of this class of polymers into viable materials occurs as solvent evaporates during their processing from molecules to membranes, understanding the factors that control solution structure provides vital insight into this compounded process. We find that small changes in the immediate electrostatic environment of the ionic clusters affect the morphology and the structure of these polymers in solutions.

This study uses sulfonated polystyrene (SPS) as the model polymer[14-19] and focuses on polymers in the ionomer regime where well-defined ionic clusters are formed.[20, 21] SANS studies have been carried out on solutions of SPS in toluene and toluene/ethanol. Atactic polystyrene is an amorphous polymer whose synthetic routes through anionic polymerization result in a narrow

26

molecular weight distribution, hence has been used in numerous studies, yielding a broad knowledge base that underline the current study.[21-27]

The structure, and mechanical response of SPS has been extensively studied,[14, 21, 23, 24, 28-31] pointing to direct correlation between clustering and rheology of the melts. Pioneering insight attained by Weiss and coworkers demonstrate a correlation between the clustering, structure and rheological characteristics of SPS melts.[27, 32-34] They have shown that the cluster formation of short oligomers of approximately ~ 4kg/mol, constrains the polymer motion, resulting in rheological response akin to those of long entangled polymers.[32] Swelling the polymer with small amounts of polar solvents perturbs the clusters as evidenced by the decreasing intensity of the ionic-peak in small angle X-ray measurements.[27] Further, they have shown that suppressing the formation of clustering, the rheological characteristics become similar to that of polystyrene with the same molecular weight. Realizing the impact of clustering on the dynamics of ionomers, Castagna et al. [22, 23] provided the first direct observation of clusters in SPS through the use of microscopy. They reported ionic clusters of ~ 2nm in diameter independent of the degrees of sulfonation and neutralization. Computational studies have provided direct molecular insight into the factors that control cluster formation and stability. Agrawal et al.[21] have shown that with increasing dielectric constant of the SPS, the cluster size decreases, and their shape shifts from ladder-like structures toward more spherical objects. Mohottalalage et al.[28] have shown that distribution of ionic groups along the polymer chain backbone affects the shape, size and packing of ionizable groups within the clusters. They have demonstrated that the number of discrete (unique) chains that are tethered to any individual cluster depends on the distribution of the ionizable blocks along the polymer backbone. The formation of clusters in solution is a more convoluted process, affected by additional distinct interactions of the backbone and ionic assemblies with the solvents. Examples include studies by

Weiss and coworkers who showed that in decalin, a cyclic aliphatic solvent, aggregates are formed at distinctively low sulfonation levels ($f = 0.02$).[35] Lantman et al. observed that for SPS with $f = 0.04$ in THF, the dimension of individual ionomer chains remain unchanged while forming multi chain aggregates.[36] Numerous studies pointed to effects of the counterion in both melt and solutions.[23, 25, 37, 38]

With molecular insight of large-scale atomistic MD studies coupled with nm length scale structure attained by SANS, the current study probes the solution structure of SPS on multiple length scales. MD studies were carried out on SPS with Na^+ as counterions. The static structure factor $S(q)$ calculated for the computational solutions exhibit remarkable correlation with the SANS results for SPS in its acid form. Following the fundamentals of the SANS experiments and MD simulations, the results attained from both techniques including concentration and temperature effects will be introduced. We will then discuss the impact of the addition of ethanol, a polar solvent, followed by our conclusions.

3.3 Methodology

Sample Preparation Sulfonated polystyrene with a molecular weight of the backbone of 11 kg/mol with dispersity of 1.04 was purchased from Polymer Source Inc. ™ The polymer was synthesized by anionic polymerization[39] and randomly sulfonated with sulfonation fractions of $f = 0.03$ and 0.09 of the available sites. Deuterated toluene (99.5%) and ethanol (99%) were purchased from Cambridge Isotope Laboratories, Inc., USA. The concentration was varied from 0.25 to 10 Wt% polymer in d_8-toluene and d_6-ethanol with varying ethanol fractions $f_{EtOH} = 0.00 - 0.05$. All solutions exhibit liquid like consistency and were easily transferable to the neutron cells. They remain fluid over six months, the time that elapsed between consecutive SANS measurements.

SANS Experiments SANS measurements were carried out on the General-Purpose Small Angle Neutron Scattering (GP-SANS) at the High Flux Isotope Reactor, Oak Ridge National Laboratory.[40, 41] Data were collected at three detector-to-sample distances of 1.1m, 4.8m and 19.2m to capture the momentum transfer $q = 0.005 - 0.7$ Å^{-1} using a wavelength of $\lambda = 4.75$ Å, with $\Delta\lambda/\lambda$ of 13%, where $q = 4\pi sin(\theta)/\lambda$. $I(q)$ was recorded for the solutions, empty cell, standard, and all solvent combinations of d_8-toluene and d_6-ethanol. Transmission of every sample was recorded at temperature range measured. SANS data were recorded on a He^3 LPSD (Linear position-sensitive detector), and data were converted using SPICE and integrated into one dimensional scattering patterns in Mantid available at GP-SANS instrument.[40, 41] All data were normalized by a pre-calibrated standard to obtain absolute intensity and is multiplied by the number of available neutrons per solid angle and are presented in units of cm^{-1}. This standard procedure in SANS of polymeric solutions in incorporated in the reduction software. Scattering from the solvents and the empty cell were subtracted from the data. The incoherent scattering was evaluated at high q for each of the samples and subtracted as a constant background. Further, solvents with toluene-d-toluene mixtures were run separately, with the H/D ratio to match the potential incoherent effect of the protons of the polymers and hardly any changes were observed. Thus, the incoherent scattering was treated as background following the common practice for reducing data of a 2 component polymer solutions. Further details of the data reduction are available through the instrument site. [42]

SANS Data Analysis Data analysis was done using a unified model that asserts that the scattering from soft materials can be analyzed in terms of exponential functions, each capturing features on a given length scale. The analysis was done using SasView.[43] As a function of increasing *q,* the

patterns exhibit distinctive network features in the low q regime, an interionic correlation, very broad feature, manifested as a "knee" in the pattern at intermediate q, followed by the signature of the solvated chains. The high inhomogeneity of the structural features on all length scales precludes many of the traditional pathways for data analysis. To overcome this challenge, the current study uses a feedback loop between SANS analysis and MD simulations where SANS covers a q range of 0.005 - 0.7 Å^{-1} and MD simulations, defined by the simulation box size, capture $q > 0.02$ Å^{-1}.

The initial analysis of the SANS patterns was done through determination of the slopes of the curves in a Porod Representation log I(q) as a function of log q of the data, in the low and the intermediate q regimes. The low q regime was evaluated by Guinier approximation. This approximation was done with the assumption that the large fluctuations would level off at larger dimensions that are outside the range captured by the instrument, an assumption that is often done for evaluating formation of instantaneous networks and concentration fluctuations. A simple Guinier-Porod analysis was unable to capture the intermediate q range where the inter cluster correlation signature is manifested.

As the system consists of associative polymers, the SANS data were then fit to the Correlation Model,[44] a highly intuitive approach that has been applied initially to understand the association of PEO in water.[45-48] This model was somewhat successful in the low sulfonation regime for dilute solutions. Though this model has been effective in fitting complex fluids that are locally segregated but homogenous over larger length scales, [45-48] it did not capture the multiple length scales in our solutions.

The SANS patterns were therefore analyzed using the concepts of a unified model, developed by

Beaucage.[49-51] The model asserts that the scattering from amorphous sytems can be captured by superposition of power laws or fractals scattering functions, that together capture the different length scales that contribute to the scattering, each characterized by an exponenet,

$$I(q) = \sum_{i=1}^{2}(G_i \exp\left(\frac{-q^2 R_{g,i}^2}{3}\right)$$

$$+B_i \exp\left(\frac{-q^2 R_{g,i+1}^2}{3}\right) \{[erf\left(\frac{qR_{g,i}}{\sqrt{6}}\right)^3/q]\}^{P_i}) \quad (2)$$

P_i is the power-law exponenet that chrateristic of the of the scatterer shape (or conformation for polyemr solusions). G_i is the classical Guinier prefactor, and B_i is a prefactor specific to the type of major scatterer in a given q regime.[52]

The current study employs a two-level summation where $R_{g,3} = 0$. This model contains eight parameters, which is a large number, but offers a path to bridge between length scales, if only qualitative. B_i and G_i are treated as fitting parameters only. Therefore, the crossover between different q regimes is not affected by the specific mathematical expressions of B_i presented in the original model or in a modified one that incorporates form factors of specific objects in a different way from the original generalized fractal formalism.[49, 50]

Here we assume a two-level model, where in the low q regime a network of relatively large highly swollen domains is formed. Within these domains, the chains are confined by ionic clusters,[30] with a high fraction of the polymer solvated in toluene, assuming close to a Gaussian configuration. Based on the MD simulations, the q range in which the inter ionic cluster correlation is manifested, the broad distribution of cluster size and shape smear the signature in the pattern.

The data were first analyzed in the low q regime, using traditional Guinier analysis that allowed us to extract a characteristic length scale for the network R_{g1} that together with the slope of the

data, was used as starting values in the fitting. Guidance for R_{g2} and P_2, were obtained from MD simulations. Eq. 2 presents the model conceptually. The fitting was carried out using a SasView module[43] where a background (Bk) term is added, which accounts for residual incoherent scattering. This term is slightly dependent on concentration as shown in Tables A3.1 and A3.2. These values, however, are negligible compared to the overall I(q) values. With the broad length scale and significant differences in intensity between $I(q) \to 0$ and the rest of the range, G_i serves as a scaling factor because the scattering length density differences between the swollen polymer is not a unique value. Along the same lines, since there are no well-defined scattering shapes, B_i serves as a second scaling factor. In the original derivation of the unified model, B_i, was derived for specific form factors and was later modified.[51] Herein however B_i is merely used as a bridging factor, and arbitrary fitting parameter to capture the boundary between network and chain characteristics. Changing B_i slightly changes the width of the plateau observed at the intermediary q range but does not lead to any significant differences in the network characteristics or R_g of the chains. The SasView fitting routine allows incorporation of a scaling factor and a background term, that together allows scaling to the broad disparity of $I(q)$ at various q ranges. Here as the $I(q)$ was converted to absolute scattering no scaling factor was needed.

The changes in the inter-ionic correlation signature are followed through tracking the shift in the "knee" manifested between the chain conformation and the network characteristics. Quantitative insight on this region was attained from the analysis of the MD simulations. The parameters extracted at low q from a simple Guinier analysis, correlation model (where it fits) and the unified model were only slightly dependent on the model chosen.

Computational Details Sulfonated polystyrene, toluene and ethanol were built using the polymer builder in BIOVIA[TM] Materials Studio. The systems consist of 148 unique, atatic sulfonated

polystyrene chains with sulfonation fraction $f = 0.03$, and 0.09, each with a total molecular weight of ~11 kg/mol with 106 monomer per chain with Na^+ as a counterion and solvents. The all atoms optimized potential for liquid simulations (OPLS-AA) force fields developed by Jorgensen et al.[53, 54] was used to model the systems. This potential includes bonded and non-bonded terms. The bonded potential is sum of intermolecular bond, angle, and dihedral interactions. The non-bonded interactions are described by Lennard-Jones potential with an attractive r^{-6} and repulsive r^{-12} terms and a long-range Coulomb interaction.

Simulations were initially carried out using LAMMPS.[55] Following the construction of the systems, production runs were carried out using GROMACS.[56-58] Using LAMMPS, the Newton equations of motions were integrated using a velocity-Verlet algorithm with a time step of *1 fs*.[59] The Lennard-Jones interactions are truncated at 1.2 nm. The Coulomb interactions are treated with long-range particle-particle particle-mesh (PPPM) algorithm[60] with a real space cutoff of 1.2 nm and a precision of $5x10^{-4}$. Periodic boundary conditions were used for all simulations.

The solvents were added after the polymer system was run for 100 ns at 300K in an implicit good solvent. The solutions consist of toluene and toluene/ethanol mixtures with 10 wt% polymer. Each system contains between 2.4 - 2.5 million atoms. Each system was first run at constant pressure of 1 atm using the Nosé - Hoover thermostat and barostat[61, 62] for 10 ns to obtain the correct density. The final length of the cubic cell is $L \sim 31$ nm which is significantly larger than the size of a polymer chain. To allow the chains to locally equilibrate the dielectric constant ε was increased from 1 to 30 to reduce the residual electrostatic screening between ionic groups. The solution systems were run for 30 ns at constant volume after which the dielectric constant was reset to 1. The LAMMPS data were then converted to GROMACS[56-58] to enhanced efficiency. Conversion is carried out using a combination of ParmEd and InterMol tools.[63] The electrostatics were treated

using particle mesh Ewald[64] (PME) algorithm and Fourier grid spacing of 0.12 nm. All harmonic bonds involving hydrogen atoms were replaced with constraints using the LINCS algorithm.[65] The temperature was maintained using the Bussi-Parrinello thermostat (V-rescale)[66] with a time constant of 0.1 ps. The simulations were carried out using 2 fs time step. MDAnalysis[67] toolkit was used to perform equilibrium analysis. Each system was run in GROMACS at a constant volume at $T = 300$ K for 600-800 ns. Time $t = 0$ corresponds to the beginning of the run in GROMACS after the dielectric constant was reset to 1. The system temperature was increased to 328 K and ran at constant pressure for 10 ns and then ran at constant volume for 400 ns.

Following the preparation of the solution, the static structure factor and cluster characteristics were extracted. The static structure factor $S(q)$ is computationally given by

$$S(q) = \left| \sum_i b_i e^{iq \cdot r_i} \right|^2 / \sum_i b_i^2 \qquad (3)$$

where b_i is the scattering length for neutrons and r_i is the position of atom i. The scattering length density of the solvent is set to zero. Due to the periodic boundary conditions, the wavevectors q are limited to $q = 2\pi/L$ (n_x, n_y, n_z), where L is the length of the simulation cell and n_x, n_y, and n_z are integers. The calculated $S(q)$ access the q range from $q = 2\pi/L \sim 0.02$ Å^{-1} to 0.7 Å^{-1}. The large-scale features detected by SANS at lower q are not accessible to the simulations even for these multi-million atom simulations.

The ionic groups form distinct clusters. The average cluster size was determined and followed as a function of time. Sulfur atoms residing within 6 Å radius of each other are defined to be in the the same cluster.

3.4 Results

A. Concentration Effects Solutions with 0.25 Wt.% to 10.0 Wt% of polymer in toluene, were probed by SANS. Representative patterns, at 303K are shown in Figure 3.1 a and b, and the corresponding Kratky plots are shown in Figure A3.1. All patterns exhibit an upturn at low q values with a slope that varies with sulfonation levels and concentrations. For low sulfonation fractions, $f = 0.03$, the slope changes between 3.2 to 3.8 with increasing concentration from 0.25 Wt% to 10 Wt%. These low q signatures arise from large length scale structures, attributed to bridging through clustering, that is rather surprising at these low sulfonation levels and relatively low concentrations. It is however consistent with the rheological response of SPS in solutions.[35] As the sulfonation fraction increases from $f = 0.03$ to 0.09 the onset of the low q upturn shifts to lower q values.
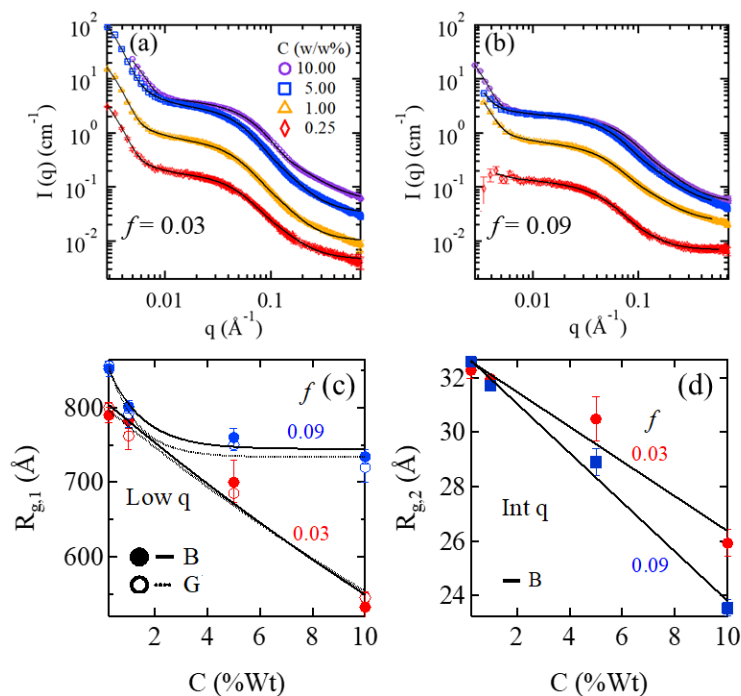
Figure 3.1: SANS patterns for SPS in toluene as a function of the polymer concentration (a) $f = 0.03$ and (b) $f = 0.09$. Symbols correspond to the experimental data and the solid lines to the fitting to Beaucage model. $R_{g,i}$ of chains in toluene as a function of the concentration of polymer, obtained from (c) Dimensions extracted from Beaucage marked by B, and Guinier, marked by G, models at low q regime ($q < 0.004$ Å⁻¹) and (d) dimensions extracted from the Beaucage model at intermediate q regime ($0.02 < q < 0.2$ Å⁻¹).

We attribute the low q signature to inhomogeneities in polymer concentration coupled with network formation, both driven by ionic assemblies. In the intermediate q range, the experimental scattering intensity $I(q)$ decays as power law $q^{-\alpha}$ with $\alpha \sim 1.8\text{-}2$. Since toluene is a good solvent for PS $\alpha \sim 2$ suggests that the chains assume Gaussian confirmation away from the ionic clusters. In contrast to the rest of the solutions, 0.25Wt% does not exhibit low q signature. This reproducible pattern is attributed to a different assembly mode where a fraction of the polymer forms smaller aggregates that do not contribute to the large-scale structures. The patterns in a Kratky format are shown in the appendix to demonstrate the crossover between the different q regions.

The dimensions extracted from the Beaucage model $R_{g,1}$ and $R_{g,2}$ is plotted in Figure 3.1 c and 1d as a function of concentration. There values, extracted from the data analysis are only slightly affected (less than 5%) depending on the fitting constants (presented in Table SI1) where the values of the R_{g1} and R_{g2} are within 5% from the values extracted directly from the Guinier analysis as shown in Figure 3.1c and MD simulations, and the P_i are similar to the experimentally measured slopes. This analysis yields two characteristic dimensions on the order of 520 Å – 820 Å and ~ 23 Å - 33 Å. The larger dimension $R_{g,1}$ is significantly larger than R_g of individual SPS molecules. It captures the length scale of the network formed by bridging of polymer by the ionic groups and points to the network structure formed in these solutions. Both $R_{g,i}$ values decrease with increasing where more sulfonated groups are present in solution, enhancing the number and size of ionic assemblies, which impacts the confinement of individual chains and affects the packing of the chains.[28] Though $R_{g,2}$ decreases as the concentration increases for both sulfonation fractions the effect is significantly stronger in solutions of $f = 0.09$.
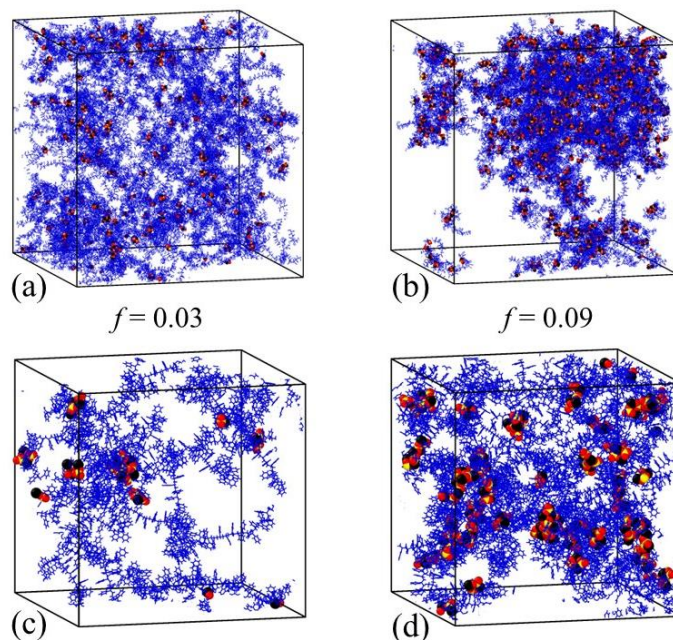
Figure 3.2: Visualization of computed solutions of 10 wt% SPS in toluene at T = 300 K for (a) f = 0.03 (310^3 Å^3), (b) f = 0.09 (307^3 Å^3) and zoomed-in images of (1/27 of the simulation box) for (c) f = 0.03 (100^3 Å^3), (d) f = 0.09 (100^3 Å^3) both at 600 ns at 300 K (blue – backbone, red – oxygen, yellow – sulfur, black-Na^+)

Molecular insight was obtained from large scale, atomistic MD simulations. Visualization of the computational solutions are shown in Figure 3.2 a,b. A zoomed in subsection of the same systems is shown in Figures 3.2 c,d to show the local arrangement of the ionic clusters and chains. For both f-values, distinctive clusters are observed. However, in the f = 0.03 solution, these are significantly small, and the chains are distributed homogeneously across the system on the length scale and time scales of the simulation. The polymer is mixed with the solvent across the entire solution linked by the ionic clusters. With increasing sulfonation fraction (f = 0.09) the clusters become significantly larger and their number increases, confining more of the PS backbone and driving distinct polymer rich and solvent rich domains.
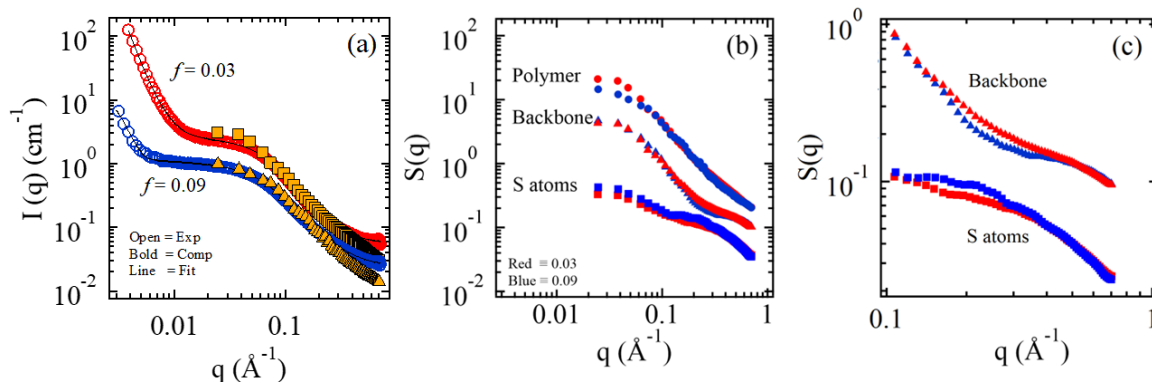
Figure 3.3: Structure factors for 10 Wt.% SPS in toluene. (a) Experimental *I(q)* and calculated *S(q)*. (b) Partial *S(q)* of the polymer, the backbones, and the sulfur atoms at the same concentrations and sulfonation levels as in (a). *S(q)* for the polymer is shifted up vertically for clarity (c) *S(q)* for the backbone and S atoms on an expanded scale for $0.1 \text{ Å}^{-1} \leq q \leq 0.7 \text{ Å}^{-1}$.

The calculated *S(q)* and the experimental scattering intensity *I(q)* are shown in Figure .33 a. The calculated *S(q)* was averaged over the last 20 ns of the run and shifted vertically to overlap with the experimental *I(q)*. The experimental and calculated results are in distinctive agreement over the range accessible to simulations as shown in Figure 3.3 a. The length scale range accessible to simulations depends on the size of the simulation box. With these multi-million atom simulations, chosen as a compromise between the desired large size and computational feasibility, the compute solutions capture the length scale of ~10 times the average R_g of a single chain. A slight shift of the simulations compared with experiments at the high q regime are attributed to finite size of the simulations.

Calculated *S(q)* was averaged over 20 ns, between 580 to 600 ns. Similar to the challenge of physical solution the question of the equilibrium state of the systems are in associative complex fluids arises. However, *S(q)* measured over different time intervals, after 300 ns were practically identical.

The partial structure factors $S(q)$, shown for the scattering solely from the polymer chains, from the backbone and from the sulfur atoms in Figure 3.3 b,c, decern the contributions of the backbone and the clusters to the scattering factor. $S(q)$ of the backbone differs slightly in solutions of $f = 0.03$ and 0.09, reflecting the confinement effects the clusters have on the chain. $S(q)$ for the S atoms exhibits a distinctive peak for $f = 0.09$ centered around inter cluster distance of 31 Å which is attributed to the ionic peak.
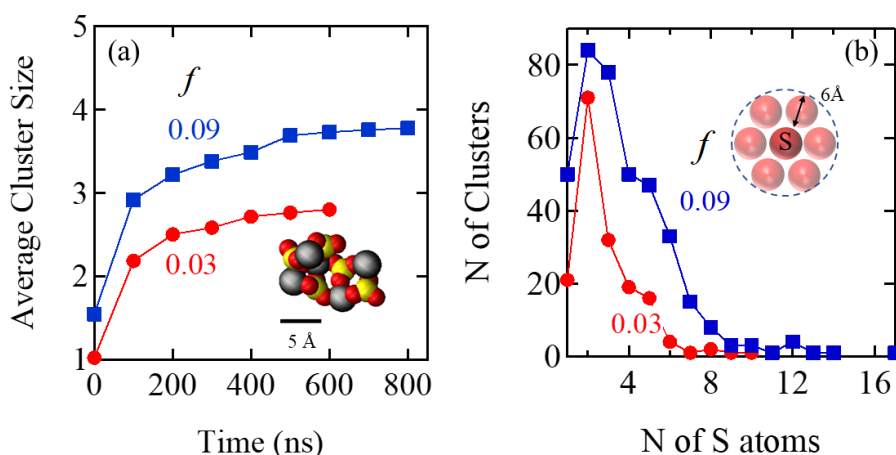
Figure 3.4: (a) Average cluster size as a function of time and (b) cluster distribution function for $f = 0.03$ and 0.09 SPS in 10 Wt% toluene, averaged over the last 10 ns of the run. The insert in (a) depicts one typical cluster at 600 ns.

The computed solutions were simulated to times where no significant difference in cluster size distribution were observed. The average cluster size as a function of time is shown in Figure 3.4 a. The final cluster size distribution, averaged over the last 10 ns of the run are shown in Figure 3.4 b. The average cluster increases with time, reaching a plateau at late time of 2.9 for $f = 0.03$ and 3.6 for $f = 0.09$. For both sulfonation fractions, a low fraction of the sulfonation groups (~3 - 4%) remain non-clusterd, and significant number reside in clusters of 2 - 4 SO_3^- groups. For $f = 0.03$ aproximatly 30% reside in, whereas for $f = 0.09$, only 12 % are in pairs and the system is dominated by large clusters. The Na^+ couterions fully condensed for both f values.

In contrast to melts[21] where clusters exhibit ladder like structures in low dielectric environment, in toluene solution, the ionic clusters are internaly disordered, and assume a variety of shapes.

B. Temperature Effects SANS measurements were carried out at several temperatures. The SANS patterns are shown in Figure 3.5 a,b and the corresponding Kratky plots, $q^2I(q)$ versus q, are shown in Figure A3.2. For both sulfonation fractions, the overall intensity slightly decreases with increasing temperature across the entire measured q range.
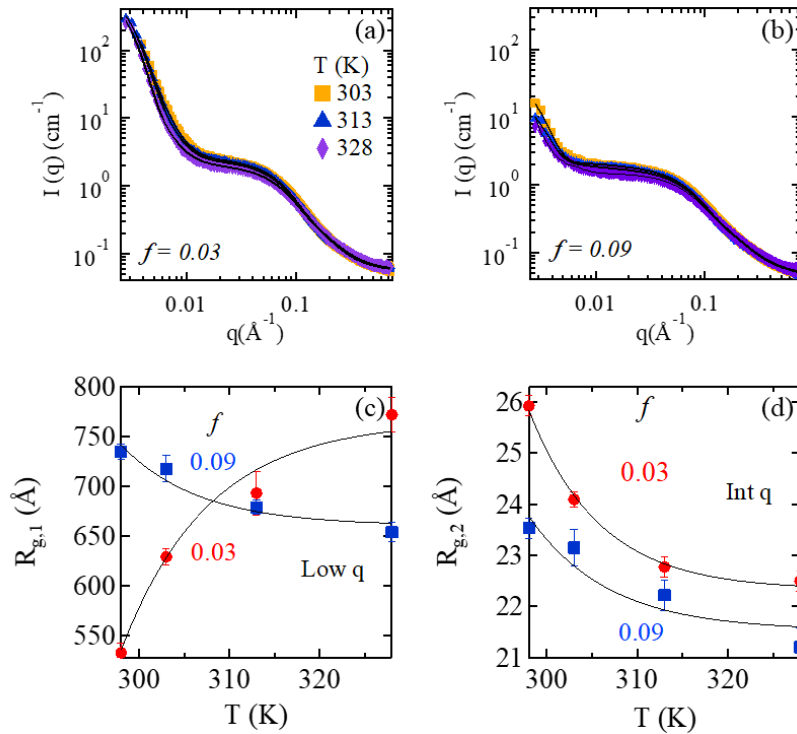
Figure 3.5: SANS pattern $I(q)$ versus q for SPS 10 Wt% in toluene for 3 temperatures for (a) $f = 0.03$ (b) $f = 0.09$. $R_{g,i}$ as a function of temperature from Beaucage model.

The change in dimensions captured from the Beaucage analysis are presented in Figure 3.5c,d. With increasing temperature, $R_{g,1}$ for the two sulfonation fractions exhibit opposite trends where for $f = 0.03$ the characteristic dimension increases whereas for $f = 0.09$, it decreases. While rather

surprising, these opposing trends are attributed to the impact of temperature on the inhomogeneous distribution of the PS backbone in the solution.

SPS toluene solutions are controlled by two energy scales, van der Waals interactions dominating the interchain chains forces as well as the interaction with the solvent and electrostatic interactions that control clustering. Since the strength of the van der Waals interactions are on the order of ~ kT, and the ionic interactions is approximately two orders of magnitude higher, in the measured temperature range, the ionic clusters are hardly impacted, as shown in Figure 3.6a, whereas the added thermal energy impacts the chain distribution. The smaller dimension, $R_{g,2,}$ however, hardly changes for both $f = 0.03$ and 0.09.
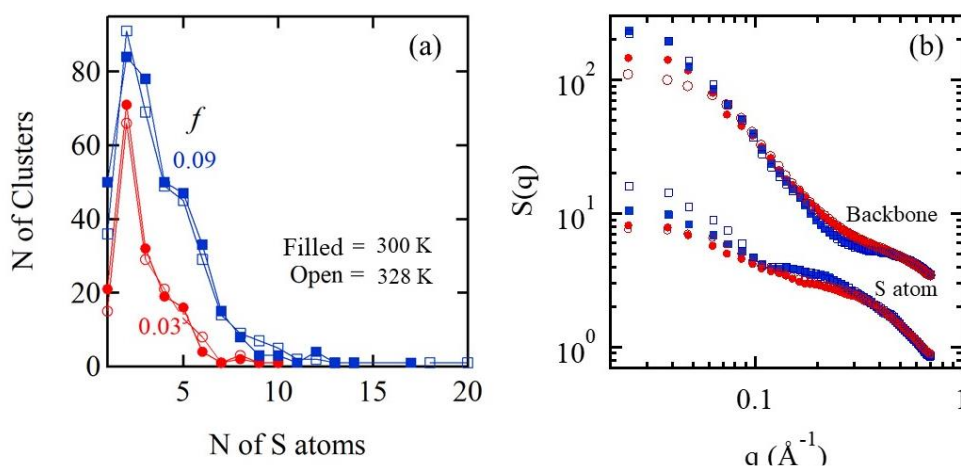
Figure 3.6: (a) Cluster distribution and (b) partial S(q) for the backbone only and the sulfur atoms for $f = 0.03$ and $f = 0.09$ at 300 to 328 K

With toluene being a good solvent for the backbone, the added thermal energy allows breathing of these networks. Lowering the sulfonation level results in expansion of the network. With increasing f more chains are associated with each cluster.[28] Partial $S(q)$ for the backbone and S atoms are shown in Figure 3.6 b. For both sulfonation fractions barely any changes are observed

in the intermediate q region. However the breathing mode of the network is reflected in the structure factors of both the network and the sulfur atoms.

C. Solvent Dielectric Effects

SANS patterns of solutions at 303 K of both sulfonations fractions in form of Kratky plots are shown Figure 3.7 a,b as the ethanol fraction is increased. The corresponding Kratky plots are shown in Figure A3.3 Upon addition of as low as 1 Wt% ethanol, the signature at low q disappears and with increasing ethanol fraction the overall scattering intensity decreases across the measured q range. The signature at intermediate q range shifts towards higher q and becomes broader, as has been previously observed for swollen melts.[27]
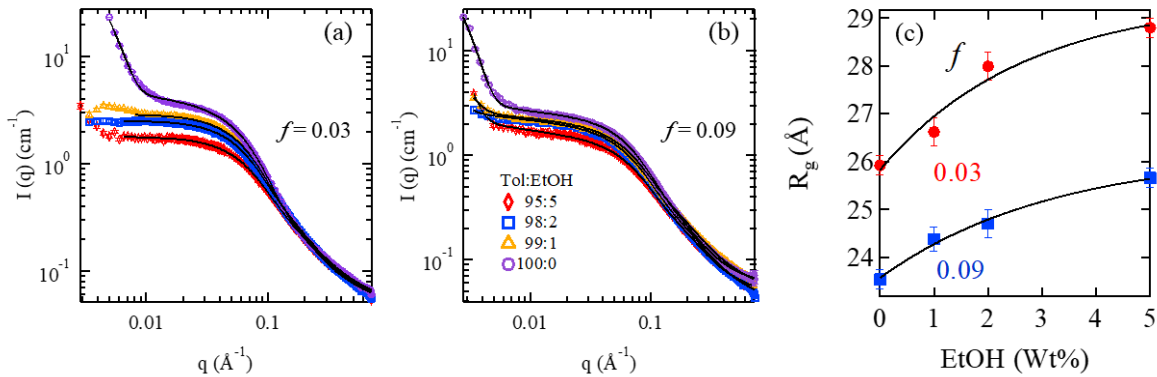
Figure 3.7: SANS patterns of $I(q)$ versus q for (a) $f = 0.03$ and (b) $f = 0.09$ for 10 Wt% SPS at 303K for different ethanol fractions (c) R_g extracted from Beaucage model in the intermediate q region for $f = 0.03$ and $f = 0.09$.

As ethanol is added, R_g increases as seen in Figure 3.7 c. This dimension change is attributed to reduced confinement of the PS chains as a result of disruption of the large clusters.
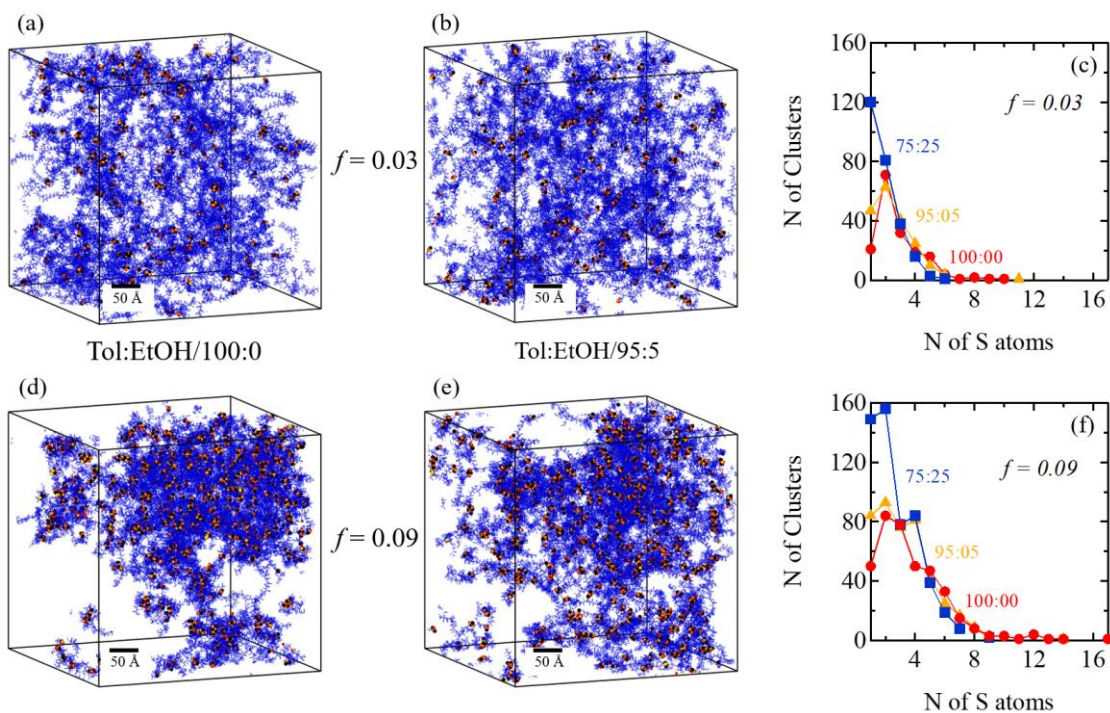
Figure 3.8: Visualization of 10 Wt% SPS for $f = 0.03$ and $f = 0.09$ in Tol:EtOH (Wt%) (a) 95:5 (b) 75:25 and for $f = 0.09$ in Tol:EtOH (Wt%) (c) 95:5 (d) 75:25 at run time of 600 ns. Number of clusters of size N of S atoms for (c) $f = 0.03$ and (f) $f = 0.09$.

Visualization of the computed solutions, presented in Figure 3.8, shows that the addition of 5% ethanol disrupts the large clusters, for both f values, as described quantitatively in Figure 3.8 c where the cluster size distribution with increasing fractions of ethanol is presented. Consequently, a more homogenous distribution of the polymer backbone is observed. Increasing the ethanol fraction to 25 Wt%, significantly increases the number of non-associated sulfonated groups, however some small clusters persist.
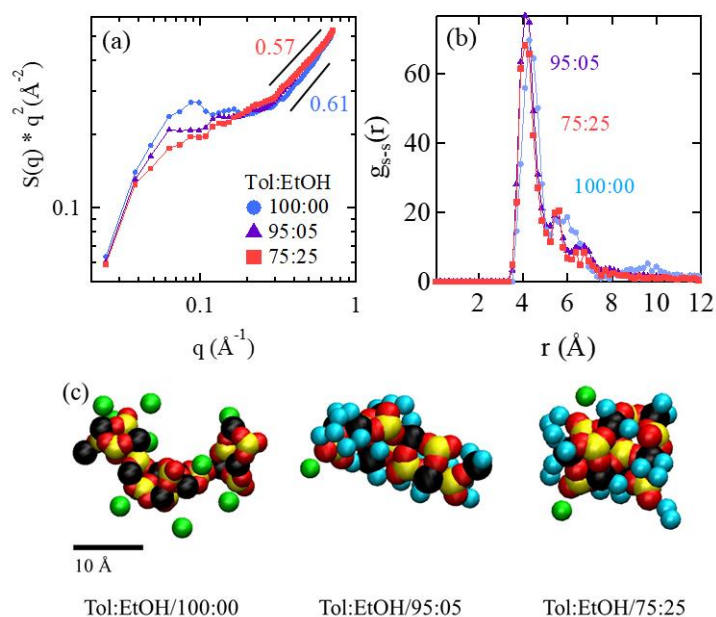
Figure 3.9: (a) Kratky plot $q^2 S(q)$ versus q for the computed solutions and (b) pair distribution function between Sulfur-Sulfur atoms from the simulations, averaged the last 20 ns of the run for $f = 0.09$, 10 Wt% at 300K for different ethanol fractions. (c) Visualization of toluene and ethanol association with an ionic group as a function of ethanol fraction. Yellow-sulfur, red-oxygen, black-Na$^+$, blue-oxygen in EtOH, and green-carbon in toluene CH$_3$ at 600 ns.

At these high levels of ethanol, the quality of the solvent decreases, and the chains are no longer Gaussian, as is depicted in the calculated $S(q)$ in Figure 3.9 a, where the slope of the curve at high q differs between the neat solutions with no ethanol and the ethanol containing solutions. These $S(q)$ patterns exhibit the characteristic "ionomer" peak at low q which decreases in intensity with increasing ethanol, indicating loss of correlation between the ionic assemblies. The high q region ($q = 0.3$ Å^{-1} – 0.7 Å^{-1}) depicts the chain packing. In this range the slope increases with increasing ethanol fraction, which suggests that the polymer chain density changes with polar solvent. With increasing ethanol concentration, the larger clusters break up, however $g(r)$ for the sulfonated groups clearly shows that significant number of the groups remain correlated defining a hydrophilic region that is less cohesive than the cluster but is segregated from the hydrophobic regions. The comparison between $S(q)$ and $g(r)$ for the same solutions clearly show

44

that with addition of polar solvents, long range cluster correlations are significantly reduced, however significant number of the sulfonated groups remain correlated as shown in *g(r)*, forming swollen ionic domains.

A representative cluster and the corresponding ionic domains containing the solvent atoms within 7 Å of S atoms is shown in Figure 3.9 c for 0, 5 and 25% ethanol. In toluene, only a limited number of toluene molecules reside within 7 Å of the sulfonated rings, where ~ 11% reside in the proximity of the backbone. Ethanol, however, is directly associated with the ionic clusters with 44% of ethanol molecules reside in the vicinity of the ionic assembly for 5% ethanol. With an excess of ethanol, 25% the ethanol molecules penetrate the clusters and drive the ionizable groups apart.

3.5 Conclusions

The conjunction of mesoscopic structure attained by SANS on SPS together with molecular insight extracted from MD simulations on SPS with Na^+ as a counterion, has provided a direct correlation between the characteristics of the assemblies of the sulfonated groups and the structure of networks formed by SPS in toluene. With both hydrogen and sodium being predominantly condensed in these solutions, the macroscopic structure is dominated by network formation driven by the assembly of the sulfonated groups. With an exceptional agreement between the structure factors measured experimentally and calculated from MD simulations we were able to answer a long-standing challenge of understanding the factors that control networks formed by ionomers, namely, corelating the packing of the sulfonated groups and the networks' structure.

The structure of these networks however depends on the polymer concentration, on the fraction of sulfonated groups, temperature, as well as solvent polarity. SANS studies capture the dimension of the network as well as intra domain structure where the signature of the clusters is expressed.

Computationally the measurements depict the intra-domain structure. With increasing concentrations and sulfonation fractions, the size and number of the ionic clusters increase, affecting the homogeneity of the solutions.

Upon addition of a polar solvent, ethanol, the large-scale network signature observed by SANS disappears, however the solutions consist of large domains that are well captured by concentration fluctuations, where the chain segments between the ionic groups remain close to Gaussian. The characteristics of the ionic assemblies, however, are strongly affected, reducing the correlation between the sulfonated groups, and often breaking some of the larger clusters.

Beyond the fundamental new physics, the ability to tweak the ionic clusters and impact the overall structure opens the way to tailor processing conditions of ionizable polymers from solutions with desired clustering for targeted applications.

3.6 Acknowledgements

3.7 Appendix

C (Wt%)	0.25	1	5	10
Bk	0.005	0.010	0.033	0.050
Rg_1	790.10	782.92	700.19	532.28
P_1	2.336	2.381	2.595	3.152
B_1	0.00196	0.011523	0.00085	0.00003
G_1	30344	38825	50419	88712
Rg_2	32.276	31.96	31.89	25.92
P_2	2.347	2.387	2.468	2.523
B_2	0.25	0.13	0.10	0.06
G_2	416.99	415.75	414.02	382.31

Table A3.1: Fitting parameters to Beaucage model for $f = 0.03$ in toluene as a function of concentration.

C (Wt%)	0.25	1	5	10
Bk	0.0063	0.0212	0.0415	0.0458
Rg_1	852.52	801.37	760.21	734.17
P_1	1.598	1.600	1.700	1.946
B_1	0.0724	0.0550	0.0167	0.0028
G_1	15231	13317	2519.3	5666.3
Rg_2	32.577	31.714	28.904	23.533
P_2	1.8227	1.9246	2.0031	2.2089
B_2	0.901	0.804	0.615	0.404
G_2	418.14	391.66	335.82	218.14

Table A3.2: Fitting parameters to Beaucage model for $f = 0.09$ in toluene as a function of concentration.
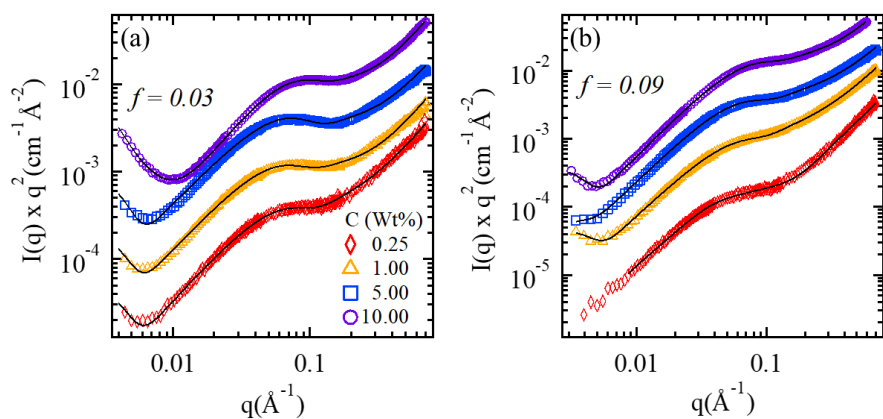
Figure A3.1: Kratky plot for (a) $f = 0.03$ and (b) $f = 0.09$ for varying polymer concentrations.
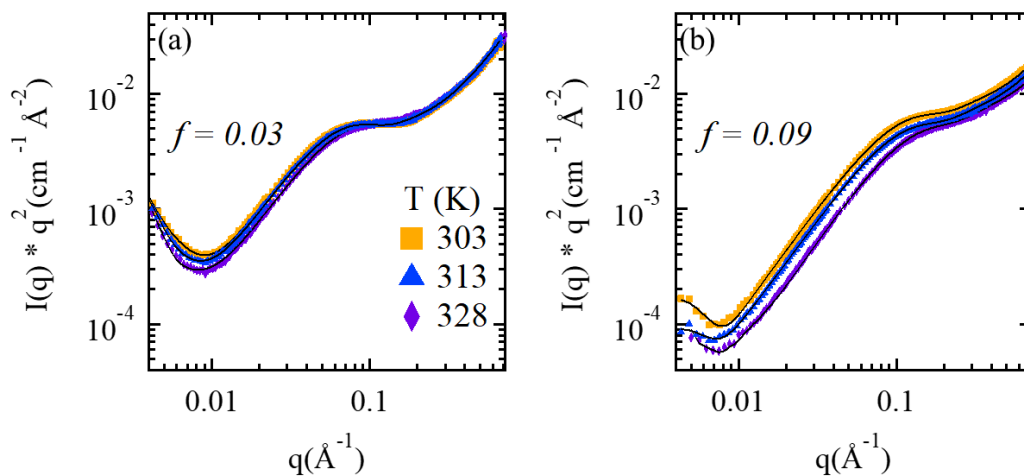
Figure A3.2: Kratky plot for (a) $f = 0.03$ and (b) $f = 0.09$ with varying temperature.
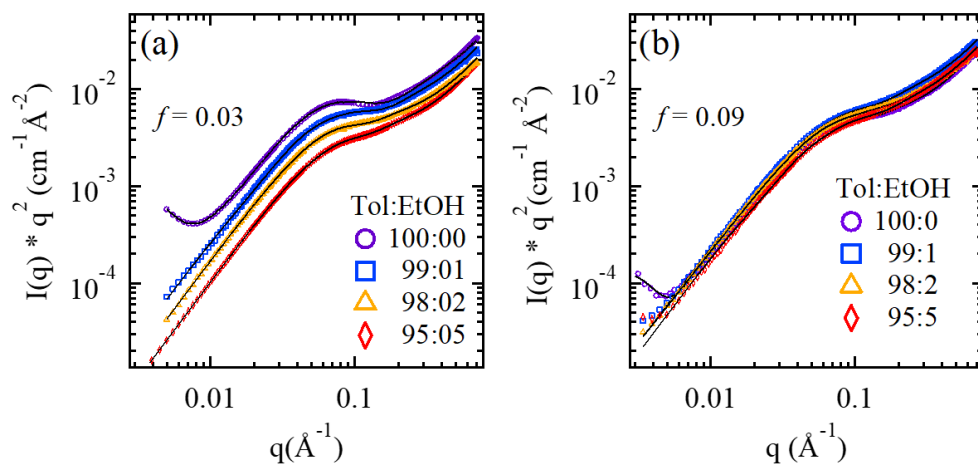
Figure A3.3: Kratky plot for (a) $f = 0.03$ and (b) $f = 0.09$ with varying EtOH fraction.

3.8 References

(1) Chabot, F.; Lee, J.; Vandenberghe, F.; Guetaz, L.; Gebel, G.; Lyonnard, S.; Porcar, L.; Rosini, S.; Morin, A. Detailed Catalyst Layer Structure of Proton Exchange Membrane Fuel Cells from Contrast Variation Small-Angle Neutron Scattering. *ACS Applied Energy Materials* **2023**, *6* (3), 1185-1196.

(2) Bordín, S. P. F.; de los Angeles Chinellato Díaz, J.; Romero, M. R. Nafion-Based Membranes for Proton Exchange Membrane Fuel Cells. *Proton Exchange Membrane Fuel Cells: Electrochemical Methods and Computational Fluid Dynamics* **2023**, 299-329.

(3) Kouhi, M.; Khodaei, M. Additive manufacturing and biomaterials in regenerative dentistry. *Frontiers in Bioengineering and Biotechnology* **2023**, *11*, 1211009.

(4) Bernat, J.; Gajewski, P.; Kołota, J.; Marcinkowska, A. Review of Soft Actuators Controlled with Electrical Stimuli: IPMC, DEAP, and MRE. *Applied Sciences* **2023**, *13* (3), 1651.

(5) Eisenberg, A.; Hird, B.; Moore, R. A new multiplet-cluster model for the morphology of random ionomers. *Macromolecules* **1990**, *23* (18), 4098-4107.

(6) Pineri, M.; Eisenberg, A. *Structure and properties of ionomers*; Springer Science & Business Media, 2012.

(7) Rigdahl, M.; Eisenberg, A. Viscoelastic properties of sulfonated styrene ionomers. *Journal of Polymer Science: Polymer Physics Edition* **1981**, *19* (10), 1641-1654.

(8) Gebel, G.; Diat, O. Neutron and X-ray scattering: suitable tools for studying ionomer membranes. *Fuel cells* **2005**, *5* (2), 261-276.

(9) Kerres, J. A. Design concepts for aromatic ionomers and ionomer membranes to be applied to fuel cells and electrolysis. *Polymer Reviews* **2015**, *55* (2), 273-306.

(10) Miyake, J.; Watanabe, T.; Shintani, H.; Sugawara, Y.; Uchida, M.; Miyatake, K. Reinforced polyphenylene ionomer membranes exhibiting high fuel cell performance and mechanical durability. *ACS Materials Au* **2021**, *1* (1), 81-88.

(11) Weiss, R. A. Polyester Ionomers. *Polyester Films: Materials, Processes and Applications* **2023**, 67-156.

(12) Kerres, J. A. Development of ionomer membranes for fuel cells. *Journal of Membrane Science* **2001**, *185* (1), 3-27.

(13) Goyal, P.; Kusoglu, A.; Weber, A. Z. Coalescing Cation Selectivity Approaches in Ionomers. *ACS Energy Letters* **2023**, *8* (3), 1551-1566.

(14) Fitzgerald, J.; Weiss, R. Synthesis, properties, and structure of sulfonate ionomers. *Polymer Reviews* **1988**, *28* (1), 99-185.

(15) Lopez, C. G. Scaling and entanglement properties of neutral and sulfonated polystyrene. *Macromolecules* **2019**, *52* (23), 9409-9415.

(16) Chen, Q.; Huang, C.; Weiss, R.; Colby, R. H. Viscoelasticity of reversible gelation for ionomers. *Macromolecules* **2015**, *48* (4), 1221-1230.

(17) Lerman, M. J.; Lembong, J.; Muramoto, S.; Gillen, G.; Fisher, J. P. The evolution of polystyrene as a cell culture material. *Tissue Engineering Part B: Reviews* **2018**, *24* (5), 359-372.

(18) Wang, K.; Zhang, Z.; Liu, C.; Fu, Q.; Xu, W.; Huang, C.; Weiss, R.; Gong, X. Efficient polymer solar cells by lithium sulfonated polystyrene as a charge transport interfacial layer. *ACS applied materials & interfaces* **2017**, *9* (6), 5348-5357.

(19) Arslanova, A.; Sanginov, E.; Dobrovol'skii, Y. A. New composite proton-conducting membranes based on nafion and cross-linked sulfonated polystyrene. *Russian Journal of Electrochemistry* **2018**, *54*, 318-323.

(20) Middleton, L. R.; Winey, K. I. Nanoscale aggregation in acid-and ion-containing polymers. *Annual review of chemical and biomolecular engineering* **2017**, *8*, 499-523.

(21) Agrawal, A.; Perahia, D.; Grest, G. S. Clustering effects in ionic polymers: Molecular dynamics simulations. *Physical Review E* **2015**, *92* (2), 022601.

(22) Castagna, A. M.; Wang, W.; Winey, K. I.; Runt, J. Influence of the degree of sulfonation on the structure and dynamics of sulfonated polystyrene copolymers. *Macromolecules* **2010**, *43* (24), 10498-10504.

(23) Castagna, A. M.; Wang, W.; Winey, K. I.; Runt, J. Structure and dynamics of zinc-neutralized sulfonated polystyrene ionomers. *Macromolecules* **2011**, *44* (8), 2791-2798.

(24) Castagna, A. M.; Wang, W.; Winey, K. I.; Runt, J. Influence of cation type on structure and dynamics in sulfonated polystyrene ionomers. *Macromolecules* **2011**, *44* (13), 5420-5426.

(25) Lefelar, J. A.; Weiss, R. A. Concentration and counterion dependence of cluster formation in sulfonated polystyrene. *Macromolecules* **1984**, *17* (6), 1145-1148.

(26) Essafi, W.; Spiteri, M.-N.; Williams, C.; Boué, F. Hydrophobic polyelectrolytes in better polar solvent. Structure and chain conformation as seen by SAXS and SANS. *Macromolecules* **2009**, *42* (24), 9568-9580.

(27) Fitzgerald, J.; Kim, D.; Weiss, R. The effect of diluents on the ionic interactions in sulfonated polystyrene ionomers. *Journal of Polymer Science Part C: Polymer Letters* **1986**, *24* (6), 263-268.

(28) Mohottalalage, S. S.; Aryal, D.; Thurston, B. A.; Grest, G. S.; Perahia, D. Effects of ionic group distribution on the structure and dynamics of amorphous polymer melts. *Macromolecules* **2021**, *55* (1), 217-223.

(29) Xie, R.; Weiss, R. Molecular dynamics simulation of chain collapse of random ionomers in a poor solvent. *Computational and Theoretical Polymer Science* **1997**, *7* (2), 65-74.

(30) Mohottalalage, S. S.; Kosgallana, C.; Senanayake, M.; Wijesinghe, S.; Osti, N. C.; Perahia, D. Molecular Insight into the Effects of Clustering on the Dynamics of Ionomers in Solutions. *ACS Macro Letters* **2023**, *12*, 1118-1124.

(31) Mohottalalage, S. S.; Kosgallana, C.; Meedin, S.; O'Connor, T. C.; Grest, G. S.; Perahia, D. Response of Sulfonated Polystyrene Melts to Nonlinear Elongation Flows. *Macromolecules* **2023**, *56* (3), 947-953.

(32) Ling, G. H.; Wang, Y.; Weiss, R. Linear viscoelastic and uniaxial extensional rheology of alkali metal neutralized sulfonated oligostyrene ionomer melts. *Macromolecules* **2012**, *45* (1), 481-490.

(33) Qiao, X.; Weiss, R. Nonlinear rheology of lightly sulfonated polystyrene ionomers. *Macromolecules* **2013**, *46* (6), 2417-2424.

(34) Weiss, R.; Yu, W.-C. Viscoelastic behavior of very lightly sulfonated polystyrene ionomers. *Macromolecules* **2007**, *40* (10), 3640-3643.

(35) Chakrabarty, K.; Weiss, R.; Sehgal, A.; Seery, T. Characterization of ionomer solutions. 2. Dynamic light scattering studies on sulfonated polystyrene ionomers in a nonpolar solvent. *Macromolecules* **1998**, *31* (21), 7390-7397.

(36) Lantman, C.; MacKnight, W.; Higgins, J.; Peiffer, D.; Sinha, S.; Lundberg, R. Small-angle neutron scattering from sulfonate ionomer solutions. 1. Associating polymer behavior. *Macromolecules* **1988**, *21* (5), 1339-1343.

(37) Agrawal, A.; Perahia, D.; Grest, G. S. Cluster morphology-polymer dynamics correlations in sulfonated polystyrene melts: computational study. *Physical review letters* **2016**, *116* (15), 158001.
(38) Zhou, N. C.; Chan, C. D.; Winey, K. I. Reconciling STEM and X-ray scattering data to determine the nanoscale ionic aggregate morphology in sulfonated polystyrene ionomers. *Macromolecules* **2008**, *41* (16), 6134-6140.
(39) Bouix, M.; Gouzi, J.; Charleux, B.; Vairon, J. P.; Guinot, P. Synthesis of amphiphilic polyelectrolyte block copolymers using "living" radical polymerization. Application as stabilizers in emulsion polymerization. *Macromolecular rapid communications* **1998**, *19* (4), 209-213.
(40) Littrell, K.; Atchley, K.; Cheng, G.; Melnichenko, Y.; Wignall, G. General purpose small-angle neutron scattering instrument on HFIR Oak Ridge. *Neutron news* **2008**, *19* (3), 20-21.
(41) Wignall, G. D.; Littrell, K. C.; Heller, W. T.; Melnichenko, Y. B.; Bailey, K. M.; Lynn, G. W.; Myles, D. A.; Urban, V. S.; Buchanan, M. V.; Selby, D. L. The 40 m general purpose small-angle neutron scattering instrument at Oak Ridge National Laboratory. *J. App. Crystallography* **2012**, *45*, 990-998.
(42) *SANS Data Reduction for CG2(GP-SANS)*. https://neutrons.ornl.gov/sites/default/files/SANS%20Data%20Reduction%20for%20CG2.pdf (accessed 11/30/23).
(43) *SasView Software*. https://www.sasview.org/ (accessed.
(44) Hammouda, B.; Ho, D. L. Insight into chain dimensions in PEO/water solutions. *Journal of Polymer Science Part B: Polymer Physics* **2007**, *45* (16), 2196-2200.
(45) Rossi, B.; Paciaroni, A.; Venuti, V.; Fadda, G.; Melone, L.; Punta, C.; Crupi, V.; Majolino, D.; Mele, A. SANS investigation of water adsorption in tunable cyclodextrin-based polymeric hydrogels. *Physical chemistry chemical physics* **2017**, *19* (8), 6022-6029.
(46) O'Connell, R. i. n. A.; Sharratt, W. N.; Aelmans, N. J.; Higgins, J. S.; Cabral, J. o. T. SANS Study of PPPO in Mixed Solvents and Impact on Polymer Nanoprecipitation. *Macromolecules* **2022**, *55* (3), 1050-1059.
(47) Fajalia, A. I.; Tsianou, M. Charging and uncharging a neutral polymer in solution: A small-angle neutron scattering investigation. *The Journal of Physical Chemistry B* **2014**, *118* (36), 10725-10739.
(48) Kancharla, S.; Bedrov, D.; Tsianou, M.; Alexandridis, P. Structure and composition of mixed micelles formed by nonionic block copolymers and ionic surfactants in water determined by small-angle neutron scattering with contrast variation. *Journal of Colloid and Interface Science* **2022**, *609*, 456-468.
(49) Beaucage, G. Small-angle scattering from polymeric mass fractals of arbitrary mass-fractal dimension. *Journal of applied crystallography* **1996**, *29* (2), 134-146.
(50) Beaucage, G. Approximations leading to a unified exponential/power-law approach to small-angle scattering. *Journal of Applied Crystallography* **1995**, *28* (6), 717-728.
(51) Hammouda, B. Analysis of the Beaucage model. *Journal of Applied Crystallography* **2010**, *43* (6), 1474-1478.
(52) Feigin, L.; Svergun, D. I. *Structure analysis by small-angle X-ray and neutron scattering*; Springer, 1987.
(53) Jorgensen, W. L.; Maxwell, D. S.; Tirado-Rives, J. Development and testing of the OPLS all-atom force field on conformational energetics and properties of organic liquids. *Journal of the American Chemical Society* **1996**, *118* (45), 11225-11236.
(54) Jorgensen, W. L.; Madura, J. D.; Swenson, C. J. Optimized intermolecular potential functions for liquid hydrocarbons. *Journal of the American Chemical Society* **1984**, *106* (22), 6638-6646.

(55) Thompson, A. P.; Aktulga, H. M.; Berger, R.; Bolintineanu, D. S.; Brown, W. M.; Crozier, P. S.; in't Veld, P. J.; Kohlmeyer, A.; Moore, S. G.; Nguyen, T. D. LAMMPS-A flexible simulation tool for particle-based materials modeling at the atomic, meso, and continuum scales. *Comp. Phys. Comm.* **2022**, *271*, 108171.

(56) Pronk, S.; Páll, S.; Schulz, R.; Larsson, P.; Bjelkmar, P.; Apostolov, R.; Shirts, M. R.; Smith, J. C.; Kasson, P. M.; Van Der Spoel, D. GROMACS 4.5: a high-throughput and highly parallel open source molecular simulation toolkit. *Bioinformatics* **2013**, *29* (7), 845-854.

(57) Abraham, M. J.; Murtola, T.; Schulz, R.; Páll, S.; Smith, J. C.; Hess, B.; Lindahl, E. GROMACS: High performance molecular simulations through multi-level parallelism from laptops to supercomputers. *SoftwareX* **2015**, *1*, 19-25.

(58) Berendsen, H. J.; van der Spoel, D.; van Drunen, R. GROMACS: A message-passing parallel molecular dynamics implementation. *Computer physics communications* **1995**, *91* (1-3), 43-56.

(59) Allen, M. P. Introduction to molecular dynamics simulation. *Computational soft matter: from synthetic polymers to proteins* **2004**, *23* (1), 1-28.

(60) Hockney, R. W.; Eastwood, J. W. *Computer simulation using particles*; crc Press, 2021.

(61) Nosé, S. A unified formulation of the constant temperature molecular dynamics methods. *The Journal of chemical physics* **1984**, *81* (1), 511-519.

(62) Hoover, W. G. Canonical dynamics: Equilibrium phase-space distributions. *Physical review A* **1985**, *31* (3), 1695.

(63) Shirts, M. R.; Klein, C.; Swails, J. M.; Yin, J.; Gilson, M. K.; Mobley, D. L.; Case, D. A.; Zhong, E. D. Lessons learned from comparing molecular dynamics engines on the SAMPL5 dataset. *Journal of computer-aided molecular design* **2017**, *31*, 147-161.

(64) Essmann, U.; Perera, L.; Berkowitz, M. L.; Darden, T.; Lee, H.; Pedersen, L. G. A smooth particle mesh Ewald method. *The Journal of chemical physics* **1995**, *103* (19), 8577-8593.

(65) Hess, B.; Bekker, H.; Berendsen, H. J.; Fraaije, J. G. LINCS: A linear constraint solver for molecular simulations. *Journal of computational chemistry* **1997**, *18* (12), 1463-1472.

(66) Bussi, G.; Donadio, D.; Parrinello, M. Canonical sampling through velocity rescaling. *The Journal of chemical physics* **2007**, *126* (1), 014101.

(67) Michaud-Agrawal, N.; Denning, E. J.; Woolf, T. B.; Beckstein, O. MDAnalysis: a toolkit for the analysis of molecular dynamics simulations. *Journal of computational chemistry* **2011**, *32* (10), 2319-2327.

CHAPTER FOUR

FROM MOLECULAR CONSTRAINTS TO MACROSCOPIC DYNAMICS IN ASSOCIATIVE NETWORKS FORMED BY IONIZABLE POLYMERS: A NEUTRON SPIN ECHO AND MOLECULAR DYNAMICS SIMULATIONS STUDY

4.1 Abstract

The association of ionizable polymers strongly affects their motion in solutions, where the constraints arising from the clustering of the ionizable groups alter the macroscopic dynamics. The interrelation between the motion on multiple length and time scales is fundamental to a broad range of complex fluids, including physical networks, gels, and polymer-nanoparticle complexes, where long-lived associations control their structure and dynamics. Using neutron spin echo and fully atomistic, multimillion atom molecular dynamics (MD) simulations carried out to times comparable to that of chain segmental motion, the current study resolves the dynamics of networks formed by polystyrene sulfonate solutions for sulfonation fractions $0 \leq f \leq 0.09$ across time and length scales. The experimental dynamic structure factors were measured and compared with computational ones, calculated from MD simulations, and analyzed in terms of a sum of two exponential functions, providing two distinctive time scales. These time constants correspond to constrained motion, where the slower time is correlated with the effects of the ionic clusters, and the faster one with non-confined dynamics is associated with highly solvated segments. A unique relationship between the polymer dynamics and the size and distribution of the ionic clusters was established and correlated with the number of polymer chains that participate in each cluster. The correlation of dynamics in associative complex fluids across time and length scales, enabled by combining the understanding attained from reciprocal space through neutron spin echo and real

space through large-scale MD studies, addresses a fundamental, long-standing challenge that underlines the behavior of soft materials and affects their potential uses.

4.2 Introduction

The dynamic processes in networks of ionizable polymers drive their unique characteristics and enable their many current and potential applications in lightweight technologies ranging from clean energy generation and storage to biotechnology.[1-3] Their structure and dynamics in melts and solutions are governed by the coupling of two distinctive energy scales, van der Waals interactions and electrostatic forces, resulting in the coupling of responses on multiple length and time scales. Beyond ionizable polymeric networks, the coupling between processes that occur on distinctive length scales is a key to resolving the behavior of associative soft materials including networks, gels and nanoparticles-polymer hybrids as well as polymer-membrane complexes, all driven by dynamic constraints formed by physical association of chains.[4-9]

Ionizable polymers cluster into long-lived physical networks where the ionizable groups form long lived assemblies, affecting both the segmental dynamics of the macromolecules and their ability to rearrange. Tethering a very small number of ionizable groups to the polymer backbone is sufficient to affect the motion of the polymer,[10, 11] influencing their properties, including their mechanical response. Though the constraints of ionic clustering exerted on the motion of ionizable polymers are evident in their flow characteristics,[10, 12] the molecular processes that underline the macroscopic lock-in of macromolecules is yet to be resolved.

Here, enabled by a conjunction of neutron spin echo (NSE) measurements and exascale atomistic molecular dynamics (MD) simulations, the dynamics of an ionizable model polymer, sulfonated polystyrene (SPS), in solutions are probed across length and time scales. NSE is among the very few methods that can directly resolve dynamics on the mesoscopic length scale ca. 1-15nm.[13-15]

Large scale atomistic MD simulations, that capture the time scales of the actual relaxation times of the chains, provide real-space insight,[16, 17] enabling the translation of knowledge across time length scales.

The correlation between the ionic cluster characteristics and the overall properties of ionizable polymers stems from the balance of the chain elasticity, or pull-out forces, and that of ionic electrostatic interactions as was postulated by Moore, Eisenberg, and co-workers, and Dreyfus.[18-21] The pioneering observation of Weise and co-workers.[22-24] who demonstrated that a small number of ionizable groups tethered to the polystyrene backbone results in a strong increase in the viscoelastic response[25-27] that differs significantly from that of short, non-entangled flexible van der Waals polymers, has driven the quest to resolve the pathways in which clustering affects the dynamics of ionizable polymers in melts and in solutions. This impact, as reflected in the dynamic structure factor $S(q,t)$ and shear viscosity, was captured by Agrawal et al. using MD simulations.[17] They showed that in melts, dynamics of the polymer depends on the counter ion and cluster morphology. A direct correlation between flow response and clustering has been recently demonstrated, where the flow viscosity is directly impacted by the size, shape and distribution of the clusters.[12, 28]

Early NSE studies of SPS with low sulfonation levels in THF and DMSO solvents resolved the polymer relaxation time in terms of a correlation length x that captures interchain correlations.[29] These studies have provided a glimpse into the correlation of chain relaxation and viscosity, providing the knowledge base that underlies the current studies. Further studies probed SPS in toluene at the low sulfonation regime and high molecular weight showed that even at concentrations as low as 1% the ionic clusters have a large impact on polymer motion on the nanosecond time scale.[30] Our recent quasi elastic neutron scattering (QENS) studies have shown

that the dynamics of SPS in its acid form, in cyclohexane, a poor solvent for both the backbone and the sulfonated groups at room temperature, is constrained on the length scale of the rigid segment of the polymer, the length scale accessible to QENS. This motion increases with increasing temperature with a distinctive transition to a faster dynamics at the θ temperature of the polystyrene backbone in cyclohexane.[31]

With results from real and reciprocal space, the current study strives to correlate the effects of clustering on the translation of constraint dynamics from the atomistic level and segmental length scales to the overall motion of the polymers, using sulfonated polystyrene in the ionomer regime. SPS in its ionomer regime, where well defined clusters are formed, is a well-studied polymer whose synthetic routes lead to narrow molecular weight distribution and the degree of sulfonation can be controlled. The study focuses on short, lightly sulfonated polystyrene with low molecular weights of ~11 kg/mol in toluene which is a good solvent for the polystyrene backbone. The small number of ionizable groups tethered to the backbone is sufficient to form clusters that constrain macroscopic motion, as shown by rheology, while the polymer backbone remains dynamic.

4.3 Methodology

Sulfonated polystyrene in its acid form with a molecular weight of ~11 kg/mol with a polydispersity index of 1.2 was purchased from Polymer Source™ Inc. The polymer was synthesized by anionic polymerization and was randomly sulfonated to sulfonation fractions of f = 0.03 and 0.09 of the available sites. Samples were made by dissolving 10 Wt% of the polymer in d-toluene purchased from Cambridge Isotope Laboratories, Inc., USA. At these low concentrations, the polymer readily dissolves. Samples were then allowed to equilibrate for several days under ambient conditions. The polymer concentration is typical of that used in solution

56

casting of ionic polymers and is just above the overlap concentration (~6.4Wt%) of the polystyrene with similar molecular weights.

Neutron Spin Echo NSE experiments were performed at the spallation neutron source (SNS, Oak Ridge, TN, USA).[13] Data from two neutron wavelengths 8 Å and 11 Å were combined to cover a wide q-range of 0.057 Å^{-1} to 0.32 Å^{-1} and Fourier times of 0.04 –100 ns. The q range and the Fourier time probed were determined by sample characteristics and instrument limits.

Two reference samples, a sheet of graphite and Al_2O_3 powder, were measured and used to correct for instrument resolution. The solvent was run separately and subtracted from the data. The data were collected by an in-house program, developed initially in Jülich Center for Neutron Science, Germany, and reduced to the form of *S(q,t)* using DrSpine program.[32] The temperature was controlled at 303 K by an SP FTS ThermoJet control system (SP Industries Warminster, PA) with the accuracy of +/- 0.5 K. Samples were encapsulated in 3 mm thick quartz rectangular Hellma cells (Müllheim, Germany).

Molecular Dynamics Simulations Comparable systems were studied by MD simulations. Sulfonated polystyrene and toluene were built using the polymer builder in BIOVIA^{TM} Materials Studio. The system contained 148 unique, atatic sulfonated polystyrene chains with sulfonation fraction $f = 0$, 0.03, and 0.09, each with a total molecular weight of ~11 kg/mol with 106 monomer per chain with Na^+ as a counterion. Similar to the experiments, the computer solutions consist of 10 wt% polymer in toluene. Each system contains between 2.4 - 2.5 million atoms. The final dimension of the cell is $L \sim 31.0$ nm for the 3 values of f; dimensions that are much larger than the size of a polymer chain whose radius of gyration R_g is 28 – 31 Å. The all atoms optimized potentials for liquid simulations (OPLS-AA) force fields, developed by Jorgensen et al.[33, 34] were used to model the system. The initial simulations were carried out using the LAMMPS[35] software

package and converted to GROMACS[36-38] for enhanced efficiency.

Each system was first run at constant pressure of 1 atm for 10 ns to obtain equilibrium density. The dielectric constant ε was increased from 1 to 30 to reduce the residual electrostatic screening between ionic groups. This step breaks the ionic clusters allowing the chains to locally equilibrate. Each solution was run for 30 ns at constant volume after which the dielectric constant was reset to 1 and ran for 600-800 ns at temperature 300 K.

4.4 Results
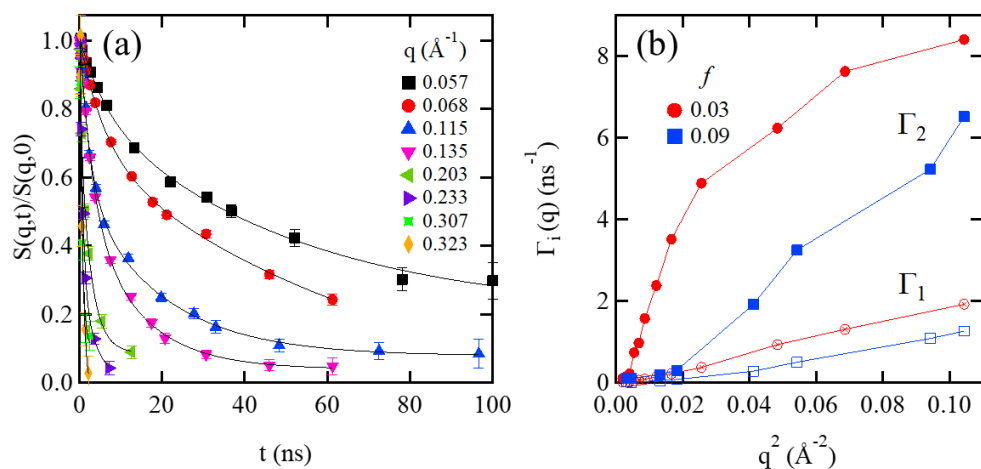
Figure 4.1: (a) Dynamic structure factor $S(q,t)$ from NSE for $f = 0.03$ at 303 K as a function of q. (b) Effective diffusion coefficient $\Gamma_1(q)$ (open) and $\Gamma_2(q)$ (filled) extracted from the fits to a double exponential function

The dynamic structure factor, $S(q,t)$ at different wave vectors q values for a solution of $f = 0.03$ in toluene, are presented in Figure 4.1. The lowest q attainable on the instrument, 0.057 Å^{-1}, captures the dimensions of the correlations between ionic clusters detected by SANS.[39] At these dimensions, $S(q,t)$ decreases significantly slower than at higher q and does not fully decay within Fourier times accessible. For $q > 0.11$ Å^{-1}, where segmental dynamics is manifested, $S(q,t)$ fully decays within the time range accessible. With the multitude of time and length scales of dynamics in these solutions, a stretched exponential Kohlrausch–Williams–Watts *(KWW)* model was first

58

attempted but was unable to capture the entire q range. The patterns were thus analyzed in terms

of a sum of two exponentials,

$$S(q,t)/S(q,0) = A_1 exp(-t/\tau_1) + A_2 exp(-t/\tau_2) \qquad (1)$$

where A_1 and A_2 are pre-exponentials that weighs the contributions of each of the processes in

$S(q,t)$, t is time, and τ_1 and τ_2 are relaxation times. The sum of $A_1 + A_2 \rightarrow 1$ for all q.

The results obtained by fitting $S(q,t)$ to a sum of two exponential and the relaxation times are

extracted. The relaxation rates Γ_1(q) and Γ_2(q), with $\Gamma_i(q) = 1/\tau_i(q)$ plotted in Figure 4.1b, show are

on the same order of magnitude, with $\Gamma_1(q) < \Gamma_2$(q). However, both are essential to capture the

relaxation of the polymer in toluene across the entire q range. For the slower relaxation rate, A_1

=0.78 at $q = 0.057$ Å^{-1} decreases to 0.39 at $q = 0.323$ Å^{-1} whereas for the faster one, A_2 increases

from 0.22 to 0.60 across this q range for $f = 0.03$. For $f = 0.09$, the slow relaxation rate, A_1 =0.83

at $q = 0.057$ Å^{-1} decreases to 0.30 at $q = 0.323$ Å^{-1} whereas for the fast relaxation rate, A_2 increases

from 0.17 to 0.70 across this q range.

For a simple, non-constraint process the relaxation rates $\Gamma_i(q)$ vary linearly with q^2. However, $\Gamma_i(q)$

as a function of q^2 clearly deviates from linearity, as seen in Figure 4.1b, pointing to constraint

dynamics. These data are plotted in terms of "effective diffusion" $\Gamma_i(q)/q^2$, commonly used for

diffusive systems, as a function of q in Figure A4.1, demonstrating that in contrast to diffusive

motion the effective diffusion exhibits a strong q dependance. With increasing q, Γ_1(q), increases

with a lower slope than $\Gamma_2(q)$ and exhibits a cross over to a faster motion at $q = 0.135$ Å^{-1}. Notable

differences are observed between $f = 0.03$ and 0.09 solutions, where the relaxation rates of $f =$

0.03 solution is faster than that of $f = 0.09$ across the entire q range. With increasing q, $\Gamma_2(q)$ first

increases slightly followed by a cross over to a rapid change that transitions to a slower increase

at high q.

These results depict two interdependent dynamic processes, a slow motion that takes place on the length scale of the inter ionic-cluster correlation and a faster segmental motion that exhibits a strong q dependence that diverges from simple diffusion, indicative of constraints motion of the chains beyond the mesoscopic length scale of the inter cluster correlation.

In these solutions, SPS whose backbone below the entanglement length of PS in the melt, constitute only 10% of the solution. The rest is toluene, which is good for the PS backbone. Therefore, the constraint dynamics is attributed to direct confinement of segments to the ionic clusters and bridging between clusters through individual chains residing in several clusters simultaneously. Direct confinement varies as a distance from the tethering point of the chains as depicted from the MD simulations.
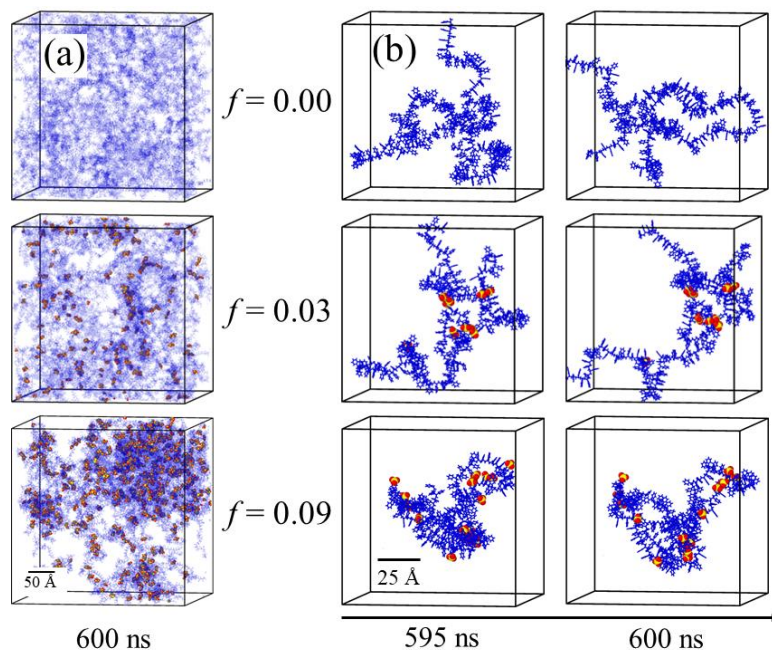
Figure 4.2: a) Visualization of polymer domains in solutions of $f = 0$, 0.03 and 0.09, at 300K. Toluene is removed for clarity. b) Visualization of two chains in all solutions at 5 ns intervals with only 1/27 of the simulation cells shown. (blue – backbone, red – oxygen, yellow – sulfur, black- Na$^+$

Visualization of computed solutions of PS and SPS with $f = 0$, 0.03 and 0.09 are shown in Figure 4.2. The solution of $f = 0$ is rather homogeneous. With increasing sulfonation *to f=0.03*, clusters

are formed, driving the formation of polymer-rich and solvent rich regions, where the polymer rich domains propagate across the solution. In f = 0.09 solutions, well defined clusters are observed, the polymer rich domains become denser and often segregated from the toluene. This significant phase segregation between the polymer-rich and solvent domains as has been previously reported by SANS.[39] This inherent inhomogeneous in these associative systems drives the complex dynamics observed in $S(q,t)$.

Visualization of representative chains in the solutions, shown in Figure 4.2 b, captures the motion of the chains 5 ns apart for f = 0, 0.03 and 0.09. The Na^+ counter ions are condensed and do not move away from the ionic groups within the time scale observed.
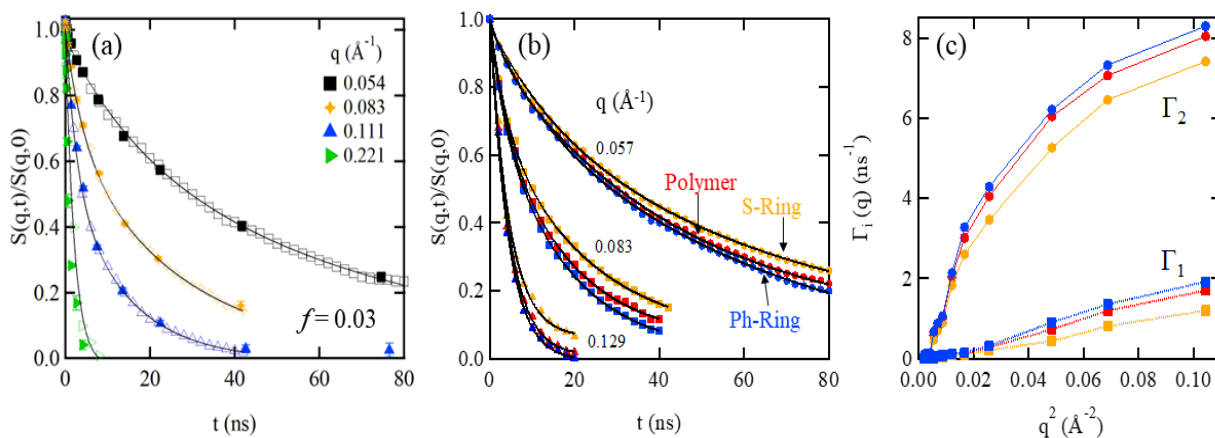
Figure 4.3: (a) Experimental (filled)) and computed (open) $S(q,t)$ for f = 0.03. (b) Computed partial dynamic structure factors $S(q,t)$ of the indicated polymer segments. The solid lines in a) and b) correspond to the results of fitting to a sum of two exponents. (c) The relaxation rates $\Gamma_i(q)$ extracted from the fitting of the computed dynamic structure factors as a function of q^2 for the polymer (red), the phenyl rings (Ph-ring, orange) and the sulfonated phenyl rings (S-rings blue) for f = 0.03 solutions.

In this time frame, only the fast motion is visually captured, the large-scale breathing mode of the entire network is observed only through the change in the position of the clusters. The chain segments closer to the clusters however show comparatively less motion than those further away and the overall chain mobility increases with their distance from the clusters.

The dynamic structure factor $S(q,t)$ was calculated for the computed solutions using

$$S(q,t) = \sum_{i,j=1}^{N} b_i \, b_j e^{[iq.(r_i(t)-r_j(0))]} \, / \, \sum_{i=1}^{N} b_i^2 \qquad (2)$$

where b_i are the neutron scattering lengths of atom i and $r_i(t)$ position of atom i at time t. These computational results in comparison with the experimental measurements are presented in Figure 4.3. The computed $S(q,t)$ for $f = 0.03$ is compared with the corresponding experimental results in Figure 4.3 a. The two are in distinctive agreement, which allows a direct correlation of the reciprocal space results with the molecular insight attained from computational studies.

The computed $S(q,t)$ for the polymer, phenyl, and S rings of the SPS are shown for representative q values in Figure 4.3 b. As expected, for all three q values, the dynamic structural factor of the non-sulphonated phenyl ring decays faster than the sulfonated and the polymer ring. The dynamic structure factor for the entire polymer follows the motion of the non-sulfonated ring. With increasing q, the phenyl ring motion shows higher deviation from the sulfonated one and the polymer motion. Similar trends have been previously obtained for SPS melts.[17] As $S(q,t)$ averages over clustered and non-clustered S-rings, together with coupling of the polymer backbone to the solvent, the differences in local dynamics of the S-rings and the rest of the chains are smaller. The effective diffusion constants extracted from the computed $S(q,t),$ shown in Figure 4.3 c, follow the same trend as the experimental one for the entire polymer.
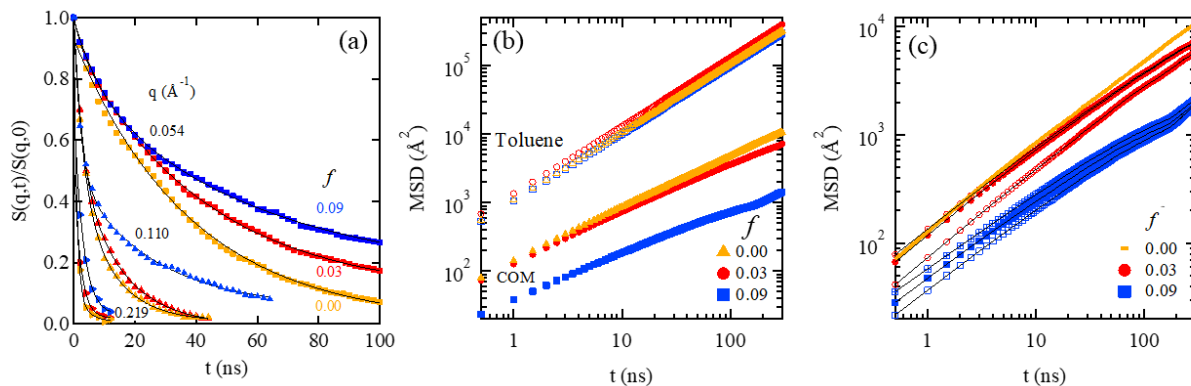
Figure 4.4: (a) Calculated $S(q,t)$ at the indicated sulfonation fractions for $f = 0$, 0.03, and 0.09 at the indicated q values. The solid lines are the results of fitting to the sum of two exponents, eq. 1. (b) MSD of the center of mass as a function of time at the indicated sulfonation fractions and MSD of the toluene (c) MSD the polymer backbone marked by full symbols the Ph-ring marked be empty ones, and S-Ring by a crossed symbol. The PS is marked by a line only.

The impact of the degree of clustering and their size is reflected in computed $S(q,t)$, where increasing sulfonation fraction results in slower decay as shown in Figure 4.4 a. However, the effects vary with length scale. At low q, where the inter-cluster correlations and direct tethering of the chains dominate, the effect of f is the largest and $S(q,t)$ for $f = 0.03$ and 0.09 are distinctive. At intermediate q ($q = 0.1$ Å^{-1}), the dynamics of $f = 0.09$ captures slower dynamics compared with that of $f = 0$ and 0.03. As q increases, probing smaller dimensions, the motion the dynamics becomes faster where $f = 0$ and 0.03 are hardly distinguishable and $f = 0.09$ is only slightly slower. The motion of the entire chains is captured by the mean square displacement (MSD) shown in Figure 4.4 b for the center of mass (COM) of the polymers, where $MSD = \sum_{i=1}^{N} < |r_i(t) - r_i(0)|^2 >/N$ with N in the number of atoms, $r_i(t)$ and $r_i(0)$ are the position of atom i at times t and 0, respectively. The average is over different starting times. MSD clearly decreases with increasing sulfonation, where MSD of the non-sulfonated chain increases linearly with time, that of $f = 0.03$ and 0.09 solutions curve towards leveling off at longer times, typical for constraint diffusion. This

effect is further manifested in MSD of the separate constituents of the polymer, shown in Figure 4.4 c where MSD of the sulfonated ring is slower than that of the non-sulfonated ones.

Comparing the motion depicted by MSD with segmental dynamics attained from NSE, translate the molecular insight into the mesoscopic length scale. For $f = 0.03$, the time for a monomer on the backbone to move an average distance of order $l = 2\pi/q$ is approximately the time it takes for $S(q,t)$ to decay by 90%. This indicates that decay times measured by the dynamic structure factor are dominated by the single chain relaxation. However, for $f = 0.09$, in the time $S(q,t)$ decays by 90%, the average distance a monomer on the backbone moves is much less than $2\pi/q$, indicating that the decay of $S(q,t)$ is dominated by the collection motion of the chains. For example, for $q = 0.011$ Å^{-1}, $l = 57$ Å, in the time for $S(q,t)$ to decay, the average displacement of monomers on backbone is ~ 55 Å for f = 0.03 and $\sim$32 Å for $f = 0.09$. Similar behavior characterizes all q values measured.
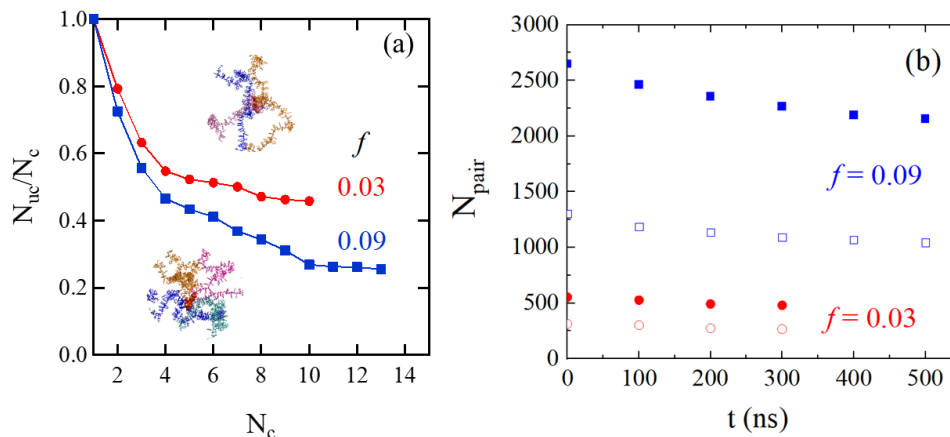
Figure 4.5: a) Number of unique chains N_{UC} normalized to the number of sulfur atoms N_c in a cluster for $f = 0.03$ and 0.09, together with visualization of one cluster and the associated chains for each case. b) Number of pairs N_{pair} of sulfur atoms that remain in the same cluster as a function of time for all S pairs (filled) and for S pairs tethered to different chains (open).

The polymer chains are confined to the network through clustering, however the network remains mobile and moves in the solvent, while polymer remains confined to the cluster. The number of

distinctive, unique chains that participate in each of the clusters normalized to the number of sulfur atoms in a cluster N_c, is shown in Figure 4.5 a. Sulfur atoms residing within 6 Å radius of each other are defined to be in the the same cluster.[39] The average cluster size for $f = 0.03$ is 2.8 and for $f = 0.09$, it is 3.8. On average more than one chain associated with each cluster for clusters of size $N_c > 2$. Therefore, the clusters consist of sulfur groups from distinctive chains as well as intra-molecular association. With the long-lived nature of these clusters, chains directly participate in more than one cluster driving macroscopic constraint motion. The clusters' "survival time" was measured by calculating the number N_{pair} of pairs of sulfur atoms that remain in the same cluster as a function of time (Figure 4.5 b). These results show that over times scale where $S(q,t)$ decays, the ionic clusters hardly change.

4.5 Conclusions

The results attained from neutron spin echo studies and MD simulations, combing real and reciprocal space, have resolved a long-standing critical challenge of how constraints exerted by assembly of limited number of ionic segments affects macroscopic dynamics in networks formed by ionizable polymer solutions. NSE and MD simulations were carried out on a model system of low sulfonation SPS in the acid and sodium salt respectively, in toluene. We show that SPS forms long lived clusters of the ionizable groups, whose survival time is longer than microsecond, directly affecting the motion of the segments that are confined to the clusters. These clusters consist of ionizable groups that reside either on the same chain or on distinctive chains, where those who reside on different chains, constrain the dynamics on the mesoscopic length scale. Direct bridging between clusters, even by very few chains drive the larger scale constraint of the motion observed by rheology. Combining the results from real spaces and reciprocal space have enabled

the realization of a long-standing challenge in polymers, an approach that will facilitate the understanding of complex systems and whose dynamics is coupled across time and length scales.

4.6 Acknowledgements

4.7 Appendix

Element	Scattering lengths (10^{-15} m)
H	-3.74
D	6.67
C	6.65
S	2.80
O	5.80
Na	3.63

Table A4.1: Neutron scattering lengths for selected elements.
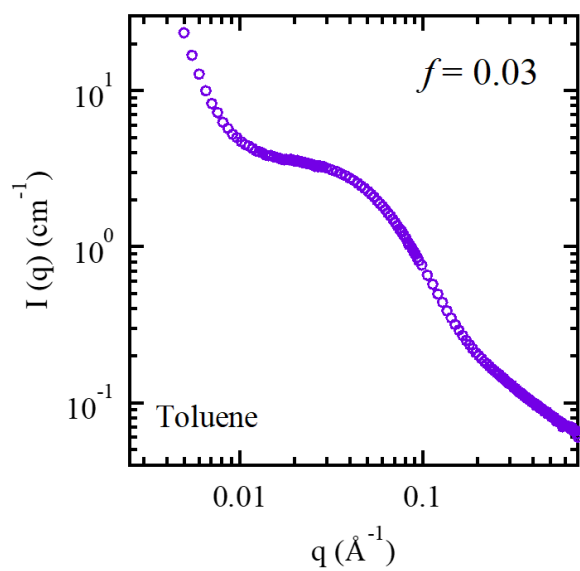
Figure A4.1: SANS patterns of *I(q)* versus *q* for *f* = 0.03 for 10 Wt% SPS in toluene at 303K
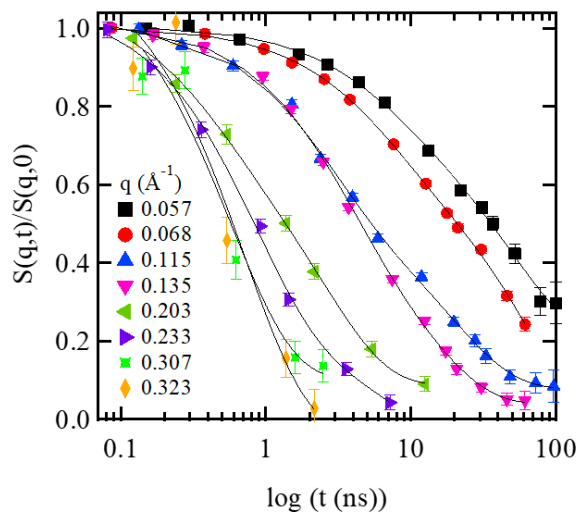
Figure A4.2: Dynamic structure factor *S(q,t)* versus log(t) from NSE for *f* = 0.03 at 303 K in a range of q values
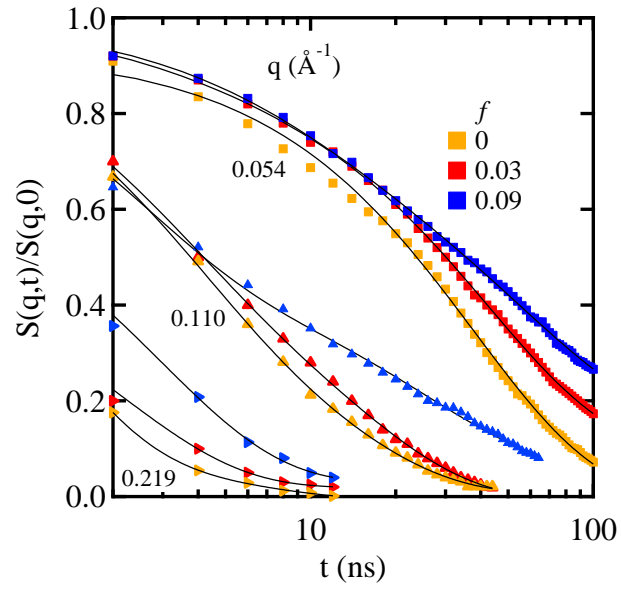
Figure A4.3: Dynamic structure factor $S(q,t)$ versus log(t) from simulations for $f = 0$ (yellow), $f = 0.03$ (red) and $f = 0.09$ (blue) at 303 K in a range of q values
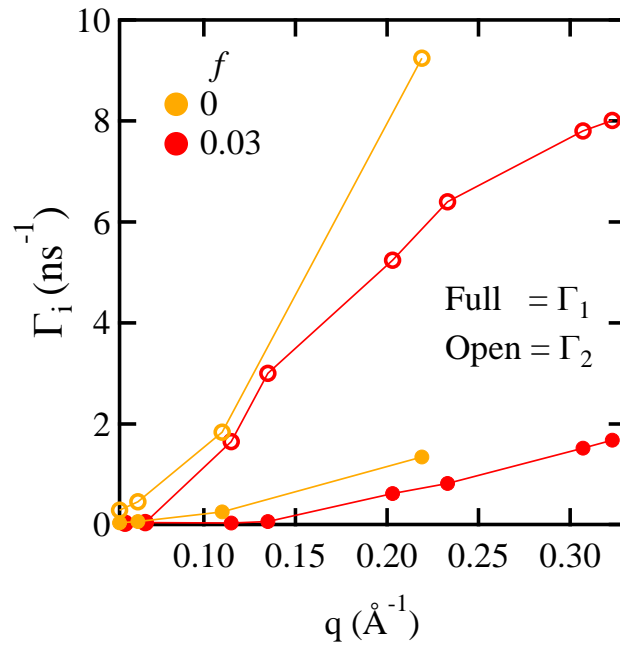
Figure A4.4: The relaxation rates Γ_1 (full) and Γ_2 (open) extracted from the fitting to double exponential function for the computed dynamic structure factors as a function of q for the $f = 0$ (yellow) and $f = 0.03$ (red)
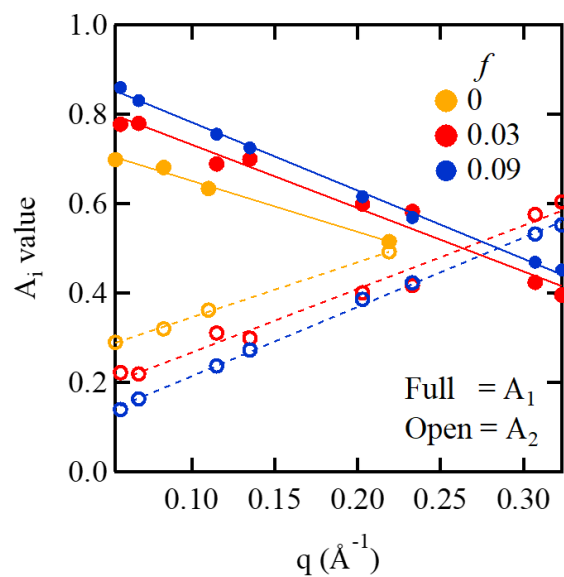
Figure A4.5: A_1 and A_2 values for $f = 0$, $f = 0.03$ and $f = 0.09$ from double exponential
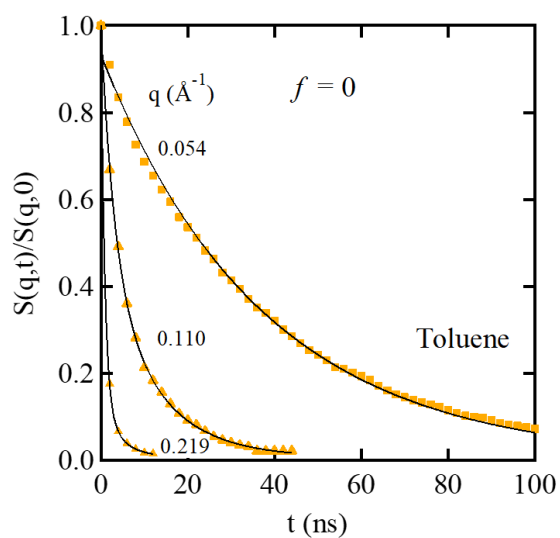
Figure A4.6: Calculated $S(q,t)$ for $f = 0$ at the indicated q values. The solid lines are the results of fitting to the sum of two exponents.
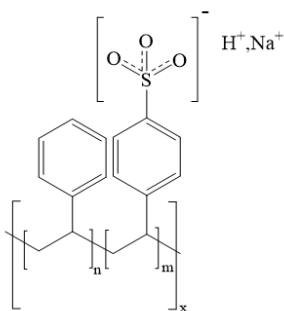
Figure A4.7: Structure of SPS

4.8 References

(1) Goyal, P.; Kusoglu, A.; Weber, A. Z. Coalescing Cation Selectivity Approaches in Ionomers. *ACS Energy Letters* **2023**, *8* (3), 1551-1566.

(2) Mardle, P.; Chen, B.; Holdcroft, S. Opportunities of Ionomer Development for Anion-Exchange Membrane Water Electrolysis: Focus Review. *ACS Energy Letters* **2023**, *8*, 3330-3342.

(3) Wang, J.; Wu, B.; Wei, P.; Sun, S.; Wu, P. Fatigue-free artificial ionic skin toughened by self-healable elastic nanomesh. *Nature Communications* **2022**, *13*, 4411.

(4) Shivers, J. L.; Sharma, A.; MacKintosh, F. C. Strain-Controlled Critical Slowing Down in the Rheology of Disordered Networks. *Phys. Rev, Lett.* **2023**, *131*, 178201.

(5) Jones, T. J.; Dupuis, T.; Jambon-Puillet, E.; Marthelot, J.; Brun, P.-T. Soft deployable structures via core-shell inflatables. *Phys. Rev. Lett.* **2023**, *130*, 128201.

(6) Lou, Y. Appetizer on soft matter physics concepts in mechanobiology. *Develop. Growth Differ.* **2023**, *65*, 234-244.

(7) Rao, A.; Olsen, B. D. Structural and dynamic heterogeneity in associative networks formed by artificially engineered protein polymers. *Soft Matter* **2023**, *19*, 6314-6328.

(8) Webber, M. J.; Tibbitt, M. W. Dynamic and reconfigurable materials from reversible network interactions. *Nature Rev. Mater.* **2022**, *7*, 541-556.

(9) Zhao, J.; Meng, F. Modeling Viscoelasticity and Dynamic Nematic Order of Exchangeable Liquid Crystal Elastomers. *Phys. Rev. Lett.* **2023**, *131*, 068101.

(10) Weiss, R.; Zhao, H. Rheological behavior of oligomeric ionomers. *J. Rheology* **2009**, *53*, 191-213.

(11) Colby, R.; Zheng, X.; Rafailovich, M.; Sokolov, J.; Peiffer, D.; Schwarz, S.; Strzhemechny, Y.; Nguyen, D. Dynamics of lightly sulfonated polystyrene ionomers. *Physical review letters* **1998**, *81* (18), 3876.

(12) Mohottalalage, S. S.; Kosgallana, C.; Meedin, S.; O'Connor, T. C.; Grest, G. S.; Perahia, D. Response of Sulfonated Polystyrene Melts to Nonlinear Elongation Flows. *Macromolecules* **2023**, *56* (3), 947-953.

(13) Ohl, M.; Monkenbusch, M.; Arend, N.; Kozielewski, T.; Vehres, G.; Tiemann, C.; Butzek, M.; Soltner, H.; Giesen, U.; Achten, R. The spin-echo spectrometer at the Spallation Neutron Source (SNS). *Nuclear Instruments and Methods in Physics Research Section A: Accelerators, Spectrometers, Detectors and Associated Equipment* **2012**, *696*, 85-99.

(14) Zamponi, M.; Kruteva, M.; Monkenbusch, M.; Willner, L.; Wischnewski, A.; Hoffmann, I.; Richter, D. Cooperative Chain Dynamics of Tracer Chains in Highly Entangled Polyethylene Melts. *Phys. Rev. Lett.* **2021**, *126*, 187801.

(15) Arrighi, V.; Higgins, J. S. Local effects of ring topology observed in polymer conformation and dynamics by neutron scattering—A review. *Polymers* **2020**, *12*, 1884.

(16) Agrawal, A.; Perahia, D.; Grest, G. S. Clustering effects in ionic polymers: Molecular dynamics simulations. *Physical Review E* **2015**, *92* (2), 022601.

(17) Agrawal, A.; Perahia, D.; Grest, G. S. Cluster morphology-polymer dynamics correlations in sulfonated polystyrene melts: computational study. *Physical review letters* **2016**, *116* (15), 158001.

(18) Eisenberg, A. Clustering of ions in organic polymers. A theoretical approach. *Macromolecules* **1970**, *3* (2), 147-154.

(19) Bazuin, C.; Eisenberg, A. Ion containing polymers: Ionomers. ACS Publications: 1981.

(20) Eisenberg, A.; Hird, B.; Moore, R. A new multiplet-cluster model for the morphology of random ionomers. *Macromolecules* **1990**, *23* (18), 4098-4107.

(21) Rigdahl, M.; Eisenberg, A. Viscoelastic properties of sulfonated styrene ionomers. *Journal of Polymer Science: Polymer Physics Edition* **1981**, *19* (10), 1641-1654.

(22) Lu, X.; Steckle, W.; Weiss, R. Ionic aggregation in a block copolymer ionomer. *Macromolecules* **1993**, *26* (22), 5876-5884.

(23) Qiao, X. Nonlinear Rheology of Lightly Sulfonated Polystyrene Ionomers. *Macromolecules* **2013**, *v. 46* (no. 6), pp. 2417-2424-2013 v.2446 no.2416. DOI: 10.1021/ma3026496 From National Agricultural Library PubAg.

(24) Zhang, L.; Brostowitz, N. R.; Cavicchi, K. A.; Weiss, R. Perspective: Ionomer research and applications. *Macromolecular Reaction Engineering* **2014**, *8* (2), 81-99.

(25) Weiss, R.; Yu, W.-C. Viscoelastic behavior of very lightly sulfonated polystyrene ionomers. *Macromolecules* **2007**, *40* (10), 3640-3643.

(26) Chen, Q.; Huang, C.; Weiss, R.; Colby, R. H. Viscoelasticity of reversible gelation for ionomers. *Macromolecules* **2015**, *48* (4), 1221-1230.

(27) Ling, G. H.; Wang, Y.; Weiss, R. Linear viscoelastic and uniaxial extensional rheology of alkali metal neutralized sulfonated oligostyrene ionomer melts. *Macromolecules* **2012**, *45* (1), 481-490.

(28) Mohottalalage, S. S.; Senanayake, M.; Clemmer, J. T.; Perahia, D.; Grest, G. S.; O'Connor, T. Nonlinear elongation flows in associating polymer melts: from homogeneous to heterogeneous flow. *Physical Review X* **2022**, *12* (2), 021024.

(29) Nyström, B.; Roots, J.; Higgins, J.; Gabrys, B.; Peiffer, D.; Mezei, F.; Sarkissian, B. Dynamics of polystyrene sulfonate ionomers in solution. A neutron spin-echo study. *Journal of Polymer Science Part C: Polymer Letters* **1986**, *24* (6), 273-281.

(30) De Luca, E.; Waigh, T. A.; Monkenbusch, M.; Kim, J. S.; Jeon, H. S. Neutron spin echo study of the dynamics of micellar solutions of randomly sulphonated polystyrene. *Polymer* **2007**, *48* (14), 3930-3934.

(31) Mohottalalage, S. S.; Kosgallana, C.; Senanayake, M.; Wijesinghe, S.; Osti, N. C.; Perahia, D. Molecular Insight into the Effects of Clustering on the Dynamics of Ionomers in Solutions. *ACS Macro Letters* **2023**, *12*, 1118-1124.

(32) Zolnierczuk, P.; Holderer, O.; Pasini, S.; Kozielewski, T.; Stingaciu, L.; Monkenbusch, M. Efficient data extraction from neutron time-of-flight spin-echo raw data. *Journal of applied crystallography* **2019**, *52* (5), 1022-1034.

(33) Jorgensen, W. L.; Maxwell, D. S.; Tirado-Rives, J. Development and testing of the OPLS all-atom force field on conformational energetics and properties of organic liquids. *Journal of the American Chemical Society* **1996**, *118* (45), 11225-11236.

(34) Jorgensen, W. L.; Madura, J. D.; Swenson, C. J. Optimized intermolecular potential functions for liquid hydrocarbons. *Journal of the American Chemical Society* **1984**, *106* (22), 6638-6646.

(35) Thompson, A. P.; Aktulga, H. M.; Berger, R.; Bolintineanu, D. S.; Brown, W. M.; Crozier, P. S.; in't Veld, P. J.; Kohlmeyer, A.; Moore, S. G.; Nguyen, T. D. LAMMPS-a flexible simulation tool for particle-based materials modeling at the atomic, meso, and continuum scales. *Computer Physics Communications* **2022**, *271*, 108171.

(36) Berendsen, H. J.; van der Spoel, D.; van Drunen, R. GROMACS: A message-passing parallel molecular dynamics implementation. *Computer physics communications* **1995**, *91* (1-3), 43-56.

(37) Abraham, M. J.; Murtola, T.; Schulz, R.; Páll, S.; Smith, J. C.; Hess, B.; Lindahl, E. GROMACS: High performance molecular simulations through multi-level parallelism from laptops to supercomputers. *SoftwareX* **2015**, *1*, 19-25.

(38) Pronk, S.; Páll, S.; Schulz, R.; Larsson, P.; Bjelkmar, P.; Apostolov, R.; Shirts, M. R.; Smith, J. C.; Kasson, P. M.; Van Der Spoel, D. GROMACS 4.5: a high-throughput and highly parallel open source molecular simulation toolkit. *Bioinformatics* **2013**, *29* (7), 845-854.

(39) Kosgallana, C.; Senanayake, M.; Wijesinghe, S.; Mohottalalage, S.; He, L.; Grest, G. S.; Perahia, D. Clustering Effects on the Structure of Ionomer Solutions: A Combined SANS and Simulations Study. *Macromolecules (in review)* **2024**.

CHAPTER FIVE

FROM IONIC CLUSTERS DYNAMICS TO NETWORK CONSTRAINTS IN IONIC POLYMER SOLUTIONS

5.1 Abstract

Physical networks formed by ionizable polymers with ionic clusters as crosslinks are controlled by coupled dynamic events that transcend the ionic clusters through chain motion to macroscopic response. Here coupled dynamics, across length scales, from the ionic clusters to the networks in toluene swollen polystyrene sulfonate networks, was directly correlated using neutron spin echo measurements and molecular dynamics simulations carried out to times typical of relaxation of polymers in solutions. The experimental dynamic structure factor is correlated with the calculated one for computed solutions as the networks are perturbed by elevating the temperature and changing the electrostatic environment. In toluene, the long-lived clusters remain stable over hundreds of ns across a broad temperature range, while the polymer network remains dynamic. Though the size of the clusters changes as the dielectric constant of the solvent is modified through addition of ethanol, they remain stable but morph, enhancing the polymer chain dynamics.

5.2 Introduction

Ionizable polymers form networks through physical crosslinks of clustered ionizable groups. The heterogeneity of the structure and response of these complex networks enables their many applications, ranging from biotechnology to clean energy generation and storage.[1-4] In contrast to chemically crosslinked networks, the clusters constitute a dynamic bridge whose properties affect the network behavior in melts and in solutions.[5-7] Determining coupled dynamics across distinctive length scales remains a challenging open question, fundamental to these complex networks, and

critical to the design of ionizable polymers assemblies for targeted applications. Combining neutron spin echo (NSE) measurements with groundbreaking atomistic-level molecular dynamics (MD) simulations, a direct correlation between dynamics of intra-cluster events to network motion was attained. Reaching time scales of polymer chains dynamics in solutions was enabled by exascale computing and is a key to bridging between length scales. NSE probes mesoscopic length scales (0.5-40 nm) on a time scale of up to ~150 ns here and MD simulations access intra-cluster dynamics in correlation with that of the mesoscopic response of the networks. We find that small changes in intra-cluster structure is sufficient to impact the mesoscopic network dynamics and ultimately affect their macroscopic motion.

The dynamic processes across length scales of networks formed by a model polymer, sulfonated polystyrene (SPS) in toluene, a good solvent for the backbone and poor for the polar groups, are probed as the systems are perturbed by increasing the temperature and adding a polar solvent. Pioneering studies of Weiss and coworkers demonstrated the confining effects of ionic clusters on the rheology of SPS solutions.[8-12] Early NSE studies of SPS [13, 14] further affirmed that the ionic clusters confine segmental dynamics in solutions. Our recent NSE-MD study of SPS in toluene[7] have shown that while the network dynamics is constraint by the clusters, the highly solvated individual polymer chains remain dynamic.

The realization that clusters affect the structure and dynamics of these has driven several studies where their electrostatic environment was tweaked by controlling the counterion or changing the dielectric constant of the solvent.[10] Weiss and co-workers have shown that the counterions affect the structure and rheology of short oligomers.[9] Molecular insight attained by Agrawal et al.[15] showed that increasing the dielectric constant of the system decreases the cluster size, affecting their shape, and enhances the dynamics of SPS melt systems. Our quasi-elastic neutron scattering

(QENS) studies, have shown that the addition of small amounts of high dielectric solvents such as ethanol to SPS solutions in cyclohexane increases segmental dynamics on short length scales.[6] This enhanced motion has been attributed to reduced cluster dimensions in presence of ethanol, impacting the number of unique chains that reside in each of the clusters, thus reducing the bridging that controls the network. These studies have clearly shown that clustering affects the overall motion of the networks from directly confined network to macroscopic rheology response. However, the direct correlation between internal cluster dynamics, across length scales to the mesoscopic and macroscopic motion of ionomer networks, critical to the ability to tune the structure of these complex fluids, remains an outstanding challenge. This fundamental challenge is probed herein, through temperature and dielectric perturbations of the system, while simultaneously following their effects on intra-cluster characteristics and network dynamics.

5.3 Methodology

Here, experiments were carried out on randomly sulfonated polystyrene in its acid form, synthesized through anionic polymerizations, with sulfonation fractions of $f = 0.03$ and 0.09 and molecular weight of 11 kg/mol with a polydispersity index of 1.2 (Polymer Source [TM] Inc.). The polymer readily dissolves in d-toluene (Tol) and d-toluene/d-ethanol (Tol/EtOH) (Cambridge Isotope Laboratories, Inc.) to form 10 wt% solutions.

NSE experiments were performed at the spallation neutron source (SNS),[16] combining data from wavelengths 8 Å and 11 Å and Fourier times of 0.04 –100 ns. A sheet of graphite and Al_2O_3 powder, were measured and used to correct for instrument resolution. The solvents were run separately and subtracted from the data. The data were collected by an in-house program, and reduced to the form of $S(q,t)$ using the DrSpine program.[17] The temperature was controlled by SP FTS ThermoJet system with the accuracy of +/-0.5 K. Samples were encapsulated in 3 mm thick

quartz rectangular Hellma cells (Müllheim, Germany). Temprature dependence runs were carried out over a smaller q to enable measurements of all temperatures on the same solution. $S(q,t)$ were analyzed as a sum of two exponentials, extracting relaxation rates for a slow and a fast processes.[18] Fitting to a χ^2 of 4-6 were carries out, depending on the specific solution with an overall 10% error for the individual fitting parameters.

Comparable systems to the experiments were studied by MD simulations. The molecules were built using the polymer builder in BIOVIA[TM] Materials Studio with 148 unique, atatic sulfonated polystyrene chains and sulfonation fraction $f = 0$, 0.03, and 0.09, each with a total molecular weight of ~11 kg/mol with 106 monomers per chain with Na^+ as a counterion. The all atoms optimized potentials for liquid simulations (OPLS-AA) force fields [19, 20] were used to model the system. The initial simulations were carried out using the LAMMPS [21] and converted to GROMACS.[22-24] Each system contains between 2.4 - 2.5 million atoms and was run for 600-800 ns. The evolution of ionic clusters with time is given in Figure A5.1. These systems represent realistic states of the polymer in solutions that may often be in long lasting kinetically trapped states. Simulation details are given in the appendix.

5.4 Results

The experimentally measured $S(q,t)$ for $f=0.03$ as ethanol with a dielectric constant $\varepsilon = 25$ is added to toluene whose $\varepsilon = 2.37$ [25, 26] are shown in Figure 5.1 and are compared with $S(q,t)$ measured for toluene.[7] As little as 5 wt% ethanol added to toluene is manifested in a significantly faster decay of $S(q,t)$. The acceleration of dynamics takes place across all q values, with the largest effect is predominantly at the lower q regime where the inter ionic clusters correlations are expressed. At higher q values, where segmental dynamics is manifested, $S(q,t)$ decays to 0 within $4 - 40$ ns, and it is only slightly affected by the addition of ethanol. This q dependance provides direct evidence that cluster characteristics are critical to understanding their impact on mesoscopic motion of the network, where in addition to cluster size and morphology, inter-cluster dynamic events are critical.
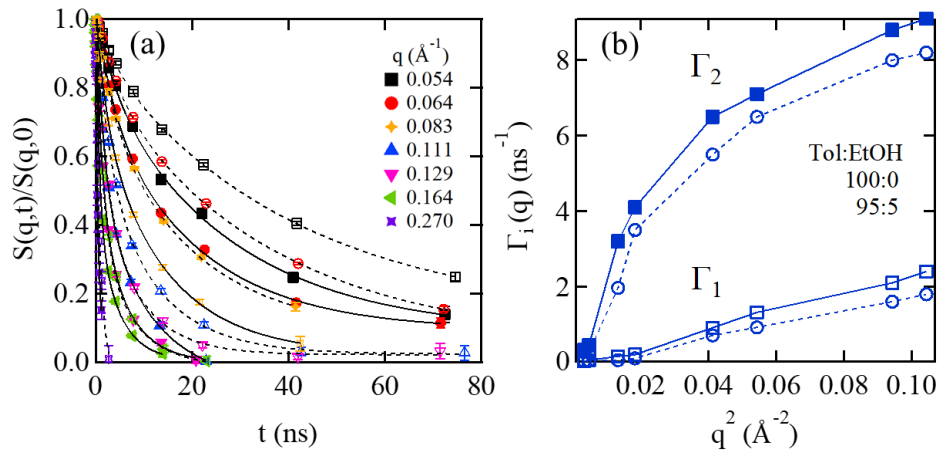
Figure 5.1: (a) NSE $S(q,t)$ for 10Wt% SPS solutions with $f = 0.03$ at 303 K as a function of time for the indicated q value for 95:5 Tol:EtOH (full lines) in comparison with toluene only (dashed lines) and (b) the relaxation rate constants $\Gamma_1(q)$ and $\Gamma_2(q)$ extracted from the fits to a double exponential function for NSE for 95:5 (bold) Tol:EtOH 100:0 (open).

$S(q,t)$ was analyzed in terms of a sum of two exponentials,

$$S(q,t)/S(q,0) = A_1 exp(-t/\tau_1(q)) + A_2 exp(-t/\tau_2(q))$$

where A_1 and A_2 are pre-exponentials that weigh the contributions of each of the process to $S(q,t)$, t is the time, and $\tau_1(q)$ and $\tau_2(q)$ are relaxation times.[18, 27] The data were initially fit to a KWW model,[28] which was unsuccessful capturing the entire q range for most systems. The relaxation rates $\Gamma_i(q)$, with $\Gamma_i(q) = 1/\tau_i(q)$, are plotted as a function of q^2 in Figure 5.1 b, with $\Gamma_1(q) < \Gamma_2(q)$. The coresponding representaion of these data in terms of effective diffusion constants $\Gamma_i(q)/q^2$ are plotted in Figure A5.2. The pre-exponential factors are presented in Table A5.1 of the appendix where $A_1 + A_2 \sim 1$. The relaxation rates exhibit two distinctive regions, with a crossover at $q \sim 0.02$ $Å^{-1}$. At low q, correlations on the inter-cluster dimensions are reflected, and segmental dynamics is expressed predominantly at higher q values. Even though $\Gamma_1(q)$ and $\Gamma_2(q)$ increase across the entire q range as ethanol is added, the dynamics remains that of a confined system.
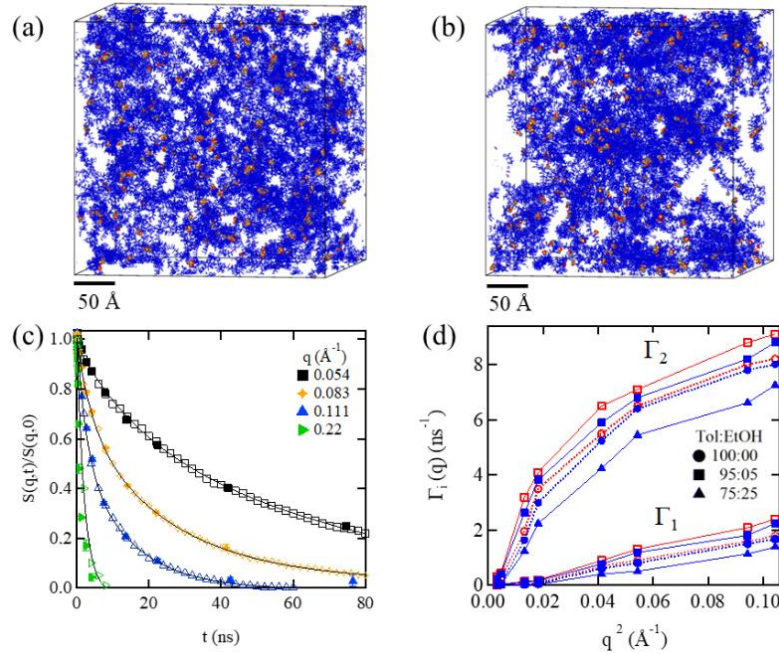
Figure 5.2: Visualization of 10Wt% $f = 0.03$ SPS in solution of Tol:EtOH (a) 95:5 and (b) 100:0, at 600 ns. Solvent molecules are removed for clarity. (c) Dynamic structure factor $S(q,t)$ as a function of q for Tol:EtOH 95:5 computational (open) and NSE (solid). The lines correspond to fitting of the computational data. (d) Relaxation rate Γ_i as a function of q^2, NSE (red) and simulations (blue) for Tol: EtOH 100:00 (circle) 95:5 (square) and 75:25 (triangle) at 300K.

Visualizations of computed solutions of Tol:EtOH 95:5 and 75:25 are shown in Fig 5.2 a,b. In both solutions, the size of the ionic clusters visually decreases, as shown in the cluster size evolution with time shown in Figure A5.1. With increasing ethanol levels, the chains agglomerate enhancing the heterogeneity of the networks for both solutions. However, the effect is more pronounced in the 75:25 Tol:EtOH solutions.

$S(q,t)$ calculated for the computed solutions is in distinctive agreement with the experimental measured values, as shown in Figure 5.2c. $\Gamma_1(q)$ and $\Gamma_2(q)$ of the computed solutions and the experimentally extracted ones, are presented in Figure 5.2d. $\Gamma_1(q)$ and $\Gamma_2(q)$ for 95:5 Tol:EtOH, are accelerated compared with those of toluene solutions, whereas for 75:25 Tol:EtOH are slower. The q dependence for both solutions follows that of toluene swollen networks.
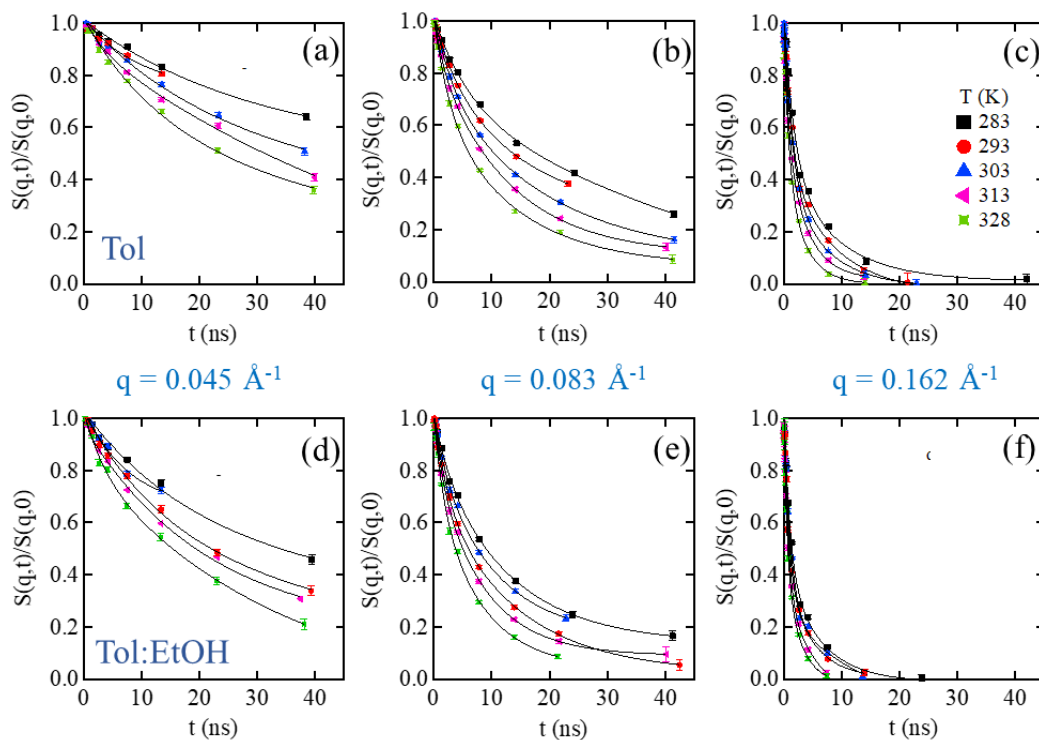
Figure 5.3: Representative NSE dynamic structure factor $S(q,t)$ for 10 wt% solutions of SPS $f = 0.03$ in toluene at (a) $q = 0.045$ Å^{-1} (b) 0.083 Å^{-1} and (c) 0.165 Å^{-1} and for $f = 0.03$ in 95:5 Tol:EtOH at the indicated q and temperature.

The networks are perturbed by increasing the temperature from 283K to 328 K for $f = 0.03$ in toluene and toluene-ethanol. Representative NSE spectra for low, intermediate, and high q regions for different temperatures are shown in Figure 5.3a and the corresponding $\Gamma_1(q)$ and $\Gamma_2(q)$ are presented in Figure 5.3 b,c. With increasing temperature $S(q,t)$ decays faster for both solutions. The response of the Tol:EtOH solutions to temperature increase is larger than that of Tol solutions. At all temperatures $\Gamma_1(q)$ and $\Gamma_2(q)$ exhibit two distinct length scales with a cross over region. However, at low q, $\Gamma_1(q)$ hardly changes up to $q \sim 0.1$ Å^{-1}, and above, it increases almost linearly. $\Gamma_2(q)$, the faster motion constant, exhibits a similar trend however the crossover takes place across a broader q range. In this temperature range, despite the enhanced motion, the dependence $\Gamma_i(q)$ on q^2 diverge from linearity as the chains remain confined.
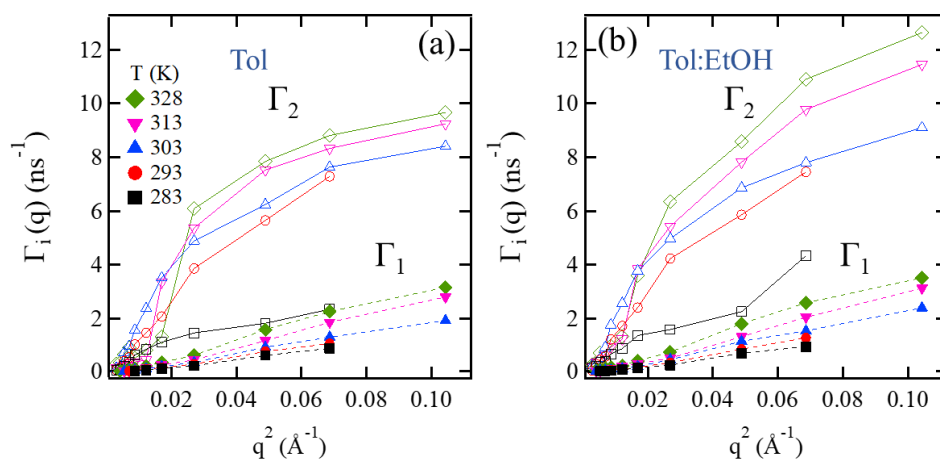
Figure 5.4: Relaxation rates $\Gamma_1(q)$ (dashed lines) and $\Gamma_2(q)$ (solid lines) a function of q^2 for 10% SPS solutions $f = 0.03$ in (a) toluene and (b) 95:5 Tol:EtOH, at the indicated temperatures.
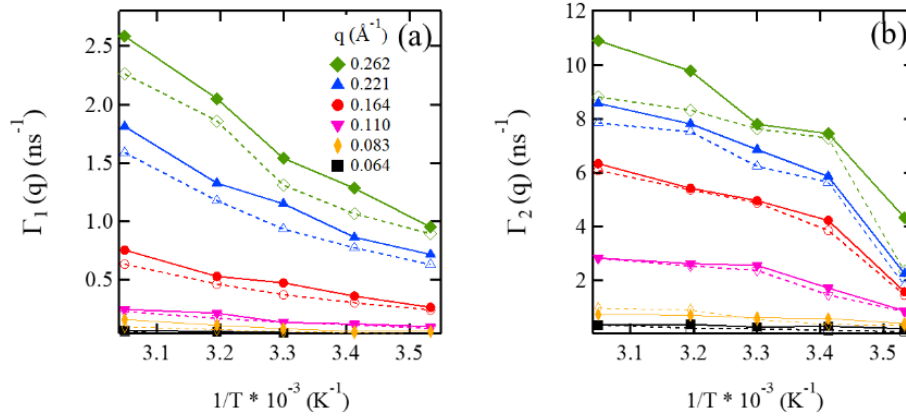
Figure 5.5: Relaxation rates (a) $\Gamma_1(q)$ and (b) $\Gamma_2(q)$ as a function of 1/T for $f = 0.03$ 10Wt.% SPS in toluene (open) and 95:5 Tol:EtOH (filled) at the indicated q values.

$\Gamma_i(q)$ are plotted as a function of $1/T$ for selected q values in Figure 5.5. At low q values, increasing temperature has a minimal effect on $\Gamma_1(q)$. However, at higher q, $\Gamma_1(q)$ varies significantly more with temperature. $\Gamma_2(q)$ increases with increasing temperature for all q values. Both $\Gamma_i(q)$ increase with increasing temperature, where the slow relaxation constant, is linear within the accuracy of the fitting which is ~10%. The faster relaxation rate diverges from linearity with a crossover at ~303K. The difference in temperature response reveals that cluster intercorrelation is hardly affected by temperature. The temperature, however, affects segmental motion of the highly solvated chains. Elevating the temperature from 283K to 328K results in a small energy change of ~ 0.09 kcal/mol, which is significantly smaller than the electrostatic energy that holds together ionizable clusters however it is sufficient to impact solvated segmental dynamics.

This trend however is more pronouced in Tol:EtOH solusions where the clusters are perturbed. Together with previous observations of the impact of added alcohol on the structure[29] and

81

dynamcis[7] of ionizable polymers, it becomes evident that the internal dynamics of the clusters alters the overall motion of the polyemrs on the mesoscopic length sacle.
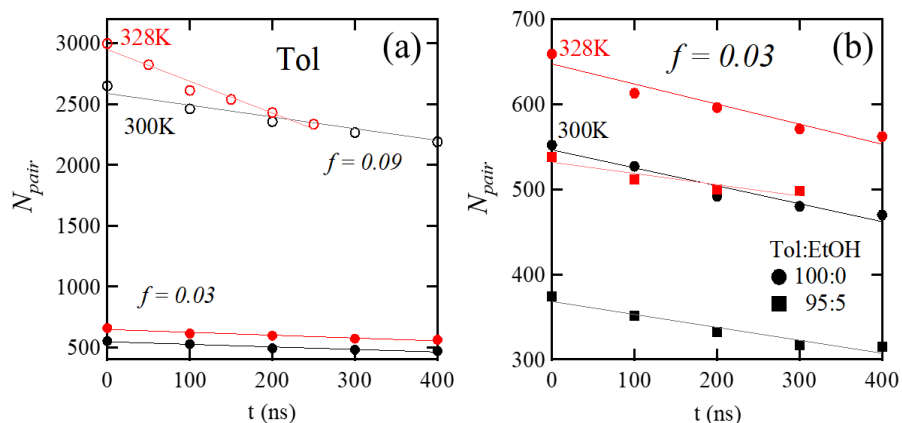
Figure 5.6: The number of S-S pairs at $t = 0$ that reside in a distinctive cluster and remain in that cluster as a function of time in 10 wt% SPS a) in toluene for $f = 0.03$ (filled) and $f = 0.09$ (open) b) in toluene (circles) and Tol:EtOH (squares(for $f = 0.03$ at 300K (black) and 328K (red).

The internal dynamics of the clusters including the survivial time of pairs of sulfonated groups across the solutions and the time dependance of the intra-cluster correlations were measured for the computed solusions. The survival time of pairs of sulfur atoms that initally reside in the same ionic clusters as time evolves, are shown in Figure 5.6 a for $f=0.03$ and $f=0.09$ in toluene at two temperatures. Surprisingly, though over long times their number decreases; there is hardly any exchange of ionizable groups between clusters over the time of the network dynamcis. Though the addition of alcohol changes the total number of pairs, seen in Figure 5.6 b, the average cluster size increases (Figure A5.2), the rate at which sulfur atoms leave the clusters remain the same, independend of the presence of alcohol.
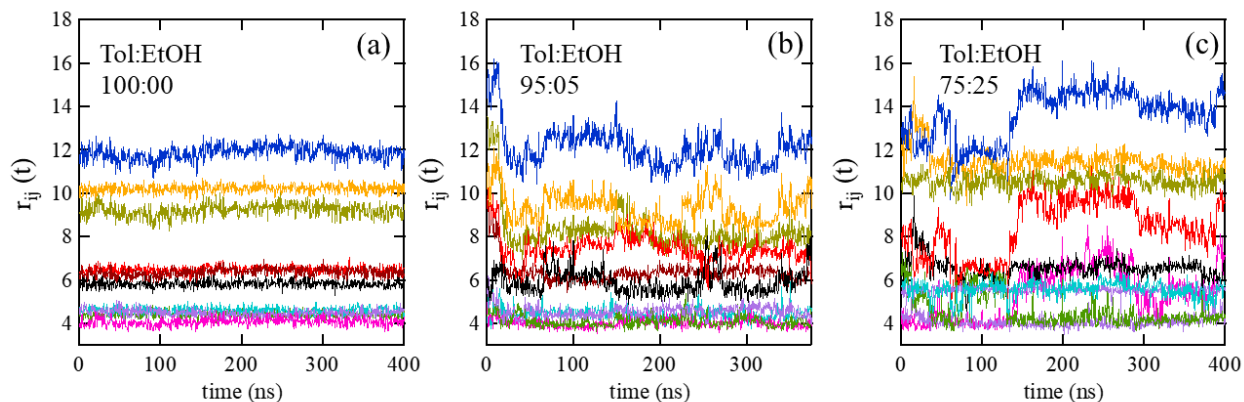
Figure 5.7: Distance $r_{ij}(t)$ between all sulfur atoms i and j in a representative cluster of size 6 as a function of time for 10 wt% SPS with $f = 0.09$ for Tol:EtOH a) 100:0 b) 95:5 and c) 75:5.

The internal dynamics was followed through measurement of the distance $r_{ij}(t)$ between all sulfur atoms i and j that reside in an ionic cluster, as a function of time. Shown in Figure 5.7 are the results for all 15 S-S pairs for a representative cluster of size 6 for $f = 0.09$ with Tol:EtOH ratios of 100:0, 95:5 and 75:25. In pure toluene, the cluster moves as a rigid body with no exchange of neighbors and little fluctuations in the internal distances over 400 ns. Raising the temperature to 328K, does not affect this pattern. With the addition of ethanol, the sulfur atoms within the cluster become more dynamic where $r_{ij}(t)$ increases over the 400 ns. At the higher temperature, intra cluster neighbor exchanges, which is strongly manifested in 75:25 Tol:EtOH.

Screening the electrostatic interactions by ethanol, even though the solvent molecules remain localized around the cluster, is sufficient to allow internal motion that enables the clusters to morph and change their shape. As it has been previously shown, the shape of the clusters affects network dynamics on the length scale captured by NSE.[7] Therefore, this dynamics on short time scales, is coupled through instantaneous shape change to the much slower motion of the clusters and the entire network.

5.5 Conclusions

With insight from NSE measurements and real space results, from MD simulations, we were able to extract and bridge dynamic events across the time and length scales that control the behavior of highly heterogeneous networks formed by solutions of ionizable polymers. A unique agreement between $S(q,t)$ extracted from both techniques allows transposing of data across length scales from intra cluster events to that of the networks. $S(q,t)$ is analyzed in terms of two characteristic relaxation rates, slow and fast, where the slow one is associated with inter ionic cluster correlations and the faster one captures segmental dynamics of the solvated chains. Internal cluster dynamics is attained from MD simulations.

In both networks, the clusters are long lived, and significant numbers of sulfur pairs remain in the same clusters for 600-800ns, with very little exchange of ionizable groups between the clusters. In toluene, the internal structure of these clusters hardly changes with time and is not affected by temprature, while the network, however, remains dynamic on the mesoscopic length scale, as evident by NSE measurements. The addition of a polar solvent hardly affects the survival times of the clusters, but does affect the intrinsic dynamics, allowing the clusters to morph and in turn enhances the network dynamics. Temprature enhances the dynamics of the solvated chains independent of the nature of the solvent.

With this two-prong approach, this study was able to identify the dynamics within ionic clusters of a model highly swollen ionic polymer network and provide a first direct correlation between intrinsic dynamics of the ionic assemblies and that of the network. Beyond the impact of the results on ionic polymers' enabling technologies, this approach of combining neutron scattering and simulation would impact a broad range of soft matter systems that are governed by highly distinctive interactions.

5.6 Acknowledgements

5.7 Appendix

Molecular Dynamics Simulations

Sulfonated polystyrene, toluene and ethanol was built using the polymer builder in BIOVIA^{TM} Materials Studio. The system contained 148 unique, atatic sulfonated polystyrene chains with sulfonation fraction f = 0, 0.03 and 0.09, each with a total molecular weight of ∼11 kg/mol with 106 monomer per chain with Na^+ as a counterion. As in the experiments, the computer solutions consist of 10 wt% polymer in pure toluene and toluene, ethanol mixtures. Each system contains between 2.4 - 2.5 million atoms.

The all atoms optimized potentials for liquid simulations (OPLS-AA) force fields, developed by Jorgensen et al. [19, 20] were used to model the system. This potential includes bonded and non-bonded terms. The bonded potential is sum of intermolecular bond, angle, and dihedral interactions. The non-bonded interactions are described by Lennard-Jones potential with an attractive r^{-6} and repulsive r^{-12} terms and a long-range Coulomb interaction.

Simulations were initially carried out using LAMMPS [21]. The Newton equations of motions were integrated using a velocity-Verlet algorithm with a time step of *1 fs*. The Lennard-Jones interactions are truncated at 1.2 nm. The Coulomb interactions are treated with long-range particle-

particle particle-mesh (PPPM) algorithm with a real space cutoff of 1.2 nm and a precision of 5×10^{-4}. Periodic boundary conditions were used for all simulations.

The solvents were added after the polymer system was run for 100 ns at 300K in an implicit good solvent. Each system was first run at constant pressure of 1 atm using the Nosé-Hoover thermostat and barostat [30, 31] for 10 ns to obtain the correct density. The final dimension of the cell is $L \sim 31.0$ nm for the 3 values of f, which is much larger than the size of a polymer chain whose radius of gyration R_g is $28 - 31$ Å. To allow the chains to locally equilibrate the dielectric constant ε was increased from 1 to 30 to reduce the residual electrostatic screening between ionic groups. The solution systems were run for 30 ns at constant volume after which the dielectric constant was reset to 1.

The LAMMPS data were then converted to GROMACS [22-24] to enhanced efficiency. The electrostatics were treated using particle mesh Ewald [32] (PME) algorithm and Fourier grid spacing of 0.12 nm. All harmonic bonds involving hydrogen atoms were replaced with constraints. The temperature was maintained using the Bussi-Parrinello thermostat (V-rescale) [33] with a time constant of 0.1 ps. The simulations were carried out using 2 fs time step. Each system was then run at a constant volume at $T = 300$ K for 600-800 ns. Time $t = 0$ corresponds to the beginning of the run in GROMACS. The temperature was then increased to 328 K and ran at constant pressure for 10 ns and then ran at constant volume for 300-400 ns.

The dynamic structure factor $S(q,t)$ was calculated for the computed solutions using

$$S(q,t) = \sum_{i,j=1}^{N} b_i\, b_j e^{[i\boldsymbol{q}\cdot(\boldsymbol{r}_i(t)-\boldsymbol{r}_j(0))]} \, / \, \sum_{i=1}^{N} b_i^2 \qquad (A1)$$

where b_i are the neutron scattering lengths of atom i and $r_i(t)$ position of atom i at time t. Due to the periodic boundary conditions, the wavevectors q are limited to $q = 2\pi/L$ (n_x, n_y, n_z), where L is the length of the simulation cell and n_x, n_y, and n_z are integers.
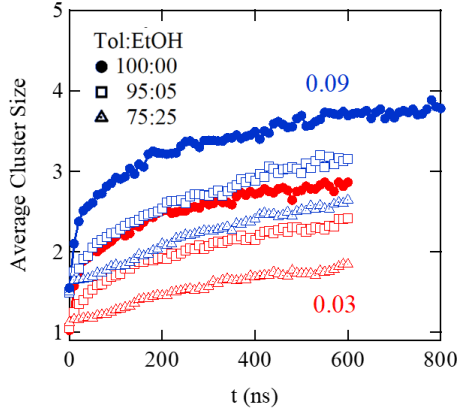
Figure A5.1. Cluster size as a function of time for the indicated solutions. Cluster size is calculated by the number of S atoms within 6 Å.
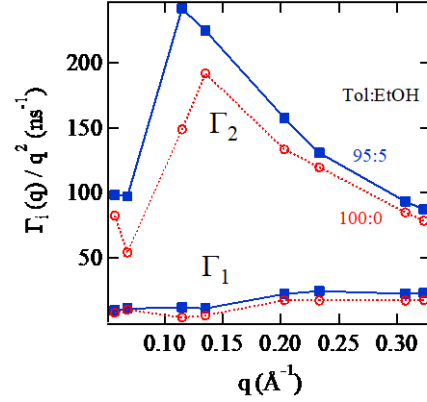
Figure A5.2: Effective diffusion constants $\Gamma_i(q)/q^2$ extracted from fitting to a sum of two exponential functions as a function of q^2. NSE data for Tol:EtOH 100:00 (open circles) and 95:5 (filled squares) for $f = 0.03$ at $T = 303$ K

Tol				Tol:EtOH 95:5		
q (Å^{-1})	A_1	A_2		q (Å^{-1})	A_1	A_2
0.057	0.778	0.222		0.057	0.871	0.162
0.068	0.780	0.219		0.068	0.792	0.182
0.115	0.689	0.311		0.115	0.714	0.274
0.135	0.700	0.299		0.135	0.672	0.291
0.203	0.599	0.401		0.203	0.558	0.472
0.233	0.583	0.417		0.233	0.482	0.492
0.307	0.424	0.576		0.307	0.351	0.621
0.323	0.396	0.604		0.323	0.311	0.674

Table A5.1: Examples for A_i values extracted from the fitting of the NSE data to a sum of two exponentials for $f = 0.03$ and $T = 303$ K. An error of 10% is associated with these fitted parameters.

5.7 References

(1) Favero, S.; Stephens, I. E.; Titirci, M. M. Anion Exchange Ionomers: Design Considerations and Recent Advances-an Electrochemical Perspective. *Advanced Materials*, 2308238.

(2) Lee, J. K.; Anderson, G.; Tricker, A. W.; Babbe, F.; Madan, A.; Cullen, D. A.; Arregui-Mena, J. D.; Danilovic, N.; Mukundan, R.; Weber, A. Z. Ionomer-free and recyclable porous-transport electrode for high-performing proton-exchange-membrane water electrolysis. *Nature Communications* **2023**, *14* (1), 4592.

(3) Malik, Z.; Muhammad, N.; Kaleem, M.; Nayyar, M.; Qazi, A. S.; Butt, D. Q.; Safi, S. Z.; Khan, A. S. Anticariogenic and Mechanical Characteristics of Resin-Modified Glass Ionomer Cement Containing Lignin-Decorated Zinc Oxide Nanoparticles. *ACS Applied Bio Materials* **2023**, *6* (2), 425-435.

(4) Balding, P.; Borrelli, R.; Volkovinsky, R.; Russo, P. S. Physical properties of sodium poly (styrene sulfonate): comparison to incompletely sulfonated polystyrene. *Macromolecules* **2022**, *55*, 1747-1762.

(5) Middleton, L. R.; Winey, K. I. Nanoscale aggregation in acid-and ion-containing polymers. *Annual review of chemical and biomolecular engineering* **2017**, *8*, 499-523.

(6) Mohottalalage, S. S.; Kosgallana, C.; Senanayake, M.; Wijesinghe, S.; Osti, N. C.; Perahia, D. Molecular Insight into the Effects of Clustering on the Dynamics of Ionomers in Solutions. *ACS Macro Letters* **2023**, *12*, 1118-1124.

(7) Kosgallana, C.; Wijesinghe, S.; Senanayake, M.; Mohottalalage, S.; Ohl, M.; Zolnierczuk, P.; Grest, G. S.; Perahia, D. From Molecular Constraints to Macroscopic Dynamics in Associative Networks formed by Ionizable Polymers: A Neutron Spin Echo and Molecular Dynamics Simulations Study. *ACS Polymers Au (in review)* **2024**.

(8) Fitzgerald, J.; Kim, D.; Weiss, R. The effect of diluents on the ionic interactions in sulfonated polystyrene ionomers. *Journal of Polymer Science Part C: Polymer Letters* **1986**, *24* (6), 263-268.

(9) Chakrabarty, K.; Seery, T.; Weiss, R. Characterization of ionomer solutions. 1. Phase behavior and gelation of sulfonated polystyrene ionomers in decalin. *Macromolecules* **1998**, *31* (21), 7385-7389.

(10) Weiss, R.; Yu, W.-C. Viscoelastic behavior of very lightly sulfonated polystyrene ionomers. *Macromolecules* **2007**, *40* (10), 3640-3643.

(11) Qiao, X. Nonlinear Rheology of Lightly Sulfonated Polystyrene Ionomers. *Macromolecules* **2013**, *v. 46* (no. 6), pp. 2417-2424-2013 v.2446 no.2416. DOI: 10.1021/ma3026496 From National Agricultural Library PubAg.

(12) Chen, Q.; Huang, C.; Weiss, R.; Colby, R. H. Viscoelasticity of reversible gelation for ionomers. *Macromolecules* **2015**, *48* (4), 1221-1230.

(13) De Luca, E.; Waigh, T. A.; Monkenbusch, M.; Kim, J. S.; Jeon, H. S. Neutron spin echo study of the dynamics of micellar solutions of randomly sulphonated polystyrene. *Polymer* **2007**, *48* (14), 3930-3934.

(14) Nyström, B.; Roots, J.; Higgins, J.; Gabrys, B.; Peiffer, D.; Mezei, F.; Sarkissian, B. Dynamics of polystyrene sulfonate ionomers in solution. A neutron spin-echo study. *Journal of Polymer Science Part C: Polymer Letters* **1986**, *24* (6), 273-281.

(15) Agrawal, A.; Perahia, D.; Grest, G. S. Clustering effects in ionic polymers: Molecular dynamics simulations. *Physical Review E* **2015**, *92* (2), 022601.

(16) Ohl, M.; Monkenbusch, M.; Arend, N.; Kozielewski, T.; Vehres, G.; Tiemann, C.; Butzek, M.; Soltner, H.; Giesen, U.; Achten, R. The spin-echo spectrometer at the Spallation Neutron Source (SNS). *Nuclear Instruments and Methods in Physics Research Section A: Accelerators, Spectrometers, Detectors and Associated Equipment* **2012**, *696*, 85-99.

(17) Zolnierczuk, P.; Holderer, O.; Pasini, S.; Kozielewski, T.; Stingaciu, L.; Monkenbusch, M. Efficient data extraction from neutron time-of-flight spin-echo raw data. *Journal of applied crystallography* **2019**, *52* (5), 1022-1034.

(18) Richter, D.; Monkenbusch, M.; Arbe, A.; Colmenero, J. *Neutron spin echo in polymer systems*; Springer, 2005.

(19) Jorgensen, W. L.; Maxwell, D. S.; Tirado-Rives, J. Development and testing of the OPLS all-atom force field on conformational energetics and properties of organic liquids. *Journal of the American Chemical Society* **1996**, *118* (45), 11225-11236.

(20) Jorgensen, W. L.; Madura, J. D.; Swenson, C. J. Optimized intermolecular potential functions for liquid hydrocarbons. *Journal of the American Chemical Society* **1984**, *106* (22), 6638-6646.

(21) Thompson, A. P.; Aktulga, H. M.; Berger, R.; Bolintineanu, D. S.; Brown, W. M.; Crozier, P. S.; in't Veld, P. J.; Kohlmeyer, A.; Moore, S. G.; Nguyen, T. D. LAMMPS-A flexible simulation tool for particle-based materials modeling at the atomic, meso, and continuum scales. *Comp. Phys. Comm.* **2022**, *271*, 108171.

(22) Pronk, S.; Páll, S.; Schulz, R.; Larsson, P.; Bjelkmar, P.; Apostolov, R.; Shirts, M. R.; Smith, J. C.; Kasson, P. M.; Van Der Spoel, D. GROMACS 4.5: a high-throughput and highly parallel open source molecular simulation toolkit. *Bioinformatics* **2013**, *29* (7), 845-854.

(23) Abraham, M. J.; Murtola, T.; Schulz, R.; Páll, S.; Smith, J. C.; Hess, B.; Lindahl, E. GROMACS: High performance molecular simulations through multi-level parallelism from laptops to supercomputers. *SoftwareX* **2015**, *1*, 19-25.

(24) Berendsen, H. J.; van der Spoel, D.; van Drunen, R. GROMACS: A message-passing parallel molecular dynamics implementation. *Computer physics communications* **1995**, *91* (1-3), 43-56.

(25) Mohsen-Nia, M.; Amiri, H.; Jazi, B. Dielectric constants of water, methanol, ethanol, butanol and acetone: measurement and computational study. *J. Solution Chem.* **2010**, *39*, 701-708.

(26) Jezuita, A.; Wieczorkiewicz, P. A.; Szatylowicz, H.; Krygowski, T. M. Effect of the Solvent and Substituent on Tautomeric Preferences of Amine-Adenine Tautomers. *ACS omega* **2021**, *6* (29), 18890-18903.

(27) Mezei, F.; Knaak, W.; Farago, B. Neutron spin echo study of dynamic correlations near liquid-glass transition. *Physica Scripta* **1987**, *1987* (T19B), 363.

(28) Rabiei, N.; Amirshahi, S. H.; Kish, M. H. Description of physical aging kinetics of glassy polymers by interpretation of parameters of the Kohlrausch-Williams-Watts relaxation function via simulation. *Physical Review E* **2019**, *99* (3), 032502.

(29) Kosgallana, C.; Senanayake, M.; Wijesinghe, S.; Mohottalalage, S.; He, L.; Grest, G. S.; Perahia, D. Clustering Effects on the Structure of Ionomer Solutions: A Combined SANS and Simulations Study. *Macromolecules (in review)* **2024**.

(30) Nosé, S. A unified formulation of the constant temperature molecular dynamics methods. *The Journal of chemical physics* **1984**, *81* (1), 511-519.

(31) Hoover, W. G. Canonical dynamics: Equilibrium phase-space distributions. *Physical review A* **1985**, *31* (3), 1695.

(32) Essmann, U.; Perera, L.; Berkowitz, M. L.; Darden, T.; Lee, H.; Pedersen, L. G. A smooth particle mesh Ewald method. *The Journal of chemical physics* **1995**, *103* (19), 8577-8593.

(33) Bussi, G.; Donadio, D.; Parrinello, M. Canonical sampling through velocity rescaling. *The Journal of chemical physics* **2007**, *126* (1), 014101.

CHAPTER SIX

STRUCTURE AND DYNAMICS OF THF SWOLLEN POLYSTYRENE IONOMER MELTS

6.1 Abstract

Ionomers are polymers in which both backbone and ionic groups govern their properties. The ionic groups form long-lived clusters, trapping the system in metastable states, which reduces the dynamics of the system. One way of overcoming this is to process these ionic materials in solutions. However, very few solvents can dissolve both the ionic groups and the backbone of ionomers. The current study probes lightly sulfonated polystyrene (SPS) melts swollen with THF. This solvent is chosen for this study due to its ability to dissolve both components due to its hydrophobic yet polar nature. The effect of varying the sulfonation fraction and weight percent of THF on the polymer's structure and dynamics is studied using fully atomistic molecular dynamics (MD) simulations. The addition of THF releases constraints between the ionic groups, resulting in larger ionic clusters than the melts. The intensity of the ionic peak at low wavevector q in the static structure factor $S(q)$ becomes more intense as the ionic clusters grow and become more distinctive with increasing THF. The local dynamics of the different segments are strongly impacted by the amount of THF, allowing all segments to become more dynamic even though the average cluster size increases.

6.2 Introduction

The balance between electrostatic interactions and segregation between hydrophilic and hydrophobic groups in ionizable polymers drive the formation of clusters.[1] While electrostatic interactions dominate the properties of polyelectrolytes[2], ionomers' characteristics are governed

by both the backbone conformation and electrostatic forces. These ionic groups are crucial in ionic transport, mechanical behavior, and adhesion strength of the polymer. Segregation of the hydrophobic matrix and ionic clusters dominate the structure of ionomers such as sulfonated polystyrene (SPS), Nafion and polystyrene methacrylate.[3, 4] The characteristics of these ionic assemblies, such as the size, shape, number, and distribution, affect the overall structure and dynamics of polymers and their transport characteristics.

Ionic clusters have immense effects on the structure and dynamics of ionomers and exert significant constraints on the motion of polymers in solutions and in melts. One way to increase chain mobility in polymers in general is to add solvents.[5] In ionizable polymers in which the ionic groups form clusters, however the solvent must tweak the clusters without collapsing the backbone. For ionic polymers, most common solvents are selective to either the polymer backbone or the ionic groups. Kosgallana et al. showed that the addition of small amounts of ethanol to SPS ionomers in toluene solutions ethanol decreases the average cluster size and increases dynamics of the system. However, further addition of ethanol collapses the chains and dynamics of the system decreases.[6, 7] This points to polar solvents with a relatively high solubility index, that will prevent the collapse of the polymer backbone but with a dielectric constant that will enable tweaking the cohesion of the ionic clusters as good candidates to unlock the ionic clusters and enhance the dynamics of ionomer melts.

The effect of these ionic aggregates has driven many studies to understand the formation and effect of these clusters on the structure and dynamics of ionomers. Experimentally, Weiss and co-workers used electron microscopy and small angle neutron scattering and observed that a minimal number of ionic segments has a large impact on the system's dynamics, and the addition of a polar solvent impacts the cluster formation.[8, 9] Winey and co-workers studied sulfonated polystyrene

neutralized with Zn using scanning transmission electron microscopy and x-ray scattering and observed that for low sulfonation levels, spherical aggregates with ~ 2nm diameter formed independently of the sulfonation fraction and ionization degree.[10, 11] Using molecular dynamics simulations, Hall et al. have shown that SPS forms discrete clusters instead of percolated aggregates formed in polymers with ionic in the polymer backbone.[12] Agrawal et al. have shown that increasing the dielectric constant of the media decreases the size of the ionic cluster and enhances the dynamics.[13] X-ray scattering and MD simulations studied done on the precise and random poly(ethylene-co-acrylic acid) has showed that the ionomer peak is affected by the position of the charged groups. While randomness broadens the ionomer peak, spacing between the ionic groups shift the ionomer peak to lower wave vector.[14,15] Mohottalalge et al. have shown that the placement of the ionic groups on the backbone affects both the structure and dynamics of the system. The distribution of ionic groups along the polymer chain affects the shape size and packing of these ionizable groups.[16] Here, using molecular dynamics (MD) simulations we probe the effect of THF on the structure and motion of SPS, with a solvent polarity of 4, and dielectric constant of 7.43. THF is hydrophobic in nature which interacts with the backbone and contains a polar component that is able to interact with the ionic groups and release contains in both segments. We demonstrate a quantitative correlation between the THF effect on cluster formation and the effect of THF on PS. We find that THF allows the polymer to release constraints and the ionic groups to form more well-defined clusters.

6.3 Methodology

Sulfonated polystyrene and THF were built using the polymer builder in BIOVIA[TM] Materials Studio. The system contains 148 unique, atatic sulfonated polystyrene chains with sulfonation fractions f = 0, 0.03, and 0.09, each with a total molecular weight of ~11 kg/mol with 106

monomers per chain. The counterion is Na^+. The systems consist of 0, 6 and 10 wt% THF. Each system contains between 0.25 – 0.33 million atoms. Periodic boundary conditions were used for all simulations. The final dimension of the simulation cell L varies from 14.2 to 16.0 nm, depending on the fraction of THF.

The all atoms optimized potentials for liquid simulations (OPLS-AA) force fields, developed by Jorgensen et al.[17, 18] were used to model the system. In all the simulations, the Lennard-Jones interactions was truncated at 1.2 nm. The initial simulations were carried out using LAMMPS[19] and converted to GROMACS [20-22] for enhanced efficiency. In LAMMPS, the Newton equations of motions were integrated using a velocity-Verlet algorithm with a time step of 1 *fs*. The Coulomb interactions are treated with long-range particle-particle particle-mesh (PPPM) algorithm[23] with a real space cutoff of 1.2 nm and a precision of 5×10^{-4}. The temperature was maintained by coupling to a Langevin thermostat with a time constant of 0.1 ps. After equilibration, the systems were converted to GROMACS, in which case the electrostatics were treated using particle mesh Ewald[24] (PME) algorithm and Fourier grid spacing of 0.12 nm. All harmonic bonds involving hydrogen atoms were replaced with constraints using the LINCS algorithm.[25] The temperature was maintained using the Bussi-Parrinello thermostat (V-rescale)[26] with a time constant of 0.1 ps. The GROMACS simulations were carried out using 2 fs time step.

Each system was first run at a constant pressure of 1 atm for 10 ns to obtain the equilibrium density. The dielectric constant ε was increased from 1 to 30 to reduce the residual electrostatic screening between ionic groups. This step breaks the ionic clusters, allowing the chains to equilibrate locally. Each system was then run for 30 ns at constant volume after which ε was reset to 1 and ran for 1000 ns at temperature 500 K. We define $t = 0$ as the time at which ε was reset to 1.

Static quantities, including the pair correlation functions *g(r)*, ionic cluster distribution, and the

static structure factor *S(q)*, were averaged over the last 20 ns of the run. The static structure factor

S(q) of the system is computationally given by,

$$S(q) = \left| \sum_i b_i e^{iq \cdot r_i} \right|^2 / \sum_i b_i^2 \qquad (1)$$

where b_i are the scattering length for neutrons[27] and r_i is the position of atom *i*. The scattering

length density of the THF was set to zero to capture the polymer structure. Due to the periodic

boundary conditions, the wavevectors *q* are limited to $\boldsymbol{q} = 2\pi/\mathrm{L} \, (n_x, n_y, n_z)$, where n_x, n_y, and n_z are

integers. The analysis for dynamic quantities, such as the mean squared displacement and dynamic

structure factor S(q,t) was averaged over the last 800 ns of the run. The dynamic structure factor

S(q,t) was calculated using

$$S(q,t) = \sum_{i,j=1}^{N} b_i \, b_j e^{[iq \cdot (r_i(t) - r_j(0))]} \, / \, \sum_{i=1}^{N} b_i^2 \,, \qquad (2)$$

where $\boldsymbol{r_i(t)}$ position of atom *i* at time *t*.

6.4 Results
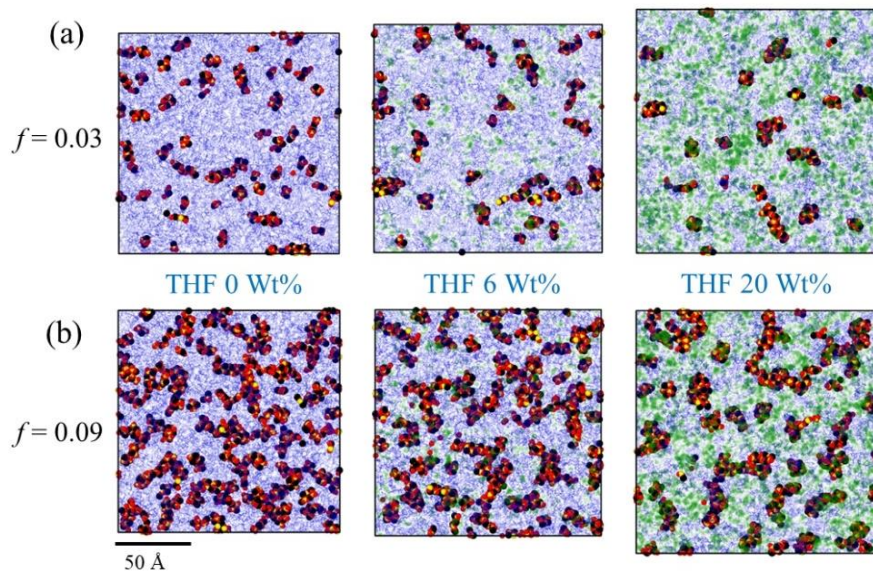
Figure 6.1: Visualization of SPS swollen melt at 1000 ns for (a) $f = 0.03$ (b) $f = 0.09$ with varying THF (Wt%). Yellow – sulfur, red- oxygen, black - Na^+, blue- polymer backbone, green - THF molecule. Backbone is transparent for clarity. Slice of 1/3 of the entire simulation box

Representataive sulfonated melts with varying THF fractions is visualized in Figure 6.1 for sulfonation fractions $f = 0.03$ and 0.09. For all melts, independent of THF fraction, clusters are observed. The THF molecules reside throughout the melt systems. As THF is added the solvent appears to drive the clusters further apart and increase their size.
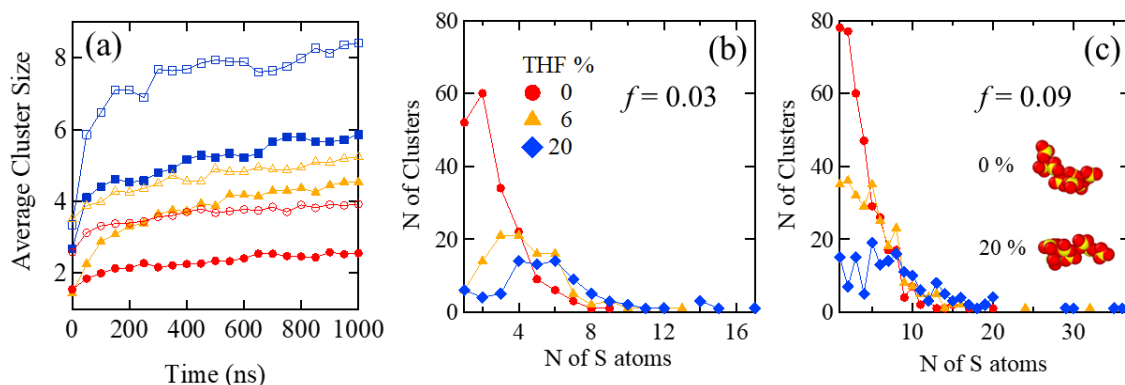
Figure 6.2: (a) Average cluster size as a function of time with varying THF fractions for $f = 0.03$ (filled) and $f = 0.09$ (open) for 0 Wt% THF (red), 6 Wt% THF (yellow) and 20 Wt% THF (blued). Cluster distribution for (b) $f = 0.03$ and (c) $f = 0.09$ with varying THF fractions (averaged over 980-1000 ns). Inset of (c) shows an example of an ionic cluster for 0 and 20 wt% THF for $f = 0.09$.

Similar to pristine melts,[13] the ionic assemblies characteristics are quantified by the cluster distribution and their average cluster size. Two sulfur atoms are defined to be in the same cluster if the distance between them is less than 6 Å. The average cluster size increases with time reaches a plateau after ~200 ns for all THF levels. Surprisingly though, with increasing THF fraction, the average cluster size increases for both sulfonation fractions. Specifically, as the system is swollen by the addition of 6 wt% THF, the average cluster size in terms of sulfur atoms per cluster, almost doubles from 2.6 to 4.5 for $f = 0.03$. Further increasing the THF fraction to 20 Wt%, the average cluster size increases only slightly to 5.2. For $f = 0.09$, addition of 6 Wt% THF increases the average cluster size from 3.9 to 5.2, while further increase in THF, shows a significant increase in cluster size to 8.4

The cluster distribution for $f = 0.03$ and $f = 0.09$ is shown in Figure 6.2 b,c for varying THF fractions. The pristine melts have a relatively large number of isolated sulfonated groups, that are not in clusters. For $f = 0.03$, the largest ionic cluster increases from size 10 in the melt to 13 with the addition of 6 wt% THF and to 17 with the addition of 20 wt% THF. For $f = 0.09$, the largest ionic cluster in the melt is of size 21, which increases to 32 with the addition of 6 wt% THF and to 37 with the addition of 20 wt% THF. The intriguing increase in size of the clusters with addition of THF is attributed this increase to this increase in constraints being released in presence of THF, which allows the polymer to form larger clusters. The cluster evolution is affected by both the solvation of the polymer backbone and the direct interaction of the ionizable groups with the solvent
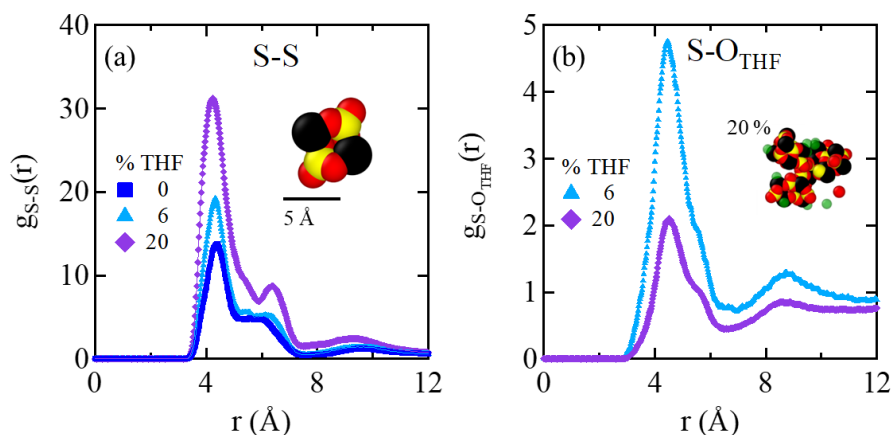
Figure 6.3: Pair correlation function between (a) two sulfur atoms. (b) Pair correlation function between sulfur and oxygen atom of THF for $f = 0.09$. Insert of (b) shows ionic cluster and counter ion with THF.

To characterize the internal correlations between the sulfur atoms in specific clusters and between a sulfur atom and THF, we measured the pair correction functions $g(r)$. The S-S pair correlation function is given by $g_{S-S}(r) = dn_{S-S}(r)/4\pi r^2 dr\rho_S$, where $4\pi r^2$ dr is the volume of spherical shell, ρ_S is the S atom density, and $dn_{S-S}(r)$ is the average number of S as a function of distance r from a S atom. The first peak in $g_{S-S}(r)$ at ~ 4.3 Å corresponds to the closest distance between

two S atoms. The second peak captures the next neighbor distance, which shifts to larger distance with increasing THF fraction. As THF is added the ionic groups relaxes and the distance between the S atoms increases. With increasing THF fraction, the average cluster size increases as seen in Figure 6.2a, which results in increase the intensity of the first peak in $g_{S-S}(r)$ an more sulfur atoms reside in the immediate surroundings of each other.

The correlation between the S atom and the O atom of the THF molecule is shown in Figure 6.3b. The first peak is at ~ 4.6 Å corresponds to the closest distance between S atom and O atom of the THF molecule with a second peak around ~ 8.7 Å. Due to THF molecular size the second peak is observed at a higher distance compared to the $g_{S-O}(r)$ second peak. The insert shows a cluster and neighboring THF molecules for $f = 0.09$ with 20 wt% THF.

System		Ratio of THF molecules to S atoms ($\pm$ 0.001)	Average number of THF associated with a S atom ($\pm$ 0.001)	Fraction of condensed Na^+ ($\pm$ 0.001)
Sulfonation fraction	THF (Wt%)			
3	6	2.99	0.46	0.995
	20	11.73	0.63	0.996
9	6	1.02	0.44	0.994
	20	3.99	0.75	0.996

Table 6.1: Solvent association (THF-O atoms within 7Å of S atom) and condensed counter ion fractions (Na^+ atoms within 6Å of S atom)

The number of THF molecules associated with the sulfur of the SO_3^- groups is given in Table 1. Here we define a THF molecule to be associated with a S atom if the distance between an O of the THF and a S atom are less than 7 Å, the distance of the first minimum in Figure 6.3b shows the solvent association with the S atoms of the ionic groups. With increasing THF fraction, the associated THF fraction increases from 0.46 to 0.63 for $f = 0.03$ and from 0.44 to 0.75 for $f = 0.09$. In all cases, the number of THF molecules associated with the ionic groups is considerably smaller

than the number of THF molecules in the entire melt. However, these numbers clearly show that THF is not a preferential solvent for the ionizable groups. The fraction of condensed Na^+ which is Na^+ atoms within 6 Å of the S atoms shows that almost all the counter ions are completely condensed with the ionic group.
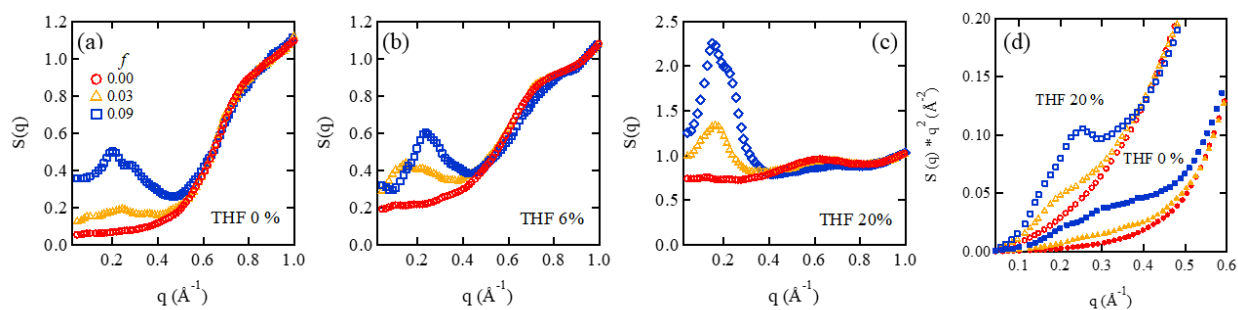

Figure 6.4: Static structure function $S(q)$ as a function of q for (a) 0 wt% (b) 6 wt% and (c) 20 wt% THF with varying sulfonation fractions $f = 0$ (red), 0.03 (yellow) and 0.09 (blue). (d) Kratky plot for 0 (filled) and 20 (open) Wt% THF.

The impact of THF of the swollen melts was encapsulating the q range where the "ionic peak" is expressed to that of chain packing. The static structure factor $S(q)$ for all melts as show Figure 6.4 a-c. A comparison of the scattering of 20% swollen melts and the pristine ones are given in terms of Kratky plots in Figure 6.4 d. for $f = 0$ pristine melts the only signature of amorphous chain-chain correlation is observed at high q. With increasing THF fraction, a more distinctive chain-chain packing signature is observed. For $f = 0.03$ and 0.09, a distinctive peak at $q \sim 0.2$ Å^{-1} for 0 and 6 wt% THF and at q ~ 0.18 Å^{-1} for 20 wt% THF is observed. The intensity of the peak grows with increasing f and THF. This peak, which is commonly referred to as the ionomer peak has been observed experimentally for a number of ionizable polymer systems.[15] It corresponds to the correlations between ionic clusters. For these low sulfonation fractions, the position of the peak corresponds to an average distance of ~31 Å for 0 and 6 wt% THF and ~ 35 Å for 20 wt% THF. The peak intensity increases with increasing f as have been previously shown for SPS melts. It

also increases with THF fraction which could be attributed to the overall degree of swelling that separates the ionic clusters, coupled with increase of their size. The Kratky plot $S(q)*q^2$ versus q for 0 and 20% THF for all three sulfonation is shown in Figure 6.4 d. Kratky representation normalizes the intensity to q^2, which is the scaling for a Gaussian chain, manifesting other structural features such as the ionic peak. The slope at higher q provides further information regarding the conformation of the chains. As THF is added the ionomer peak becomes significantly narrower for both $f = 0.03$ and $f = 0.09$ consistent with formation of well-defined ionic clusters. This surprising evolution of the clusters with THF is indicative of the release of constraints that enables further assembly of the ionic clusters. The patterns shift to lower q values, i.e. larger dimensions. This is consistent with swelling as more THF is added.
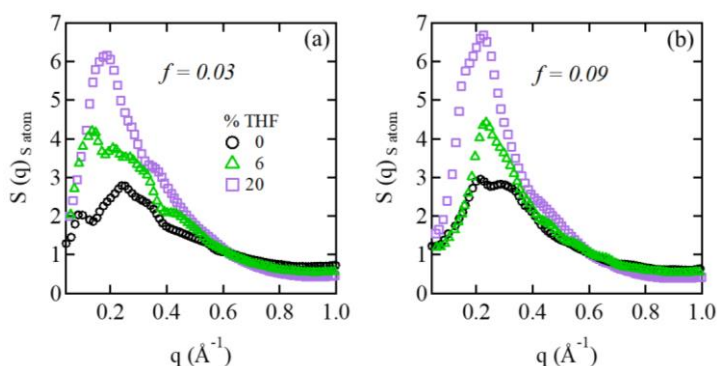
Figure 6.5: Static structure function $S(q)$ for S atoms as a function of q for (a) $f = 0.03$ and (b) $f = 0.09$ for varying THF fractions.

To further explore the nature of the clusters, $S(q)$ was calculated for the sulfur atoms, shown in Figure 6.5. $S(q)$ clearly shows that the development of well-defined clusters that shift to lower q values with increasing THF content. This peak in $S(q)$ however, is rather broad reflecting a broad distribution of cluster sizes and their inter-cluster correlations.

Figure 6.6: Mean squared displacement MSD for for $f = 0.09$ with varying THF fractions. 0 Wt% THF (red), 6 wt% THF (yellow) and 20 wt% THF (blued) (a) backbone and center of mass, (b) non-sulfonated phenyl rings and sulfonated phenyl rings, and (c) Na^+ and THF.

The mobility of the chains, counterions and solvent are determined by measuring the mean square displacement $MSD(t) = \langle \Delta r_i(t)^2 \rangle = \langle (r_i(t) - r_i(0))^2 \rangle$ as a function of time. The average is over multiple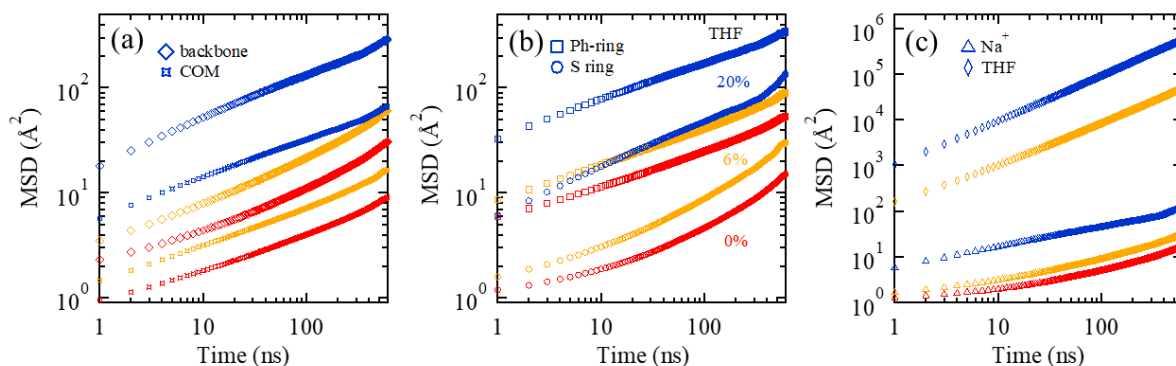 atoms and from 400 ns to 1000 ns. Figure 6.6a shows the MSD of the center of mass (COM) and the backbone. Here the backbone motion is considered as the motion of the chain without the phenyl rings. The COM motion is comparatively slower than that of the backbone on these time scales. The difference between MSD for COM and backbone increases as the THF fraction is increased. As we zoom into the system and look at the motion of the different phenyl rings, the sulfonated rings follow closely to that of the COM while the phenyl rings without S group follow closely the backbone. Due to the formation of clusters, the motion of the sulfonated rings is slower compared to that of the phenyl rings without sulfonated group at these time scales. The COM motion follows closely since the whole polymer slows down due to these clusters. The backbone follows closely to the phenyl ring motion due to the backbone having more phenyl groups compared to sulfonated rings attached to it. Similar differences in the local motion of the phenyl ring and sulfonated ring for melts has previously been observed by Agrawal etal.[13] MSD shows that the polymer has moved less than their chain size over the times that are accessible

computationally which indicates the polymer motion is restricted due to cluster formation. The coupling between MSD of the Na^+ and the sulfonated rings show that significant number of the ions are condensed. The condensation fractions are given in Table 6.1. The solvent motion increases almost 10-fold as fraction of THF increase from 6 wt% to 20 wt%.
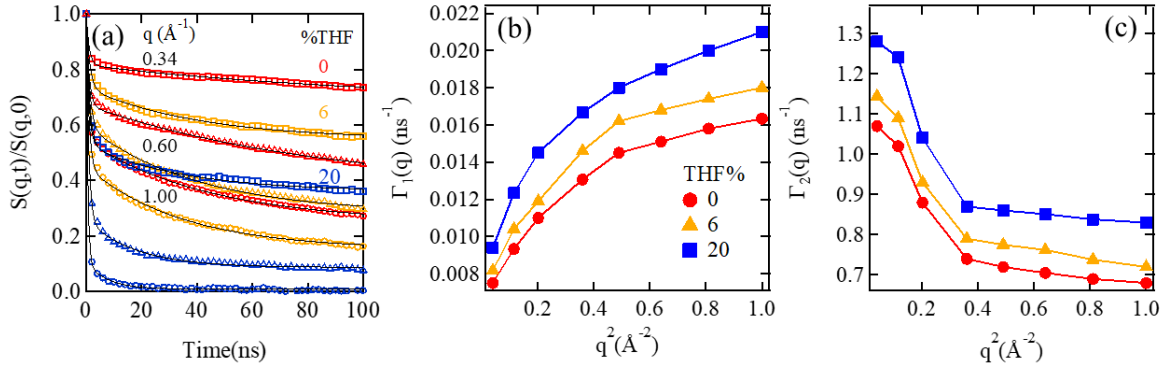

Figure 6.7: (a) Dynamic structure factor $S(q,t)$ as a function of time for 3 values of q for $f = 0.09$. Relaxation rates (b) $\Gamma_1(q)$ and (c) $\Gamma_2(q)$ extracted from the fits to a sum of two exponentials (eq. 3) as a function of q for with varying THF. 0 Wt% THF (red), 6 Wt% THF (yellow) and 20 Wt% THF (blue).

The dynamic structure factor $S(q,t)$ provides further insight into the local segmental motion of the system. $S(q,t)$ for 3 representative q values is shown in Figure 6.7a for $f = 0.09$. These systems were first analyzed by a stretched exponential Kohlrausch–Williams–Watts *(KWW)* model. But this did not capture the entire time range very well. We found that a sum of two exponentials,

$$S(q,t) = A_1 e^{-t/\tau_1(q)} + A_2 e^{-t/\tau_2(q)}, \qquad (3)$$

where A_i is constant and $\tau_i(q)$ are relaxation time, fit the data quite well. This model allows to capture two-time scales where slow and fast motions are captured within the same time scale. Results for the relaxation rates $\Gamma_i(q) \propto \tau_i^{-1}(q)$ are shown in Figure 6.7 b,c. As seen in Figure 6.7b, the slower relaxation rates $\Gamma_1(q)$ increase with increasing q as one would expect. As the THF fraction increases the motion increases at all q values, consistent with the increase in local chain mobility as seen from the MSD, Figure 6.6. Even though larger clusters are formed with

increasing THF, the solvent reduces the restrictions on the local motions, and the polymers motion increases at all length scales. For the fast motion, $\Gamma_2(q)$ shows the opposite trend as it decreases with increasing q for all THF fractions. The chains segments closer to the clusters show slower motion compared to the chain segments away from the clusters. As THF amount is increased the overall motion increase for all systems.
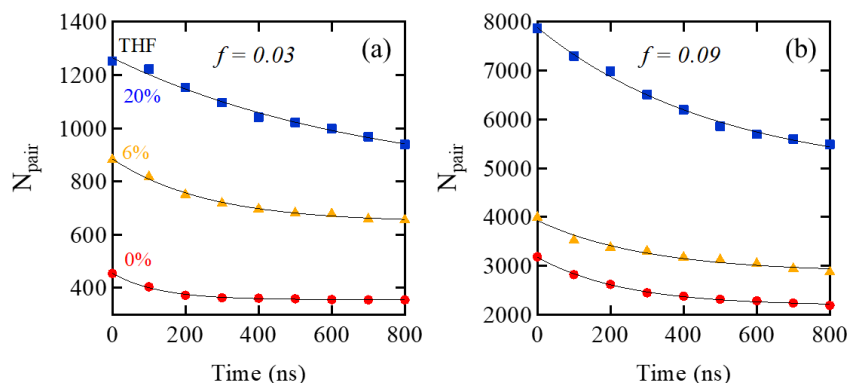

Figure 6.8: Number of pairs N_{pair} of sulfur atoms that remain in the same cluster as a function of time for all S pairs (a) $f = 0.03$ and (b) $f = 0.09$ for 0 Wt% THF (red circles), 6 Wt% THF (yellow triangles) and 20 Wt% THF (blue squares)

To obtain some insight into the lifetime of the clusters, we measured the survival rate of pairs of S atoms which remain in the same cluster as a function of time. This is calculated by first identifying all S pairs that are within the same cluster and following which pairs remain in the same cluster at a function of time. The number of such pairs N_{pair} decrease either by single S atoms leaving the cluster or the cluster breaking into two. Here N_{pair} decreases predominately by a single S atom dissociating from the cluster. As seen in Figure 6.8, N_{pair} decreases by at most 30% over 800 ns, indicating that the clusters are very long-lived clusters, with the larger decreases observed in the presence of THF. These long-lived clusters constrain the polymer mobility as seen in Figure 6.6. For $f = 0.03$, the rate of decrease of N_{pair} increases with THF fraction. As THF is added the ionic groups are less restricted and are able to move within clusters. This is more pronounced in $f = 0.09$ where the THF 20% shows a significant difference compared to the other two systems.

6.5 Conclusions

The results attained here using molecular dynamics simulations of SPS melts swollen with THF reveal the mechanism releasing constrains exerted by solvents in ionomer melts. The cluster evolution with time as THF is added is followed by the visualization of the melts, direct measurements of average cluster size and S(q), where the dynamics is resolved through MSD and S(q,t) measurements. With addition of THF, the average cluster size surprisingly increases and forms larger assemblies however the overall motion of the polymers increases. This observation contrasted previous studies that have shown that increase cluster sizes would constraint chain dynamics. A close look into the number of unique chains that reside in distinctive clusters, however, reveals that with increasing cluster size in these THF swollen melts, the number decreases. Thus, the increase in cluster size is due to intra molecular assembly rather than bridging across the melts, that does not affect the overall macroscopic motion of the chain, though it would reduce local segmental dynamics. The survival time of sulfur pairs in the same cluster decreases with increasing THF fraction proving another mechanism for constraint release in these systems. This study shows that using non-preferential solvents, such as THF, cluster formation is altered providing a mechanism to control the assembly of ionomers, impacting their processing into materials with controlled structure and dynamics, and consequently their potential use in targeted applications.

6.6 Acknowledgement

6.7 References

(1) Eisenberg, A. Clustering of ions in organic polymers. A theoretical approach. *Macromolecules* **1970**, *3* (2), 147-154.

(2) Sing, C. E.; Zwanikken, J. W.; Olvera de La Cruz, M. Electrostatic control of block copolymer morphology. *Nature materials* **2014**, *13* (7), 694-698.

(3) Zhou, N. C.; Chan, C. D.; Winey, K. I. Reconciling STEM and X-ray scattering data to determine the nanoscale ionic aggregate morphology in sulfonated polystyrene ionomers. *Macromolecules* **2008**, *41* (16), 6134-6140.

(4) Chen, Q.; Tudryn, G. J.; Colby, R. H. Ionomer dynamics and the sticky Rouse model. *Journal of Rheology* **2013**, *57* (5), 1441-1462.

(5) Lantman, C.; MacKnight, W.; Higgins, J.; Peiffer, D.; Sinha, S.; Lundberg, R. Small-angle neutron scattering from sulfonate ionomer solutions. 1. Associating polymer behavior. *Macromolecules* **1988**, *21* (5), 1339-1343.

(6) Kosgallana, C.; Senanayake, M.; Wijesinghe, S.; Mohottalalage, S.; He, L.; Grest, G. S.; Perahia, D. Clustering Effects on the Structure of Ionomer Solutions: A Combined SANS and Simulations Study. *Macromolecules (in review)* **2024**.

(7) Kosgallana, C.; Wijesinghe, S.; Senanayake, M.; Mohottalalage, S.; Ohl, M.; Zolnierczuk, P.; Grest, G. S.; Perahia, D. From Molecular Constraints to Macroscopic Dynamics in Associative Networks formed by Ionizable Polymers: A Neutron Spin Echo and Molecular Dynamics Simulations Study. *ACS Polymers Au (in review)* **2024**.

(8) Fitzgerald, J.; Weiss, R. Synthesis, properties, and structure of sulfonate ionomers. *Polymer Reviews* **1988**, *28* (1), 99-185.

(9) Fitzgerald, J.; Kim, D.; Weiss, R. The effect of diluents on the ionic interactions in sulfonated polystyrene ionomers. *Journal of Polymer Science Part C: Polymer Letters* **1986**, *24* (6), 263-268.

(10) Kirkmeyer, B. P.; Weiss, R. A.; Winey, K. I. Spherical and vesicular ionic aggregates in Zn-neutralized sulfonated polystyrene ionomers. *Journal of Polymer Science Part B: Polymer Physics* **2001**, *39* (5), 477-483.

(11) Castagna, A. M.; Wang, W.; Winey, K. I.; Runt, J. Influence of the degree of sulfonation on the structure and dynamics of sulfonated polystyrene copolymers. *Macromolecules* **2010**, *43* (24), 10498-10504.

(12) Hall, L. M.; Stevens, M. J.; Frischknecht, A. L. Effect of polymer architecture and ionic aggregation on the scattering peak in model ionomers. *Physical review letters* **2011**, *106* (12), 127801.

(13) Agrawal, A.; Perahia, D.; Grest, G. S. Clustering effects in ionic polymers: Molecular dynamics simulations. *Physical Review E* **2015**, *92* (2), 022601.

(14) Seitz, M. E.; Chan, C. D.; Opper, K. L.; Baughman, T. W.; Wagener, K. B.; Winey, K. I. Nanoscale morphology in precisely sequenced poly (ethylene-co-acrylic acid) zinc ionomers. *Journal of the American Chemical Society* **2010**, *132* (23), 8165-8174.

(15) Hall, L. M.; Seitz, M. E.; Winey, K. I.; Opper, K. L.; Wagener, K. B.; Stevens, M. J.; Frischknecht, A. L. Ionic aggregate structure in ionomer melts: effect of molecular architecture on

106

aggregates and the ionomer peak. *Journal of the American Chemical Society* **2012**, *134* (1), 574-587.

(16) Mohottalalage, S. S.; Aryal, D.; Thurston, B. A.; Grest, G. S.; Perahia, D. Effects of ionic group distribution on the structure and dynamics of amorphous polymer melts. *Macromolecules* **2021**, *55* (1), 217-223.

(17) Jorgensen, W. L.; Maxwell, D. S.; Tirado-Rives, J. Development and testing of the OPLS all-atom force field on conformational energetics and properties of organic liquids. *Journal of the American Chemical Society* **1996**, *118* (45), 11225-11236.

(18) Jorgensen, W. L.; Madura, J. D.; Swenson, C. J. Optimized intermolecular potential functions for liquid hydrocarbons. *Journal of the American Chemical Society* **1984**, *106* (22), 6638-6646.

(19) Thompson, A. P.; Aktulga, H. M.; Berger, R.; Bolintineanu, D. S.; Brown, W. M.; Crozier, P. S.; in't Veld, P. J.; Kohlmeyer, A.; Moore, S. G.; Nguyen, T. D. LAMMPS-A flexible simulation tool for particle-based materials modeling at the atomic, meso, and continuum scales. *Comp. Phys. Comm.* **2022**, *271*, 108171.

(20) Pronk, S.; Páll, S.; Schulz, R.; Larsson, P.; Bjelkmar, P.; Apostolov, R.; Shirts, M. R.; Smith, J. C.; Kasson, P. M.; Van Der Spoel, D. GROMACS 4.5: a high-throughput and highly parallel open source molecular simulation toolkit. *Bioinformatics* **2013**, *29* (7), 845-854.

(21) Abraham, M. J.; Murtola, T.; Schulz, R.; Páll, S.; Smith, J. C.; Hess, B.; Lindahl, E. GROMACS: High performance molecular simulations through multi-level parallelism from laptops to supercomputers. *SoftwareX* **2015**, *1*, 19-25.

(22) Berendsen, H. J.; van der Spoel, D.; van Drunen, R. GROMACS: A message-passing parallel molecular dynamics implementation. *Computer physics communications* **1995**, *91* (1-3), 43-56.

(23) Hockney, R. W.; Eastwood, J. W. *Computer simulation using particles*; crc Press, 2021.

(24) Essmann, U.; Perera, L.; Berkowitz, M. L.; Darden, T.; Lee, H.; Pedersen, L. G. A smooth particle mesh Ewald method. *The Journal of chemical physics* **1995**, *103* (19), 8577-8593.

(25) Hess, B.; Bekker, H.; Berendsen, H. J.; Fraaije, J. G. LINCS: A linear constraint solver for molecular simulations. *Journal of computational chemistry* **1997**, *18* (12), 1463-1472.

(26) Bussi, G.; Donadio, D.; Parrinello, M. Canonical sampling through velocity rescaling. *The Journal of chemical physics* **2007**, *126* (1), 014101.

(27) Sears, V. F. Neutron scattering lengths and cross sections. *Neutron news* **1992**, *3* (3), 26-37.

CHAPTER SEVEN

SHEAR RESPONSE ON THF SWOLLEN IONOMER POLYMER MELTS: MOLECULAR DYNAMICS SIMULATION STUDY

7.1 Abstract

Ionizable polymers contain charged groups that cluster, affecting their properties and directly impacting their potential uses, ranging from biotechnology to clean energy. Mechanical perturbation affects the clustering of these systems where they are constrained by two energy scales: electrostatic interactions of the ionic groups and van der Waals interactions of the backbone. Here, using molecular dynamics simulations, we probe the response to shear on these two energy scales for sulfonated polystyrene melts in the ionomer regime, $f = 0$ and $f = 0.09$. These melts were swollen with THF in order to reduce the constraints induced by electrostatic forces. The ionic assembly characteristics and shear viscosity were measured. We find that shear viscosity increases with the addition of even a few ionic groups compared to polystyrene. With the addition of shear, assemblies break apart in all THF fractions for $f = 0.09$. In comparison, the THF fraction shows a higher impact on the shear response of polystyrene compared to sulfonated polystyrene.

7.2 Introduction

Understanding the response of macromolecules to shear is crucial for their processing from molecules to viable materials,[1, 2] and often to their function in their many applications.[3] Understanding the response to shear provides insight into the factors that their unique viscoelastic properties.[4, 5] The behavior of polymers under shear is of particular importance in ionic polymers, where their ionizable segments drive the formation of the complex system that consists of hydrophobic van-der-Waals domains and ionic domains, each with a different response to

perturbation. The ionic clusters are known to constrain the internal dynamics of ionomer melts and solutions[6-10] and thus affect their response to shear. While it has been clear that clustering impacts the macroscopic shear response of complex fluids formed by ionizable polymers, the correlation between the molecular and macroscopic length scales remains an open question, critical to processing and fundamental to the physics of these complex systems. Here, using fully atomistic molecular dynamics (MD) simulations, we elucidate the structure evolution of THF swollen polystyrene sulfonate melts under shear. We find that the presence of ionic clusters modifies the molecular shear response, which is strongly affected by the presence of THF.

Weiss et al have extensively studied SPS ionomer structure and dynamics.[5, 8, 10-18] They have shown that the ionic groups from different chains enhance the melt viscosity as well as elasticity even without entanglement.[8] Colby and co-workers studied sulfonated polystyrene (SPS) in the polyelectrolyte regime.[19] They observed that concentration of the polymer plays a crucial part in viscosity. With high concentration above entanglement onset, relation time increases steeply. Lopez et al have studied in salt-free and excess added salt solution[20] they have found that the entanglement density and concentration are independent of added salt and solvent quality. Liu et al have studied telechelic ionomers based on either sodium carboxylate or sodium sulfonate groups.[21] by comparison of these two ionomers they found that sodium carboxylate ionomers can adjust the network under flow before the overshoot and the higher fracture stains attained after the overshoot suggest associated network can be reconstructed more easily compared to sodium sulfonate containing ionomer. Further insight was obtained by Agrawal et al who have shown that as shear is applied the chains stretch and SPS clusters break for both Na^+ and Mg^{2+} counter ions.[22] While average cluster size increases with decreasing shear rates, the average cluster size is always larger for Mg^{2+}. Gulati et al have studied the effect of salt concentration on viscosity of semi dilute

polyelectrolyte solutions.[23] They have observed that as polyelectrolytes with high molecular weight, crossovers over to semi dilute solution regime takes place in polymer concentrations where added salts and residual dominate the screening of electrostatic interactions.

This study probes the effect of slight addition of solvents on the rheology properties of sulfonated polystyrene swollen melts. As a mutual solvent THF is added, SPS melts show released constraints and larger clusters are formed but the dynamics of the systems increase.[24] Here the effect of shear on $f = 0$ and $f = 0.09$ with varying THF fraction is studied.

7.3 Methodology

Sulfonated polystyrene and THF were built using the polymer builder in BIOVIA[TM] Materials Studio. The system contains 148 unique, atatic sulfonated polystyrene chains with sulfonation fractions $f = 0$ and 0.09, each with a total molecular weight of ~11 kg/mol with 106 monomers per chain. The counterion is Na^+. The systems consist of 0, 6 and 10 wt% THF. Each system contains between 0.25 – 0.33 million atoms. Periodic boundary conditions were used for all simulations. The final dimension of the simulation cell L varies from 14.2 to 16.0 nm, depending on the fraction of THF.

The all atoms optimized potentials for liquid simulations (OPLS-AA) force fields, developed by Jorgensen et al.[25, 26] were used to model the system. In all the simulations, the Lennard-Jones interactions was truncated at 1.2 nm. The initial simulations were carried out using LAMMPS[27] and converted to GROMACS [28-30] for enhanced efficiency. In LAMMPS, the Newton equations of motions were integrated using a velocity-Verlet algorithm with a time step of 1 fs. The Coulomb interactions are treated with long-range particle-particle particle-mesh (PPPM) algorithm[31] with a real space cutoff of 1.2 nm and a precision of $5x10^{-4}$. The temperature was maintained by coupling to a Langevin thermostat with a time constant of 0.1 ps. After equilibration, the systems were

converted to GROMACS, in which case the electrostatics were treated using particle mesh Ewald[32] (PME) algorithm and Fourier grid spacing of 0.12 nm. All harmonic bonds involving hydrogen atoms were replaced with constraints using the LINCS algorithm.[33] The temperature was maintained using the Bussi-Parrinello thermostat (V-rescale)[34] with a time constant of 0.1 ps. The GROMACS simulations were carried out using 2 fs time step.

Each system was first run at a constant pressure of 1 atm for 10 ns to obtain the equilibrium density. The dielectric constant ε was increased from 1 to 30 to reduce the residual electrostatic screening between ionic groups. This step breaks the ionic clusters, allowing the chains to equilibrate locally. Each system was then run for 30 ns at constant volume after which ε was reset to 1 and ran for 200 ns at temperature 500 K. After running the built SPS melt systems at constant volume for ~200 ns in GROMACS, systems are converted to LAMMPS using MD-Analysis toolkit. Viscosity was measured using SLLOD equations of motion at strain rates of $\dot{\gamma} = 10^8$ to 10^{10} was integrated with a damping constant of 1 ps. The shear viscosity is calculated using $\eta = -\langle P_{xy} \rangle / \dot{\gamma}$, where $\langle P_{xy} \rangle$ is the xz component of the pressure tensor along the flow and gradient directions, respectively.
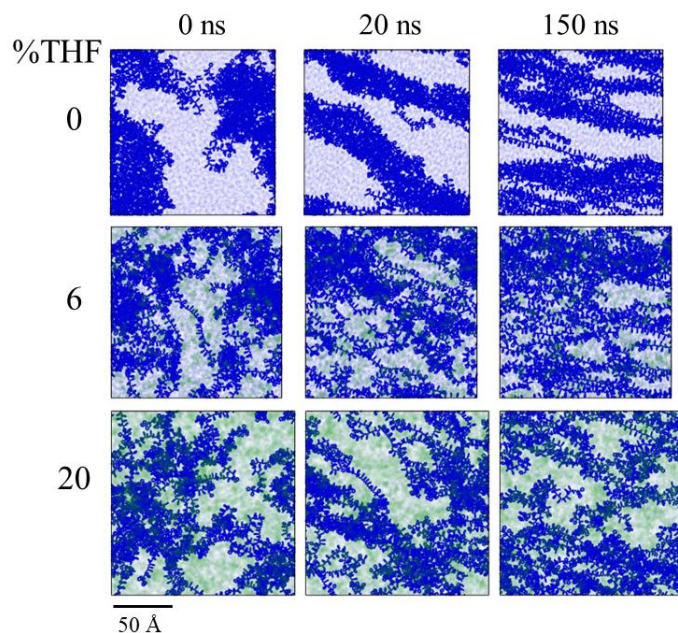
7.4 Results

Figure 7.1: 2D Visualization (xz plane) of 20 chains (total chains 148) of $f = 0$ at 0, 20 and 150ns for 0%, 6% and 20% THF for shear rate $\dot{\gamma} = 10^8$. Blue – polymer chain, Green - THF

Melts of PS and $f = 0.09$ SPS swollen with selected THF concentrations were followed as a function of time. Figure 7.1 captures the visualization of xz plant for 20 chains of $f = 0$ at 0, 20 and 150 ns as shear is applied. For the pristine melt, the quiescent state consists of collapsed chains. As shear is applied the chains stretch within 20 ns or 200 cycles. At longer times (150ns) the chains intermix with the rest of the polymer, as evident in the density of the chains. As 6% THF is added, the chains are less dense compared to the melt at quiescent state. Since shear is applied, the chains stretch out but to a lesser extent compared with the pristine melt at 20 ns. At longer times the chains stretch out. As THF concentration is further increased to 20% the chains are less stretched compared to the melt and the 6Wt% THF.
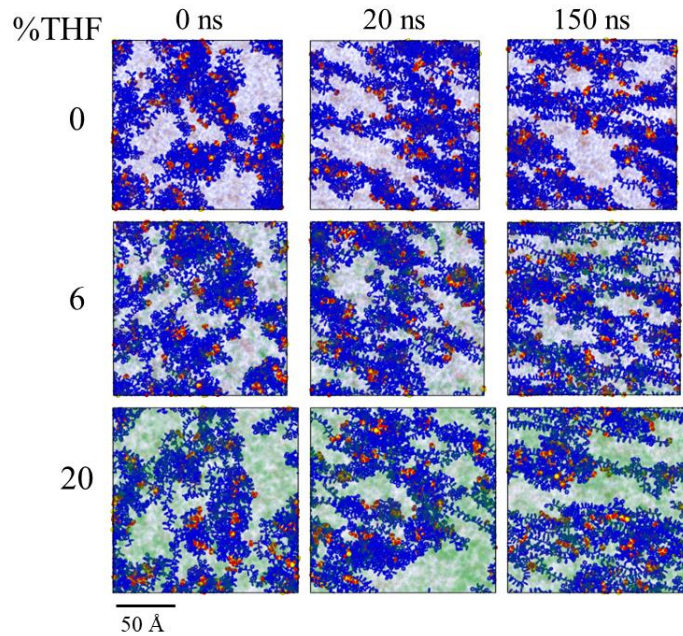
Figure 7.2: 2D Visualization (xz plane) of 20 chains (total chains 148) $f = 0.09$ at 0, 20 and 50 ns for 0%, 6% and 20% THF for shear rate $\dot{\gamma} = 10^8$. Yellow – Sulfur, Red- Oxygen, Blue- polymer backbone, Green - THF

SPS swallen melts with $f = 0.09$ are shown in Figure 7.2. In contrast to $f = 0$ system, the quiescent

state of the melt the chains are condensed due to cluster formation. As shear is applied (20 ns) the

chains stretch but regions with constrained by the clusters and with increasing shear rates, chains

further stretch. Though, compared to $f = 0$, the chains are less extended. As THF is added the

chains become more extended. At longer times the impact of the clusters become more apparent.

Similar to $f = 0$ with higher THF percentage the chains are less elongated as shear is applied. This

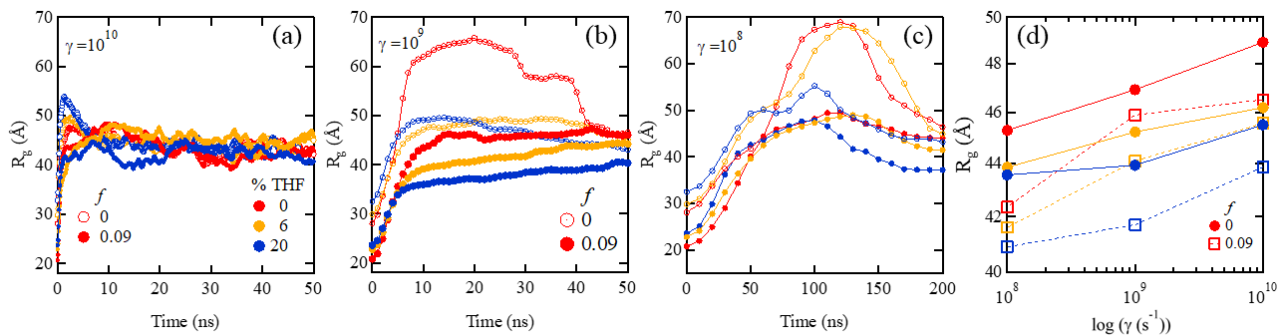is attributed to formation of the larger clusters as THF is added.[24]

Figure 7.3: Radius of gyration as a function of time for varying % THF (0 – red, 6 – yellow, 20 – blue) for $f = 0$ (open) $f = 0.09$ (full) at $\dot{\gamma}$ (a) 10^{10} (b) 10^9 and (c) 10^8 (d) Radius of gyration as a function of shear rate with varying THF for f = 0 (full) and f = 0.09 (open)

At high shear rates 10^{10} s^{-1} for all melts measured the chains stretch (Figure 7.3-a) within the first 10ns and then form a steady state with the value of 5ns. A closer look shows that at the onset of shear, the PS is further elongated compared to the SPS sample. This is ascribed to stress overshot where the chains are further extended compared with their inherent dimensions at a given shear rate. At lower shear rates ($\dot{\gamma} = 10^8$) s^{-1}, the extent of stretching depends on the degree of swelling. However, this effect diminishes at extended times and R_g levers off independent of the THF content or f. Similar to $f=0$, a significant initial increase in Rg is observed for the melt that levels off. Similar trends were observed for the slowest shear rates. The steady state Rg values for all melts are shown in Figure 7.3-d. In all systems steady state Rg increases with shear rates as expected, where instantaneous ionic clustering impact the dimensions. With increasing THF however, the chains do not elongate to the same extent.
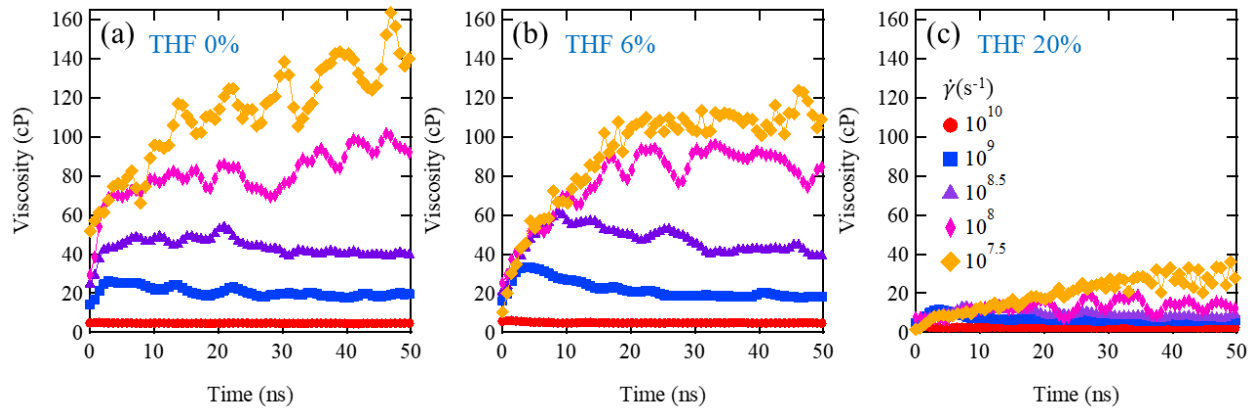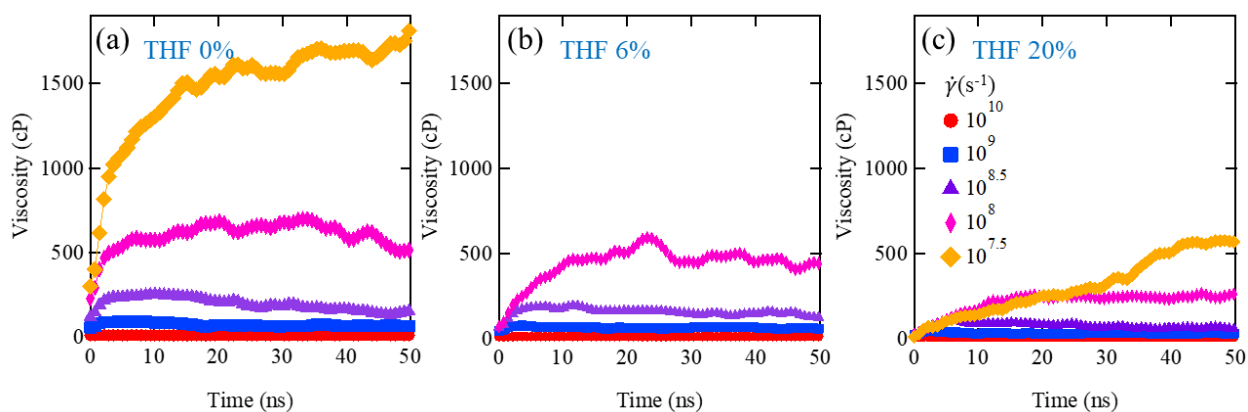

Figure 7.4: Shear viscosity vs time for $f = 0$ for $\dot{\gamma} = 10^{7.5}$ to 10^{10} s^{-1} for THF (a) 0 (b) 6 and (c) 20%

The shear viscosity η of PS melts is presented in Figure 7.4. $\eta = -\langle P_{xz} \rangle / \dot{\gamma}$ where $\langle P_{xz} \rangle$ is xz component of the pressure tensor along the flow and gradient directions respectively.

For all melts with shear, η first increases and then levels of with a significant overshoot at the higher shear rates. Reaching this state takes longer for slower shear rates. For 10^{10} the polymer begins to flow within few ns but as shear rate decrease the times increases to ~20 ns. As THF is added slower shear rates take longer to reach a fluid state and the η values within all shear rates are lower compared to the pure melt. While THF 0 and 6% response in a similar way, THF 20% shows a significant decrease in shear viscosity in all shear rates.

Figure 7.5: Shear viscosity vs time for $f = 0.09$ at $\dot{\gamma} = 10^{7.5}$ to 10^{10} s^{-1} for THF (a) 0 (b) 6 and (c) 20%

In presence of ionic clusters, η significantly increases for all systems for all shear rates compared to $f = 0$ as shown in Figure 7.5. As Ionic groups are added the systems become more constrained and viscosity increases. Melts with $f = 0.09$ show a similar trend to $f = 0$, where shear η increases with decreasing shear rate for all THF fractions. As THF is added, similar to the $f = 0$ system η significantly decreases. For THF 20% a significant decrease compared to 0 and 6% THF is observed.
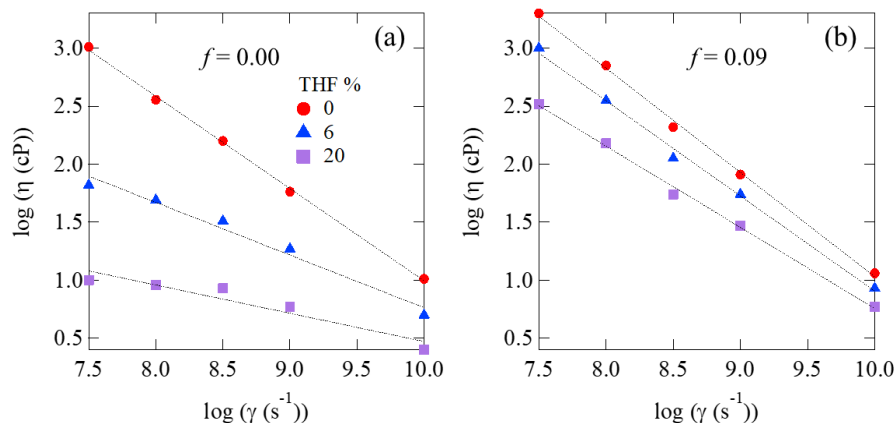
Figure 7.6: Shear viscosity (η) vs shear rate (γ) for (a) $f = 0$ and (b) $f = 0.09$ for a range of THF fractions fitted to power law model (shown in dashed lines).

Figure 7.6 shows shear viscosity as a function of shear rate for both $f = 0$ and $f = 0.09$. These data were analyzed in terms of a power-law where, $\eta \sim \dot{\gamma}^{-\alpha}$ For $f = 0$, α decreases from 0.80, 0.45 to 0.24 as THF amount in the system is increased from 0, 6 to 20 Wt%. For $f = 0.09$ the shear scaling factor α decreases from 0.90, 0.82, to 0.70 as similar THF amounts are added. This shows that with sulfonation groups and cluster formation the extent of shear thinning increases.
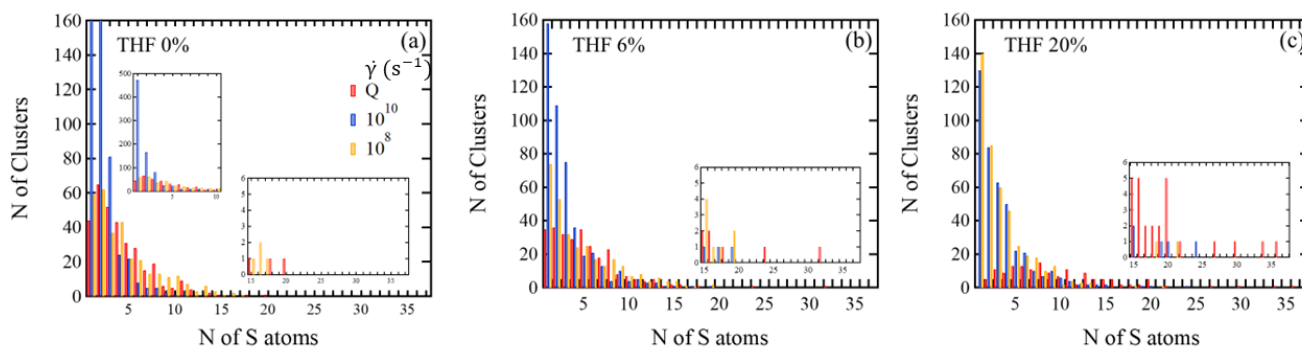

Figure 7.7: Number of clusters vs number of S atoms for $f = 0.09$ for %THF (a) 0 (b) 6 and (c) 20 at shear rates of $\dot{\gamma} = 10^{10}$(blue) and 10^8(yellow) and quiescent state (Q - red)

For $f = 0.09$ the average cluster size is measured by calculating the number of S atoms within 6 Å to each other. The quiescent state for all three sulfonation fractions is compared with shear rates of 10^8 and 10^{10}. It has been previously observed that with increasing THF fractions in SPS, larger well-defined clusters were developed.[24] As shear is applied the large clusters break for all three

THF fractions is observed. The faster shear rate of 10^{10} shows larger number of isolated SO_3^- compared with quiescent and slow shear rate 10^8 for 0 and 6% THF systems. Where 0% has 437 and 6% has 158 isolated groups SO_3^- out of the 1414 ionic groups in the system. For the slow shear rate this decreases to 59 and 74 free ionic groups for 0 and 6% THF. For 20% THF for both shear rates, a similar cluster distribution is observed.
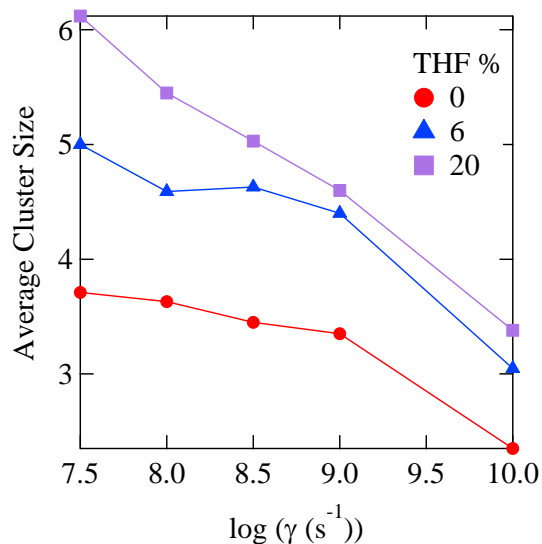

Figure 7.8: Average cluster size vs log shear rate ($\dot{\gamma}$) for $f = 0.09$ for a range of THF fractions

For $f = 0.09$ the average cluster size is measured by calculating the number of S atoms within 6 Å to each other. As the shear rate increases the average cluster size decreases. This decrease is more pronounced for the THF 20% system where the average cluster size decreases from 6.1 to 3.5. For THF 6% the cluster size barely changes within the shear rates of 8-9 and shows a large decrease at 10. For 0% THF the cluster size slowly decreases from 3.8 to 3.5 and drops to 2.5 when shear rate is increased to 10.

7.5 Conclusions

Here we use atomistic molecular simulations to determine the effect of shear response on PS and SPS ionomer melts swollen with THF. Previous study has shown that THF releases constraints and forms larger clusters. With application of shear, the chains stretch. As THF amount is increased the chains are less stretched for PS. As ionic groups are added bundles are formed due to aggregation of ionic groups. As shear is applied the chains stretch but the bundles remain intact, and the chains stretch together. As THF is added larger bundles are observed that stretch less compared to the pure melt. For both systems shear viscosity decreases with increasing shear rate. As THF is added shear viscosity decreases. With addition of ionic groups, the shear viscosity significantly increases. For the SPS systems clusters are broken and large number of free ionic groups are obtained as the systems are subjected to shear. With increasing THF fraction larger clusters are observed. With increasing shear rate smaller clusters are observed for all SPS systems.

7.6 Acknowledgement

7.7 References

(1) Farahanchi, A.; Malloy, R. A.; Sobkowicz, M. J. Extreme shear processing for exfoliating organoclay in nanocomposites with incompatible polymers. *Polymer* **2018**, *145*, 117-126.

(2) Fu, J.; Wang, Y.; Shen, K.; Fu, Q.; Zhang, J. Insight into shear-induced modification for improving processability of polymers: Effect of shear rate on the evolution of entanglement state. *Journal of Polymer Science Part B: Polymer Physics* **2019**, *57* (10), 598-606.

(3) Larson, R. G. The structure and rheology of complex fluids. *(No Title)* **1999**.

(4) Osterhold, M. *Physical Characterization of Coatings: Introduction to Rheology and Surface Analysis*; Logos Verlag, 2020.

(5) Chen, Q.; Huang, C.; Weiss, R.; Colby, R. H. Viscoelasticity of reversible gelation for ionomers. *Macromolecules* **2015**, *48* (4), 1221-1230.

(6) Agrawal, A.; Perahia, D.; Grest, G. S. Clustering effects in ionic polymers: Molecular dynamics simulations. *Physical Review E* **2015**, *92* (2), 022601.

(7) Kosgallana, C.; Wijesinghe, S.; Senanayake, M.; Mohottalalage, S.; Ohl, M.; Zolnierczuk, P.; Grest, G. S.; Perahia, D. From Molecular Constraints to Macroscopic Dynamics in Associative Networks formed by Ionizable Polymers: A Neutron Spin Echo and Molecular Dynamics Simulations Study. *ACS Polymers Au (in review)* **2024**.

(8) Qiao, X. Nonlinear Rheology of Lightly Sulfonated Polystyrene Ionomers. *Macromolecules* **2013**, *v. 46* (no. 6), pp. 2417-2424-2013 v.2446 no.2416. DOI: 10.1021/ma3026496   From National Agricultural Library PubAg.

(9) Ling, G. H.; Wang, Y.; Weiss, R. Linear viscoelastic and uniaxial extensional rheology of alkali metal neutralized sulfonated oligostyrene ionomer melts. *Macromolecules* **2012**, *45* (1), 481-490.

(10) Fitzgerald, J.; Kim, D.; Weiss, R. The effect of diluents on the ionic interactions in sulfonated polystyrene ionomers. *Journal of Polymer Science Part C: Polymer Letters* **1986**, *24* (6), 263-268.

(11) Huang, C.; Chen, Q.; Weiss, R. Nonlinear rheology of random sulfonated polystyrene ionomers: The role of the sol–gel transition. *Macromolecules* **2016**, *49* (23), 9203-9214.

(12) Zhang, L.; Brostowitz, N. R.; Cavicchi, K. A.; Weiss, R. Perspective: Ionomer research and applications. *Macromolecular Reaction Engineering* **2014**, *8* (2), 81-99.

(13) Chakrabarty, K.; Weiss, R.; Sehgal, A.; Seery, T. Characterization of ionomer solutions. 2. Dynamic light scattering studies on sulfonated polystyrene ionomers in a nonpolar solvent. *Macromolecules* **1998**, *31* (21), 7390-7397.

(14) Chakrabarty, K.; Seery, T.; Weiss, R. Characterization of ionomer solutions. 1. Phase behavior and gelation of sulfonated polystyrene ionomers in decalin. *Macromolecules* **1998**, *31* (21), 7385-7389.

(15) Xie, R.; Weiss, R. Molecular dynamics simulation of chain collapse of random ionomers in a poor solvent. *Computational and Theoretical Polymer Science* **1997**, *7* (2), 65-74.

(16) Lu, X.; Steckle, W.; Weiss, R. Ionic aggregation in a block copolymer ionomer. *Macromolecules* **1993**, *26* (22), 5876-5884.

(17) Fitzgerald, J.; Weiss, R. Synthesis, properties, and structure of sulfonate ionomers. *Polymer Reviews* **1988**, *28* (1), 99-185.

(18) Liu, S.; Cao, X.; Huang, C.; Weiss, R.; Zhang, Z.; Chen, Q. Brittle-to-ductile transition of sulfonated polystyrene ionomers. *ACS Macro Letters* **2021**, *10* (4), 503-509.

(19) Boris, D. C.; Colby, R. H. Rheology of sulfonated polystyrene solutions. *Macromolecules* **1998**, *31* (17), 5746-5755.

(20) Lopez, C. G. Scaling and entanglement properties of neutral and sulfonated polystyrene. *Macromolecules* **2019**, *52* (23), 9409-9415.

(21) Liu, S.; Zhang, Z.; Chen, Q.; Matsumiya, Y.; Watanabe, H. Nonlinear rheology of telechelic ionomers based on sodium sulfonate and carboxylate. *Macromolecules* **2021**, *54* (20), 9724-9738.

(22) Agrawal, A.; Perahia, D.; Grest, G. S. Cluster morphology-polymer dynamics correlations in sulfonated polystyrene melts: computational study. *Physical review letters* **2016**, *116* (15), 158001.

(23) Gulati, A.; Jacobs, M.; Lopez, C. G.; Dobrynin, A. V. Salt Effect on the Viscosity of Semidilute Polyelectrolyte Solutions: Sodium Polystyrenesulfonate. *Macromolecules* **2023**, *56* (5), 2183-2193.

(24) Kosgallana, C.; Grest, G. S.; Perahia, D. Structure and Dynamics of THF Swollen Polystyrene Ionomer Melts. *Macromolecules (in preperation)* **2024**.

(25) Jorgensen, W. L.; Maxwell, D. S.; Tirado-Rives, J. Development and testing of the OPLS all-atom force field on conformational energetics and properties of organic liquids. *Journal of the American Chemical Society* **1996**, *118* (45), 11225-11236.

(26) Jorgensen, W. L.; Madura, J. D.; Swenson, C. J. Optimized intermolecular potential functions for liquid hydrocarbons. *Journal of the American Chemical Society* **1984**, *106* (22), 6638-6646.

(27) Thompson, A. P.; Aktulga, H. M.; Berger, R.; Bolintineanu, D. S.; Brown, W. M.; Crozier, P. S.; in't Veld, P. J.; Kohlmeyer, A.; Moore, S. G.; Nguyen, T. D. LAMMPS-A flexible simulation tool for particle-based materials modeling at the atomic, meso, and continuum scales. *Comp. Phys. Comm.* **2022**, *271*, 108171.

(28) Pronk, S.; Páll, S.; Schulz, R.; Larsson, P.; Bjelkmar, P.; Apostolov, R.; Shirts, M. R.; Smith, J. C.; Kasson, P. M.; Van Der Spoel, D. GROMACS 4.5: a high-throughput and highly parallel open source molecular simulation toolkit. *Bioinformatics* **2013**, *29* (7), 845-854.

(29) Abraham, M. J.; Murtola, T.; Schulz, R.; Páll, S.; Smith, J. C.; Hess, B.; Lindahl, E. GROMACS: High performance molecular simulations through multi-level parallelism from laptops to supercomputers. *SoftwareX* **2015**, *1*, 19-25.

(30) Berendsen, H. J.; van der Spoel, D.; van Drunen, R. GROMACS: A message-passing parallel molecular dynamics implementation. *Computer physics communications* **1995**, *91* (1-3), 43-56.

(31) Hockney, R. W.; Eastwood, J. W. *Computer simulation using particles*; crc Press, 2021.

(32) Essmann, U.; Perera, L.; Berkowitz, M. L.; Darden, T.; Lee, H.; Pedersen, L. G. A smooth particle mesh Ewald method. *The Journal of chemical physics* **1995**, *103* (19), 8577-8593.

(33) Hess, B.; Bekker, H.; Berendsen, H. J.; Fraaije, J. G. LINCS: A linear constraint solver for molecular simulations. *Journal of computational chemistry* **1997**, *18* (12), 1463-1472.

(34) Bussi, G.; Donadio, D.; Parrinello, M. Canonical sampling through velocity rescaling. *The Journal of chemical physics* **2007**, *126* (1), 014101.

CHAPTER EIGHT

SUMMARY

This research focuses on understanding the effect of ionic aggregation on the structure, dynamics, and response to shear of ionomers in solutions as the environment is tweaked using molecular dynamics (MD) simulations and neutron scattering techniques. While large-scale atomistic MD simulations give insight into small length scales, neutron scattering is able to obtain the structure and dynamics of the polymer. The combination of neutron scattering methods with MD simulations allows the determination of structure and dynamics at multiple lengths and time scales.

1. Clustering effects on the structure of ionomer solutions: a combined SANS and simulations study

This study focused on the structure of sulfonated polystyrene (SPS) in toluene as solvent dielectrics with varied temperatures. This was done using small-angle neutron scattering (SANS) and large-scale atomistic MD simulations. The static structure scattering function extracted from both methods are in excellent agreement. While SANS was able to capture the networks at large dimensions and the ionic group relations, MD simulations were able to visualize the structure and give further insight into the cluster characteristics. As the concentration of the polymer is varied, the networks are slightly affected, and the cluster size increases due to the availability of ionic groups. As ethanol is added, smaller clusters are observed, and the large-scale networks are diminished. Temperature slightly enhances the networks and ionic groups.

2. From molecular constraints to macroscopic dynamics in associative networks formed by ionizable polymers: a neutron spin echo and molecular dynamics simulations study

Here, dynamics of the SPS in 90 Wt% toluene were probed using neutron spin echo (NSE) and MD simulations. Both methods were able to capture the segmental motion of the polymer at

various length scales. In order to capture the motion, two time scales were needed. The fast motion captures the chain motion in the solution, and slow motion captures cluster and chain segments that are directly associated. We show that SPS formed long-lived clusters for all systems that survive for long time ranges and affect the dynamics of the system.

3. From Ionic cluster dynamics to network constrains in ionic polymer solutions

Probing the dynamics of the system as external perturbations were applied was studied for SPS in toluene as solvent dielectrics and temperature were affected using NSE and MD simulations. Similar to the previous study, two-time scales were used to capture the motion of the systems. As ethanol is added, the dynamics of the system at all length scales are enhanced due to smaller clusters in the system. As temperature increases, the dynamics of both toluene and toluene-ethanol mixtures increase. By measuring the sulfur-sulfur atom distance with time, we saw that in toluene, the clusters do not exchange neighbors within a cluster, but in ethanol, ionic groups within a cluster are more dynamic and exchange neighbors.

4. Structure and dynamics of the swollen polystyrene ionomer melts

The effect of a mutual solvent on the structure and dynamics of SPS was studied using MD simulations. Here, the SPS melt was swollen with 6 Wt% and 20 Wt% THF. As solvent is added, constraints of the system are released. Cluster size and distribution, as well as static structure factor and pair correlation function, were measured to understand the structure. Surprisingly, we found that in the presence of THF, the cluster size increases. THF resides throughout the system without any preference for either chain or ionic groups. The mean squared displacement of the chains and the dynamic structure factor were measured to study the dynamics of the system. As THF is added, the dynamics of the system increase for all sulfonation fractions even though larger clusters were observed.

5. Shear response on THF swollen ionomer polymer melts: molecular dynamics simulation study.

The response to shear was studied for SPS in THF using atomistic MD simulations. As the shear rate was increased, the shear viscosity decreased for all systems. The shear viscosity decreases with the addition of THF and significantly increases with the addition of ionic groups. While PS shows less chain stretching with THF addition for all shear rates, SPS with a sulfonation fraction $f = 0.09$ shows that polymer bundles are formed, which increase with THF fraction. The bundles undergo stretching, and then the clusters are affected as shear rate increases. With increasing solvent, larger clusters remain intact while shear is applied.

APPENDIX

Clustering of Ions in Organic Polymers. A Theoretical Approach

American Physical Society
Reuse and Permissions License

Licensed Content Information

License Number:	RNP/24/JAN/074269
License date:	19-Jan-2024
DOI:	10.1103/PhysRevE.92.022601
Title:	Clustering effects in ionic polymers: Molecular dynamics simulations
Author:	Anupriya Agrawal, Dvora Perahia, and Gary S. Grest
Publication:	Physical Review E
Publisher:	American Physical Society
Cost:	USD $ 0.00

Request Details

Does your reuse require significant modifications: No

Specify intended distribution locations:	United States
Reuse Category:	Reuse in a thesis/dissertation
Requestor Type:	Author of requested content
Items for Reuse:	Figures/Tables
Number of Figure/Tables:	1
Figure/Tables Details:	FIG. 1. Mean square displacement versus time at 600 K of a sulfonated polystyrene melt
Format for Reuse:	Electronic

Information about New Publication:

University/Publisher:	Clemson University
Title of dissertation/thesis:	STRUCTURE AND DYNAMICS OF COMPLEX FLUIDS FORMED BY IONOMERS: EXPERIMENTAL-COMPUTATIONAL INSIGHT
Author(s):	Chathurika Kosgallana
Expected completion date:	Jan. 2024

License Requestor Information

Name:	Chathurika Kosgallana
Affiliation:	Individual
Email Id:	ckosgal@clemson.edu
Country:	United States

126

License Details

This Agreement between Clemson University -- Chathurika Kosgallana ("You") and John Wiley and Sons ("John Wiley and Sons") consists of your license details and the terms and conditions provided by John Wiley and Sons and Copyright Clearance Center.

Print   Copy

License Number	5712300244524
License date	Jan 19, 2024
Licensed Content Publisher	John Wiley and Sons
Licensed Content Publication	Journal of Polymer Science Part B: Polymer Physics
Licensed Content Title	Spherical and vesicular ionic aggregates in Zn-neutralized sulfonated polystyrene ionomers
Licensed Content Author	Brian P. Kirkmeyer, Robert A. Weiss, Karen I. Winey
Licensed Content Date	Jan 18, 2001
Licensed Content Volume	39
Licensed Content Issue	5
Licensed Content Pages	7
Type of Use	Dissertation/Thesis
Requestor type	University/Academic
Format	Electronic
Portion	Figure/table
Number of figures/tables	1
Will you be translating?	No
Title of new work	STRUCTURE AND DYNAMICS OF COMPLEX FLUIDS FORMED BY IONOMERS: EXPERIMENTAL-COMPUTATIONAL INSIGHT
Institution name	Clemson University
Expected presentation date	Jan 2024
Portions	Figure 1
Requestor Location	Clemson University S Palmetto Blvd, CLEMSON, SC 29634 United States Attn: Clemson University
Publisher Tax ID	EU826007151
Total	**0.00 USD**

BACK

License Details

This Agreement between Clemson University -- Chathurika Kosgallana ("You") and Springer Nature ("Springer Nature") consists of your license details and the terms and conditions provided by Springer Nature and Copyright Clearance Center.

Print   Copy

License Number	5713030341542
License date	Jan 20, 2024
Licensed Content Publisher	Springer Nature
Licensed Content Publication	Springer eBook
Licensed Content Title	Analysis of Existing Types and Protection Methods Against Neutron Radiation from Different Sources
Licensed Content Author	Valeriia Kovach, Anna Iatsyshyn, Ievhen Pylypchuk et al
Licensed Content Date	Jan 1, 2023
Type of Use	Thesis/Dissertation
Requestor type	academic/university or research institute
Format	electronic
Portion	figures/tables/illustrations
Number of figures/tables/illustrations	1
Will you be translating?	no
Circulation/distribution	1 - 29
Author of this Springer Nature content	no
Title of new work	STRUCTURE AND DYNAMICS OF COMPLEX FLUIDS FORMED BY IONOMERS: EXPERIMENTAL-COMPUTATIONAL INSIGHT
Institution name	Clemson University
Expected presentation date	Jan 2024
Portions	Fig.2 Types of ionizing radiation and their penetrating power
Requestor Location	Clemson University S Palmetto blvd
	CLEMSON, SC 29634 United States Attn: Clemson University
Total	**0.00 USD**

BACK